Cellular Targets of Guanidino Phthalocyanines

Dissertation

zur

Erlangung der naturwissenschaftlichen Doktorwürde

(Dr. sc. nat)

vorgelegt der

Mathematisch-naturwissenschaftlichen Fakultät

der

Universität Zürich

von

Bala Yeshwanth Ram Vummidi

aus

Indien

Promotionskomitee

Prof. Dr. Nathan Luedtke (Vorsitz und Leitung der Dissertation)

Prof. Dr. Andreas Plückthun

Prof. Dr. Reto Schwendener

Prof. Dr. Oliver Zerbe

Zürich, 2013

Table of Contents

Summary

DNA is a unique biomolecule that carries genetic information. While DNA is widely considered to be double helical, important processes such as replication and transcription require single-stranded DNA intermediates. Single-stranded DNA can form a variety of secondary structures, and one important example formed by G-rich sequences is the G-quadruplex. Though these structures are kinetically and thermodynamically stable *in vitro*, their existence and associated functions *in vivo* require additional evaluation. In particular, G-quadruplexes have been proposed to be attractive anti-cancer targets due to the abundance of guanine-rich sequences in the promoter regions of many oncogenes such as c-Myc. Hurley and co-workers have proposed that small molecules capable of stabilizing G-quadruplexes in promoters are capable of decreasing oncogene expression. This hypothesis, however, has only been evaluated using small molecules that exhibit little or no G-quadruplex selectivity as compared to duplex DNA. Hence, the potential role of G-quadruplex ligands in transcriptional regulation requires further study.

In this thesis, I report the utilization of cationic phthalocyanines for probing G-quadruplex structures and function *in vivo*. Ammonium and guanidium-modified phthalocyanines bind to G-quadruplex DNA *in vitro* with exceptionally high affinity ($K_d \leq 2$ nM) and high selectivity (>1'000-fold) as compared to duplex DNA. Upon G-quadruplex binding, guanidinium-modified phthalocyanines exhibit a dramatic increase in fluorescence intensity. This property can be utilized in cell-based imaging studies, where fluorescent staining is localized in perinuclear regions and lysozomes of living cells. In dead and fixed cells, however, staining was observed in the nucleolus due to the association of these compounds with RNA. Since direct observation of promoter (or telomeric) G-quadruplexes fluorescence staining was not feasible, the abilities of cationic phthalocyanines to interact with putative G-quadruplexes in promoters was evaluated by measuring their global impact on gene expression using microarray analyses. Ammonium-containing phthalocyanines caused statistically significant changes of 2-fold or more ($p < 0.001$) in the mRNA transcription of approximately 2'000 genes in B16F10 cells. Approximately 39% of these genes contain a putative G-quadruplex-forming sequence within 1'000 nucleotides of the transcription start site. This frequency does not deviate from the genome-wide % of promoters containing a puatative G-quadruplex

forming sequence. Taken together, these results do not support the presence of functional G-quadruplex structures in promoter regions capable of regulating gene expression.

According to microarray analyses, guanidinium-modified phthalocyanines exhibited a very limited ability to impact global gene expression in B16-F10 cells. One derivative, tetrakis-(diisopropyl-guanidino) zinc phthalocyanine "Zn-DIGP" consistently affected the transcription of only a single gene, CXCL10. qRT-PCR experiments demonstrated that Zn-DIGP-mediated overexpression of CXCL10 was both dose- and time- dependent, and ELISA experiments revealed that Zn-DIGP caused a 20-fold increase in extracellular CXCL10 protein concentrations at sub-toxic doses. Zn-DIGP is a competitive inhibitor of CXCL10-mediated CXCR-3 activation (IC_{50} = 4 μM), and it inhibits downstream events such as CXCL10-dependent cell migration. Interestingly, Zn-DIGP binds to the G protein-coupled receptor (GPCR) CXCR3 without activating the receptor, yet is able to cause endocytosis and degradation of CXCR3. While there are few peptide antagonists known to cause internalization of GPCRs, Zn-DIGP represents, to the best of our knowledge, the first small-molecule GPCR antagonist shown to cause receptor internalization and degradation. This process is possibly responsible for Zn-DIGP-mediated CXCL10 overexpression via dysregulation of an endogenous negative feedback loop.

CXCR3 antagonists are rapidly emerging as a new class of anti-cancer agents that can inhibit metastasis. The potential anti-metastatic activities of Zn-DIGP were therefore evaluated by an assay that mimics the hematogenous spread of malignant melanoma *in vivo*. Zn-DIGP was found to be well tolerated upon its intravenous injection into mice at 8 mg/kg and was capable of inhibiting the formation of tumor colonies in the lungs of C57BL/6 mice injected with B16F10 cells. Our results therefore provide additional evidence that CXCR3 antagonists are a new class of anti-metastatic agents. Unlike previously reported CXCR3 antagonists, however, Zn-DIGP is also a promising sensitizer for photodynamic therapy (PDT). Upon photoexcitation with red laser light (660 nm), Zn-DIGP exhibits a high quantum yield for singlet oxygen formation ($\Phi \approx 0.46$) that results in potent phototoxicity ($EC_{50} \approx 0.16$ μM) in cell cultures. Zn-DIGP can therefore be developed as a multi-functional PDT agent, where light energy can be harnessed for the treatment of primary surface tumors, while simultaneously inhibiting the formation of new tumor colonies in vital organs by interfering with chemokine signaling.

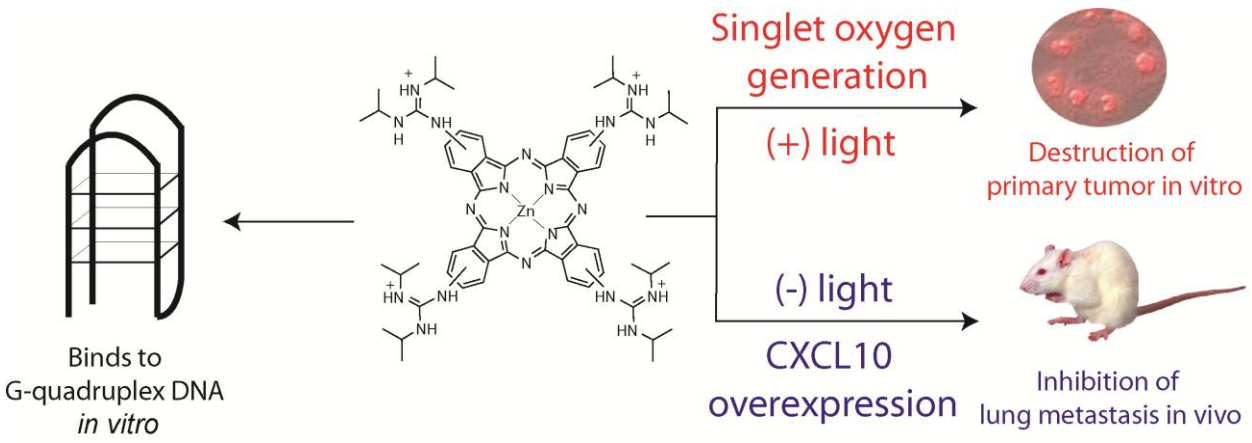
Singlet oxygen
generation
(+) light
Destruction of
primary tumor in vitro
(-) light
CXCL10
overexpression
Inhibition of
lung metastasis in vivo
Binds to
G-quadruplex DNA
in vitro

Zusammenfassung

DNA ist ein einzigartiges Biomolekül, welches genetische Informationen speichert. Obwohl DNA üblicherweise als doppelsträngig angenommen wird, treten wichtige Prozesse wie Replikation und Transkription nur auf, wenn die DNA einzelsträngig vorliegt. Basierend auf ihrer Sequenz kann einzelsträngige DNA eine Vielzahl von Sekundärstrukturen annehmen, und eine wichige Sekundärstruktur wird G-Quadruplex genannt. Obgleich diese Strukturen *in vitro* kinetisch und thermodynamisch stabil sind, ihre Existenz sowie dazugehörige Funktionen *in vivo* benötigen weitere Nachweise. Insbesondere wurden G-Quadruplexe als attraktive Angriffspunkte für Krebstherapien vorgeschlagen aufgrund der Fülle von Guanin-reichen Sequenzen in den Promotorregionen vieler Onkogene wie beispielsweise c-Myc. Hurley *et al.* berichteten, dass kleine Moleküle, welche G-Quadruplex-Strukturen in Promotorregionen stabilisieren, die Expression von Onkogenen inhibieren könnten. Diese Hypothese wurde jedoch nur mit kleinen Molekülen evaluiert, welche wenig oder keine Selektivität für G-Quadruplexe gegenüber Duplex-DNA zeigten. Deshalb erfordert die potentielle Rolle von G-Quadruplex-Liganden in der Transkriptionsregulation weitere Untersuchungen.

In dieser Arbeit berichte ich über die Nutzung kationischer Phthalocyanine für den Nachweis von G-Quadruplex-Strukturen und Funktionen *in vivo*. Ammonium- und guanidinium-modifizierte Phthalocyanine binden an G-Quadruplex-DNA *in vitro* mit ausserordentlich hoher Affinität ($K_d \leq 2$ nM) und Selektivität (> 1000fach) verglichen mit Duplex-DNA. Beim Binden an G-Quadruplex-Strukturen zeigen guanidinium-modofozierte Phthalocynine einen dramatischen Anstieg der Fluoreszenzintensität. Diese Eigenschaft wurde in Zell-basierten Experimenten genutzt, in denen Fluoreszenz in perinukleären Regionen und Lysosomen lebender Zellen lokalisiert war. In toten und fixierten Zellen jedoch wurde die fluoreszente Färbung in Nukleoli beobachtet aufgrund der Assoziation dieser Verbindungen an RNA. Da eine direkte Beobachtung der Fluoreszenzfärbung von Promoter- oder Telomer-assoziierten G-Quadruplexen nicht möglich war, die Fähigkeit der Verbindungen, mit mutmasslichen G-Quadruplex-Sequenzen in Promotoren zu interagieren, wurde indirekt untersucht durch Messung ihres globalen Effekts auf Genexpression mithilfe von Mikroarray-Analysen. Ammonium-modifizierte Phthalocyanine bewirkten statistisch signifikante Veränderungen von zweifach oder mehr ($p < 0.001$) der mRNA-Transkription von über 2000 Genen in

B16F10-Zellen. Etwa 39 % dieser Gene enthielten mutmassliche G-Quadruplex-formende Sequenzen innerhalb von 1000 Nukleotiden ausgehend von der Transkriptions-Startstelle. Dieser Wert weicht nicht ab vom Genom-weiten Vorkommen von Promotoren mit G-reichen Sequenzen. Zusammenfassend geben diese Ergebnisse keinen Hinweis auf das Vorkommen von funktionellen G-Quadruplex-Strukturen in den Promoterregionen, welche die Genexpression regulieren können.

Gemäss der Mikroarray-Analysen zeigten guanidinium-modifizierte Phthalocyanine eine sehr beschränkte Fähigkeit, die globale Genexpression in B16F10-Zellen zu beeinflussen. Ein Derivat, tetrakis-(diisopropyl-guanidino) zinc phthalocyanine „Zn-DIGP" beeinflusste die Transkription nur eines einzigen Gens konstant, CXCL10. qRT-PCR-Experimente zeigten, dass Zn-DIGP-vermittelte Überexpression von CXCL10 sowohl Dosis- als auch Zeit-abhängig war, und ELISA-Experimente offenbarten, dass nicht-toxische Mengen von Zn-DIGP einen 20fachen Anstieg der extrazellulären CXCL10-Proteinkonzentration in B16F10-Zellen bewirkten. Zn-DIGP ist ein kompetitiver Inhibitor der CXCL10-vermittelten CXCR3-Aktivierung (IC_{50} = 4 mM), und es inhibiert nachfolgende Prozesse wie beispielsweise CXCL10-abhängige Zellmigration. Interessanterweise bindet Zn-DIGP an den G-Protein-gekoppelten Rezeptor (GPCR) CXCR3, ohne diesen zu aktivieren, doch es ist in der Lage, Endozytose und Abbau von CXCR3 zu bewirken. Während nur wenige Peptid-Antagonisten bekannt sind, welche Internalisierung von GPCRs verursachen, repräsentiert Zn-DIGP nach unserem besten Wissen den ersten GPCR-Antagonisten auf Grundlage eines kleinen Moleküls, welcher Rezeptorinternalisierung und Abbau bewirkt. Dieser Vorgang ist möglicherweise verantwortlich für die Überexpression von CXCL10 durch eine endogene negative Feedback-Schleife.

CXCR3-Antagonisten treten immer mehr als eine neue Klasse von Antikrebsmitteln hervor, welche Metastasenbildung verhindern können. Die potentielle Metastasen-inhibierende Aktivität von Zn-DIGP wurde deshalb durch einen Test evaluiert, bei welchem die hämatogene Ausbreitung von bösartigen Melanomen *in vivo* nachgeahmt wird. Es zeigte sich, dass Zn-DIGP bei intravenöser Injektion in Mäusen (8 mg/kg) gut toleriert wurde, und es war in der Lage, die Bildung von Tumoren in der Lunge von C57BL/6-Mäusen, welchen B16F10-Zellen injiziert worden waren, zu verhindern. Unsere Ergebnisse bieten deshalb einen zusätzlichen Hinweis, dass CXCR3-Antagonisten eine neue Klasse von Antikrebsmitteln darstellen. Anders als frühere CXCR3-Antagonisten ist Zn-DIGP jedoch

auch ein vielversprechender Sensibilisator für photodynamische Therapien (PDT). Der Anregung mit rotem Laserlicht (660 nm) folgend weist Zn-DIGP eine hohe Quantenausbeute für die Generierung von Singlett-Sauerstoff auf ($\Phi \approx 0.46$), welcher eine potente Phototoxizität ($EC_{50} \approx 0.16$ µM) in Zellkultur zur Folge hat. Zn-DIGP kann deshalb zu einem multifunktionellen PDT-Agens weiterentwickelt werden, welches mithilfe von Lichtenergie für die Behandlung von primären Oberflächentumoren benutzt werden kann, während es gleichzeitig die Bildung von neuen Tumorkolonien in lebenswichtigen Organen verhindert, indem es Chemokin-vermittelte Signalwege beeinflusst.

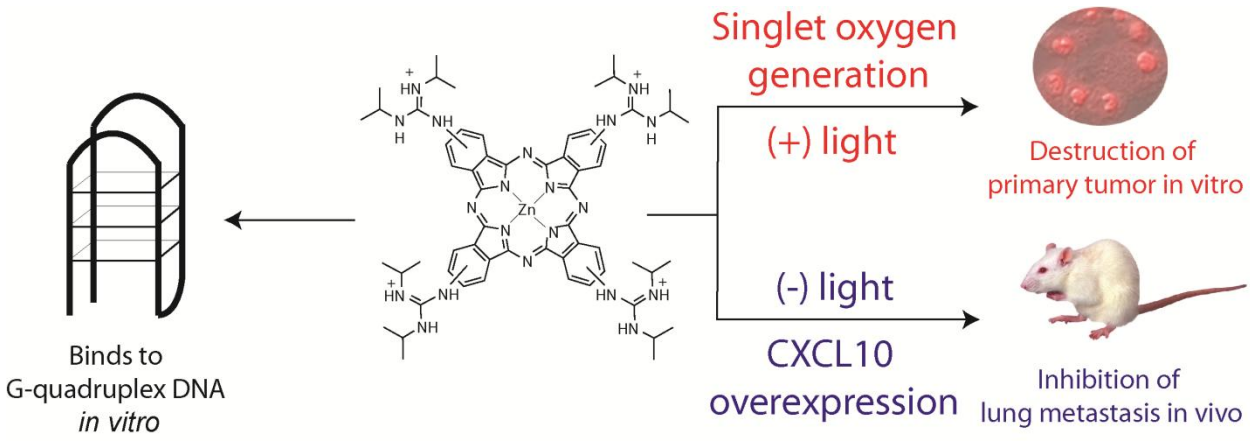

Chapter 1. Introduction

Nucleic acids are an important class of biomolecules that play diverse roles in functioning of living cells. The central dogma of biology states that deoxyribonucleic acids (DNA) are transcribed into ribonucleic acids (RNA) which encode for proteins.[1] Ever since Freidrich Miescher reported the isolation and elemental analysis of mysterious "nuclein" from nuclei of white blood cells, research on the structural and functional aspects of DNA has been rapidly mounting.[2] In 1953, Watson and Crick proposed the duplex model for 'B' form of DNA where two strands of DNA run anti-parallel to form a double helical structure consisting of a major groove and minor groove. This duplex is stabilized by hydrogen bonding and base stacking interactions between guanine-cytosine and adenine-thymine residues (Figure 1.1).[3]

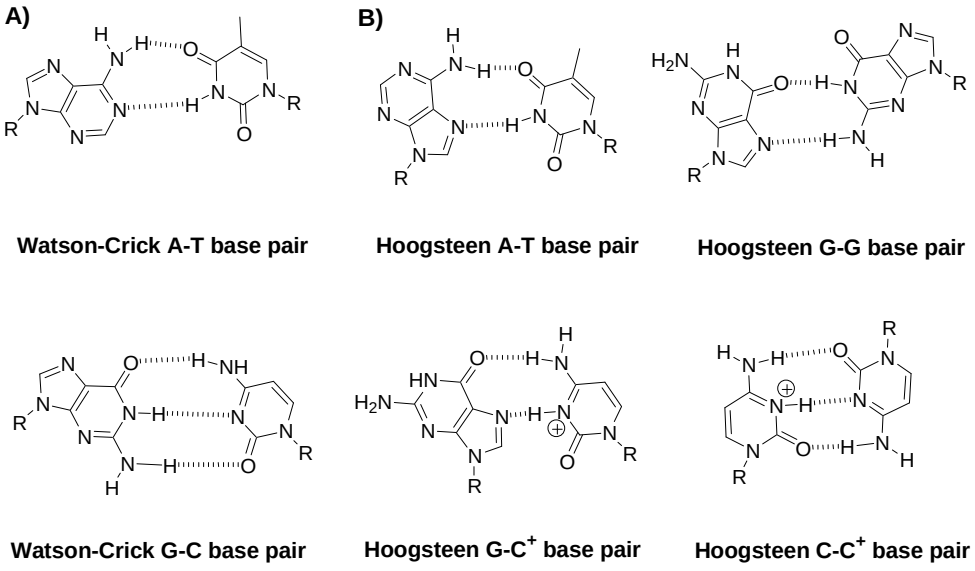

Figure 1.1. Nucleobases with A) Watson-Crick and B) non-canonical base-pairing interactions.

It is widely believed that the 'B' form of double helical structure is the (one and only) biologically relevant structure of DNA. The most important functions of DNA such as replication and transcription, however, require the presence of single stranded templates. These processes overcome the large kinetic barriers of duplex disassociation, providing the opportunity for non-duplex DNA structure to form in living cells. Some examples of non-canonical DNA structures that have been characterized *in vitro* include hairpin loop,[4] triplex,[5] i-motif [6] and G-quadruplex.[7] (Figure 1.2)

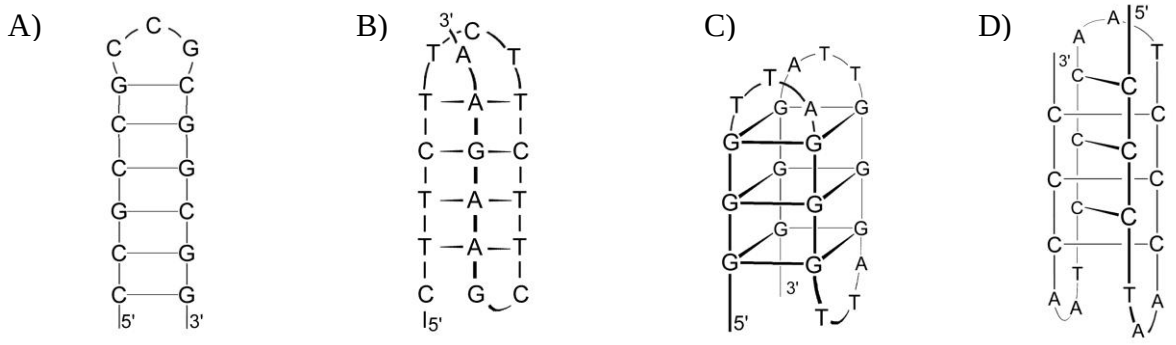

Figure 1.2. Secondary structures of single stranded DNA. A) Hairpin loop; B) Triplex; C) G-quadruplex; D) i-motif.

1.1. G-quadruplex DNA

In 1910, Bang reported that concentrated solutions of guanylic acid self-associate to form gels.[8] Using fiber diffraction studies, Gellert and coworkers concluded that polymers of guanosine can fold into a tetrameric arrangement of guanine bases that interact via Hoogsteen hydrogen bonding and metal ion binding.[9] As shown in Figure 1.3, the four guanine bases form square – coplanar arrangements that utilize the hydrogen atoms of N1 and N2 to bond with O6 and O7 of adjacent guanine to provide eight hydrogen bonds per G-tetrad. Structures containing two or more G-tetrads constitute a special family of secondary structures called G-quadruplexes.

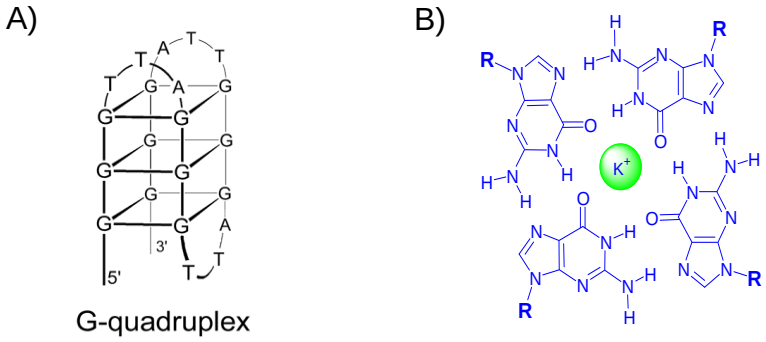

Figure 1.3. Structure of A) intramolecular G-quadruplex and B) G-tetrad.

1.1.1. Types of G-quadruplexes

G-quadruplexes can be formed from a single guanine-rich sequence (intra-molecular) or two or more strands (inter-molecular). These structures can be classified as parallel or anti-parallel based on the directionality of the phosphodiester backbones (Figure 1.4). Based on

the length and connecting nucleotides,[10, 11] the topology can be classified by diagonal, lateral, propeller[12, 13] or double-chain reversal.[13]

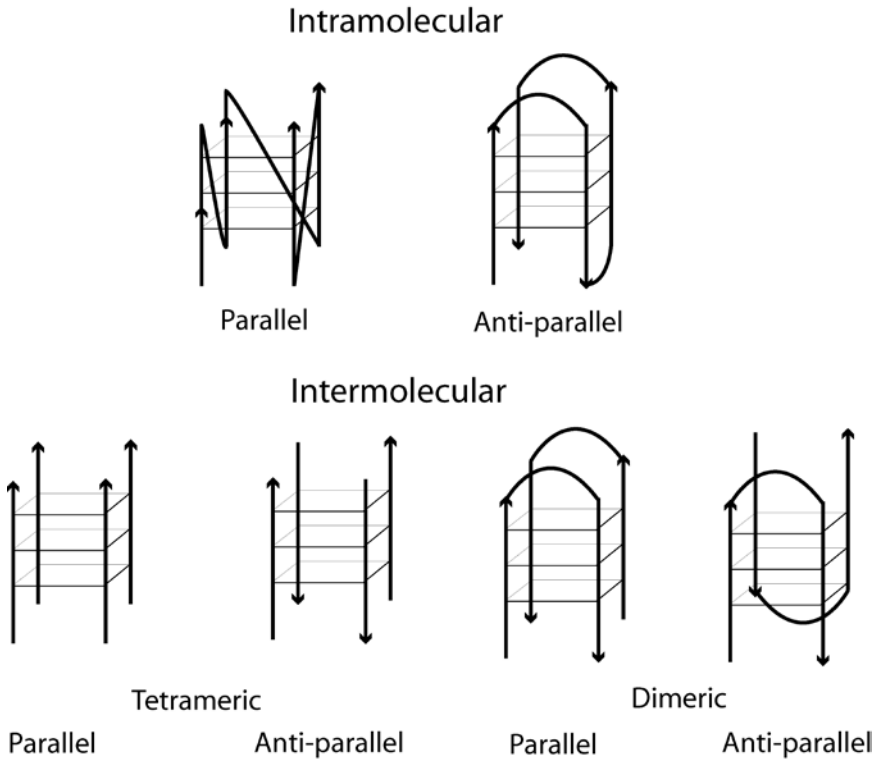

Figure 1.4. Schematic representation of different topologies of G-quadruplex structures.

1.1.2. Stabilizing factors

Stabilizing factors important for duplex DNA such as base-stacking, hydrogen bonding, hydration and electrostatic interactions are also important to G-quadruplex stability. A unique feature of G-quadruplexes is the arrangement of O6 atoms of guanine. Assembly of guanine tetrads orients the O6 of each guanine residue towards the central cavity of the G-quadruplex core. Arnott and coworkers first suggested that the negatively charged central core is stabilized by cation co-ordination.[14] The selection of a suitable cation based on its size and charge determines the overall stability of G-quadruplex structures. The general trend for preference of cationic alkali metals is $K^+ > Na^+ > Rb^+ > NH_4^+ > Cs^+ > Li^+$. Apart from these fundamental properties, loop length and sequence also determine the overall stability and topology of G-quadruplex structures. [15] The stability of G-quadruplexes generally increases until the loop reaches 5 nucleotides in length, longer loops typically do not have any additional influence on stability.[16] Among the nucleotides present in the loop, thymines tends to increase the G-quadruplex stability,[11] whereas adenine can cause destabilization.[17, 18]

1.1.3. Equilibrium between duplex and G-quadruplex

Interestingly, for every G-rich DNA sequence that is known to be capable of forming a G-quadruplex structure, its complementary C-rich sequence has been found to be capable of folding into an i-motif structure *in vitro*.[19-25] G-C rich DNA sequences can therefore exist as a mixture of G-quadruplex / i-motif and canonical duplex DNA (Figure 1.5).[26] The large kinetic barriers for duplex dissociation that are a prerequisite to establishing this equilibrium can be overcome by transcription and replication processes, as well as single-stranded DNA binding proteins,[27] chaperones,[28, 29] small-molecule binding,[30] partial dehydration/molecular crowding,[31] and/or negative supercoiling *in vivo*.[32-34] In aqueous buffer, G-quadruplex structures are typically very resistant to thermal denaturation (T_m > 70 °C),[35] while the vast majority of i-motif structures exhibit only marginal thermodynamic stabilities at neutral pH (T_m < 10 °C).[19-25] G-quadruplex structures have therefore served as the primary target for probes designed to detect this type of conformational equilibrium *in vivo*.

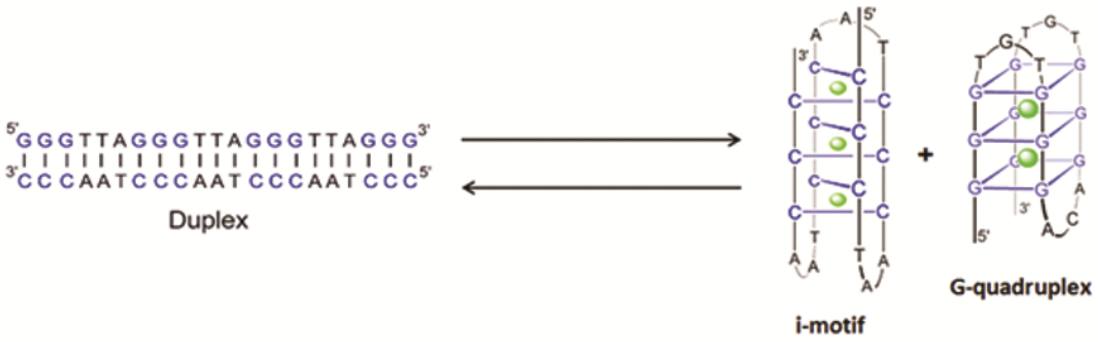

Figure 1.5. Equilibrium between G-quadruplex and duplex DNA.

1.2. Locations of G-rich sequences in the genome

Prokaryotic and eukaryotic genomes were identified to be rich in putative G-quadruplex sequences (PQS). [36-38] Bioinformatic analysis by Huppert and Balasubramanian showed that more than 376’000 PQS are present in the human genome.[39] Their enrichment was identified to be non-random and correlate with functional regions of the genome. A high frequency of PQS were found in the telomeres and the promoter regions of eukaryotic genes.

1.2.1. Telomeres

Telomeres are special DNA-protein complexes the end of chromosomes of all vertebrates. Telomeres consist of non-coding DNA, typically 8-10 kb long with single stranded 3` overhang up to 200 bp that is protected by special protein complexes called shelterin. The shelterin complex is composed of single-stranded and double-stranded DNA, DNA binding proteins (TRF1, TRF2), a single-strand DNA binding protein (Pot1), and Rap1, TPP, and TIN2 that bind via protein-protein interactions. The shelterin proteins prevent the DNA from being recognized as double stranded beaks and therefore protect the chromosome. During each round of replication, telomeres get shortened by RNA-primed DNA synthesis. This 'end replication' problem can be overcome by expression of telomerase. Telomerase is a reverse transcriptase that carries its own RNA template that can be used to extend 3` end of the telomere. Telomerase is overexpressed in cancer cells allowing for their immortality, however the telomerase activity is tightly regulated in normal cells allowing gradual telomere shortening with each cell division. A second method for telomere extension that occurs in certain tumor cells that do not overexpress telomerases is recombination-mediated process called Alternative lengthening of telomere (ALT).[40]

The 3` overhang of telomeric DNA consists of repetitive G-rich sequences. Some examples include *Sachromyces cerevisiae*: $TG_{1\text{-}3}$,[41] *Oxytricha nova*: TTTTGGGG,[42] *Arabidopsis thaliana*: TTTAGGG[43] and in mammals: TTAGGG.[44] All of these sequences can form G-quadruplex structures *in vitro*.[45, 46] The first direct evidence for the presence of telomeric G-quadruplexes *in vivo* was demonstrated using G-quadruplex specific antibodies in ciliates.[47] Further studies using RNA interference (RNAi) demonstrated that the telomere end binding proteins of ciliates – TEBPα and TEBPβ assist the formation of G-quadruplexes structures *in vivo*.[48] The human telomeric G-quadruplex can fold into at least four different G-quadruplex conformation structures *in vitro*.[49] Though their existence in eukaryotic cells is unproven, several indirect experiments supporting the formation of G-quadruplexes have been reported. For example, the shelterin protein 'Pot 1' was reported to interact with single stranded 3` overhang and destabilize G-quadruplex structures.[50] Recently, the ends of chromosomes were visualized in fixed human cells using a G-quadruplex specific antibody in fixed cells, suggesting the presence of G-quadruplexes at chromosomal ends.[51] In yeast, mutation of G-quadruplex stabilizing protein (EST1) causes telomere shortening suggesting a positive role of G-quadruplexes in telomere maintenance.[52] In another study using yeast, G-quadruplexes

structures were found to inhibit exonuclease activities at telomeric ends *in vitro*. Together, these results suggest a positive role of G-quadruplex in maintaining telomere length and stability.[53]

Given the ability of G-quadruplex folding to inhibit telomerase activity *in vitro*, it was proposed that small molecules that stabilize G-quadruplex structures could inhibit telomerase. Early studies demonstrated that the addition of a G-quadruplex specific binder, telemostatin to a cancer cells caused disassociation of telomere binding proteins from their sites and reduce cell proliferation.[54, 55] Based on these results, small molecules that stabilize G-quadruplex structures in the telomere and displace telomerase is considered as an possible anti-cancer strategy (Figure 1.6). Though several molecules were reported to inhibit the action of telomerase *in vitro*, subsequent studies showed that the telomerase inhibition was frequently a result of direct binding interactions with telomerase itself.[56] Hence, direct evidence for the therapeutic relevance of telomeric G-quadruplexes remain elusive.

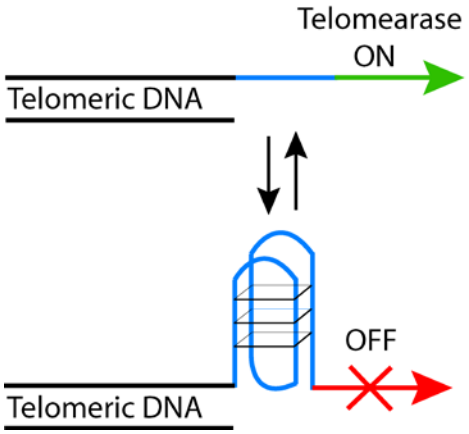

Figure 1.6. Possible role of G-quadruplex in telomerase inhibition.

1.2.2. Nucleolus

The nucleolus originates from nucleolar organizing regions (NOR) assembled from tandem rDNA genes that are present on different chromosomes.[57] Interestingly, rDNA has a C-rich template strand and G-rich non-template strand. Due to constitutive transcription of rDNA genes, the two strands are stabily disassociated into single-stranded DNA, providing opportunity for the G-rich strands to fold into G-quadruplex structures.[58, 59]

Electron microscope studies in *E.coli* identified novel DNA structures (loops) being formed during rDNA transcription. These loops were proposed to have G-quadruplexes in the G-rich

strand and DNA/RNA hybrids in the complimentary strand.[60] The formation of G-quadruplex structures in the nucleolus of eukaryotic cells has been proposed to be mediated by nucleolin and various helicases. The high abundance of nucleolin in nucleolus, together with its high affinity for G-quadruplex structures (K_d = 1 nM) *in vitro*, implies the presence of G-quadruplex structures in the nucleolus.[58, 59] In contrast, WRN[61] and BLM[62] helicases were reported to unwind G-quadruplex structures *in vitro*. WRN is localized primarily in the nucleolus[63] and serves to increase the rate of rDNA transcription.[64] Together, these results provide a contradicting view of the importance of G-quadruplex unfolding for active transcription.

A potent G-quadruplex binder, CX-3543, is known to localize in the nucleolus and it inhibits rRNA biogenesis.[65] CX-3543 is the only drug-like G-quadruplex binder that reached Phase 2 clinical trials. However, due to bioavailability problems, CX-3543 failed Phase 2 clinical trials, and its proposed cellular target of rDNA has never been fully validated as a drug target.

1.2.3. Recombination sites

Class-switch recombination is a highly regulated, essential process that alters the genomic structure of the heavy chains of immunoglobulin. Recombination occurs at the immunoglobulin switch regions (S regions) which comprise repeats from 2-10 kb in length. This repeat region contains a G-rich sequence that has the ability to form G-quadruplex structures *in vitro*. Upon transcription of the S region, atomic force microscope (AFM) images identified large loops consisting of G-quadruplex and a DNA/RNA hybrid.[66, 67] The protein MutSα binds to a G-quadruplex from the S-region (K_d = 1 nM) and it promotes a "synapsis step" which is essential for class switching.[68] The importance of G-quadruplex structures as recombination elements was clearly demonstrated in *Neisseria gonorrhoeae*. *Neisseria gonorrhoeae* is a pathogen that expresses antigenic variation in its pili. The antigenic variation is a result of recombination. The removal of 16 bp G-rich sequence shuts down antigenic variation, suggesting the importance of this sequence. Circular dichroism studies showed that this G-rich sequence can fold into a G-quadruplex structure *in vitro*. Mutations of this sequence that destabilize the G-quadruplex structure cause recombination failure. Furthermore, the addition of a G-quadruplex-specific binder, pyridostatin, inhibited antigenic variation, further confirming the utilization of a G-quadruplex structure in the recombination sites.[69] This study demonstrated the importance of G-quadruplex in

prokaryotes. However, such direct demonstration of functional G-quadruplex structures in mammalian cells remains elusive.

1.2.4. Promoter regions of oncogenes

Bioinformatics-based searches for $G_{3+}N_{1-7}G_{3+}N_{1-7}G_{3+}N_{1-7}G_{3+}$ identified strong enrichment of this PQS in promoters, 5'-UTRs and 3'-UTRs of human genes. 42.7% of 19'628 characterized genes contain at least one PQS less than 1000 nucleotides from the transcription start site.[70] In addition, the density of PQSs was very high near transcription start sites, possibly as a result of evolutionary pressure. 12% of the 5`-UTR,[70] 15% of 3`-UTR[70] and 16% of the first 100 nucleotides of first introns[71] also exhibited a high frequency of PQSs. Though not all the PQSs are validated experimentally, the strong enrichment of PQSs in gene regulatory regions raises the possibility of functional G-quadruplex structures functional in gene regulation.[72]

Initial evidence for G-quadruplex dynamics in regulating gene expression was reported in the β-globulin gene.[73, 74] Since then, many oncogenes such as c-Kit,[75] PDGF,[76] VEGF,[30] RetB[77] were reported to have PQSs in their promoter region that can form G-quadruplexes *in vitro*. c-Myc is a proto-oncogene that contains a G-quadruplex forming motif in a nuclease hypersensitive element located 130 nucleotides upstream of transcription start site. This sequence can form a propeller-type parallel G-quadruplex *in vitro*.[78] Mutation studies of the guanines in this Myc PQS demonstrated that the disruption of G-quadruplex stability could increase gene expression, suggesting that the G-quadruplex inhibits transcription.[72] Consistent with this model, proteins that either induce (nucleolin) or resolve (NM23-H2) G-quadruplex were found to repress and activate c-Myc transcription, respectively.[59] [79, 80] Given these results, Prof. Hurley has proposed that a structure-selective stabilization of G-quadruplexes by small molecules can also regulate gene expression. Since then, several G-quadruplex ligands such as TmPyP4,[10] quindoline,[81] and actinomycin[82] have been shown to inhibit c-Myc transcription.

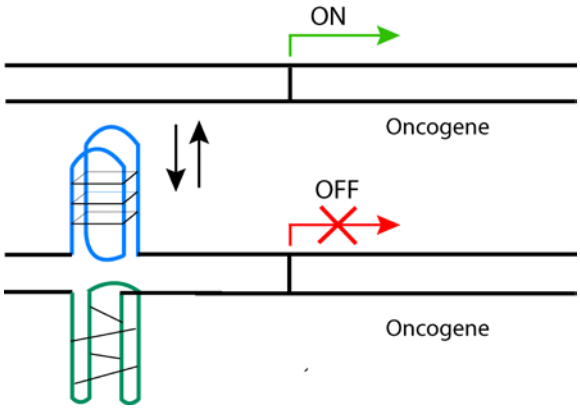

Figure 1.7. Possible role of G-quadruplex in gene regulation.

Genome-wide microarray analyses of *S.cerevisiae* that had been treated with the G-quadruplex-selective ligand N-methylmesoporphyrin (NMM) demonstrated increased transcription of genes having a PQS in the promoter, and decreased transcription of rDNA-associated genes.[83] In contrast, deletion of Sgs1p helicase (unwinds G-quadruplexes *in vitro*) caused downregulation of genes containing a PQS in their promoter, implying that G-quadruplexes inhibit transcription.[83] Furthermore, a genome wide analysis of TmPyP4-treated cancer cells demonstrate that 60% of the affected genes contained at least one PQS in the promoter. However, a toxic dose of 100 μM of TmPyP4 was used in these experiments.[84]

In 2000, Hanahan and Weinberg proposed six crucial events in the malignancy process, namely self-sufficiency in growth signals, decreased sensitive to normal growth signals, evasion of apoptosis, angiogenesis, unlimited replication and metastasis.[85] Given the vast abundance of PQSs in the human genome, there is at least one gene involved in each of these processes that possess G-quadruplex forming sequence in the promoter region. These genes include Myc and Kras for self sufficiency, RB1 for insensitivity, BCL2 for apoptosis evasion, VEGF for angiogenesis, TERT for unlimited replication and PDGF for metastasis.[79] This highlights the potentially broad importance of G-quadruplex in cancer (Figure 1.8). Targeting of promoter G-quadruplexes with small molecules is therefore a potentially attractive anti-cancer strategy that can impact many different malignancy processes at once.

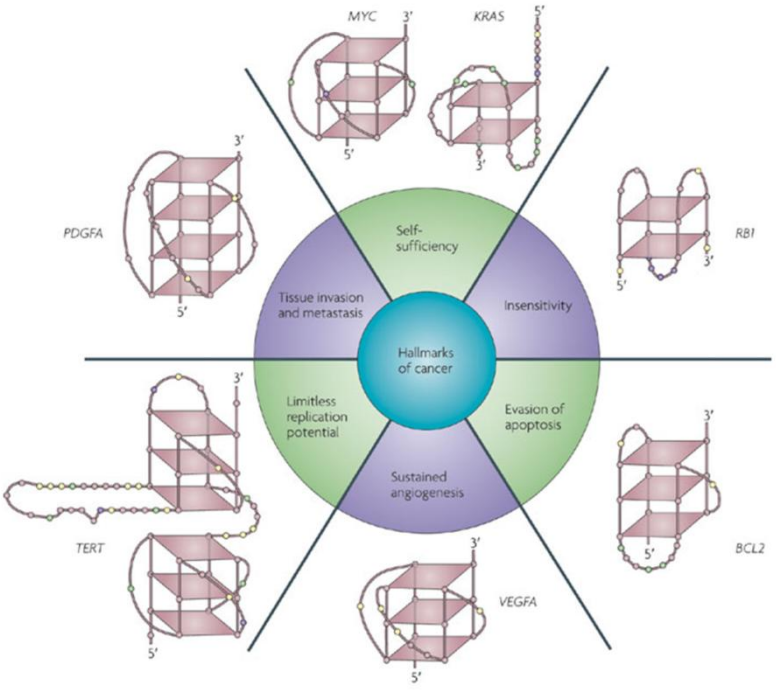

Figure 1.8. G-quadruplexes proposed to be involved in different stages of malignancy.[79]

1.3. Targeting G-quadruplexes with small molecules

Despite the growing indirect evidence supporting the presence of G-quadruplexes in mammalian cells, direct evidence is still lacking. The development of structure-selective fluorescent probes is an attractive strategy for identifying G-quadruplexes inside the cells. Targeting G-quadruplex *in vivo* with small molecules is a challenging task due to the dynamic nature of these structures and their limited abundance as compared to duplex DNA.

Ever since Zahler and coworkers demonstrated G-quadruplex mediated telomerase inhibition,[86] G-quadruplex ligands have been gaining notoriety as potential anti-cancer agents.[87-93] Many different scaffolds have been tested for their ability to bind G-quadruplex DNA.[92, 94] G-quadruplexes can bind to small molecules via end-stacking interactions on G-tetrad and/or binding to the groove regions (Figure 1.9). Binding selectivity between various G-quadruplex structures can be accomplished by developing molecules that interact selectively with the loop regions. Though several reviews have classified the G-quadruplex probes from different perspectives,[88, 91] here we will present a review of fluorescent small molecules as potential G-quadruplex probes.

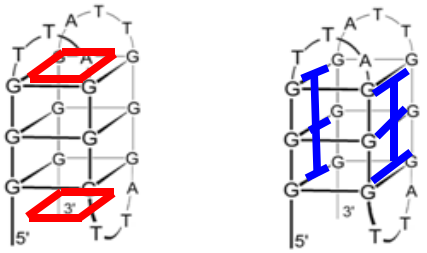

Figure 1.9. Possible binding sites of small molecules on G-quadruplexes. Red and blue represent end stacking and groove binding, respectively.

1.3.1. Fluorescent Probes

Fluorescent probes provide powerful and direct means for studying the folding and localization of biological macromolecules in living cells and whole animals. Fluorescent probes capable of structure-specific reporting of G-quadruplex structures *in vivo* will provide tools for basic biological research and the exploration of G-quadruplex DNA as a potential drug target.

Intercalating agents: Classic intercalating agents such as 9-aminoacridine and ethidium bromide bind to DNA via intercalation into layers of nucleobases.[95] This type of binding mode is not normally observed in G-quadruplex-ligand complexes.[91, 96, 97] A true intercalation mode for G-quadruplex-small molecule binding has only been reported for synthetic "G4-DNA wires" under non-physiological conditions that lack sodium and potassium ions.[98-100] The large, solvent-exposed surface areas of G-tetrads provide good receptors for aromatic cations to stack onto (Figure 1).[91, 96, 97] While classic intercalating agents can bind to G-quadruplexes via this "end-stacking" mode, they typically exhibit low G-quadruplex affinity and selectivity,[101, 102] and their fluorescence is readily quenched by guanine residues.[103, 104]

Anthraquinones (AQ) : Anthraquinones (**1**) were among the first molecules reported to interact with parallel G-quadruplexes via end-stacking interactions.[105] Several derivatives of 1,5-diamidoanthraquinones and 2,6-diamidoanthroquinones were also analysed for cytotoxicity and telomerase inhibition. 2,6-derivatives such as **2** have shown remarkable cytotoxicity and IC_{50} values for telomerase inhibition.[106] Since benzimidazole and anthraquinone derivatives were reported to be telomerase inhibitors, Huang and coworkers fused the imidazole ring and anthraquinone rings to obtain improved IC_{50} values for

telomerase inhibition. These studies suggested that by extending a planar aromatic surface improved telomerase inhibition could be achieved.[107] The anthraquinone moieties were further derivatized at different positions (2,6-, 2,7-, 1,8- and 1,5-) with protonatable amino acids (Lys, Arg) and hydrophobic spacers to increase selectivity of the scaffold for G-quadruplex over duplex.[108] The binding affinity for one of the anthraquinone derivatives 4,11-bis[(2-[acetamido]amino)ethyl)amino]anthrax[2,3-b]thiopene-5,10-dioone (**3**) (Figure 1.10) to anti-parallel telomeric DNA was measured in the micromolar range with an 100-fold selectivity for G-quadruplex over duplex DNA. Interestingly, these molecules were reported to cause destabilization of G-quadruplex structures.[109] Subsequent studies demonstrated that inhibition of telomerase was due to direct binding interactions with telomerase rather than G-quaduplex DNA. Though these molecules are fluorescent, no fluorescent based studies were performed with G-quadruplex DNA.

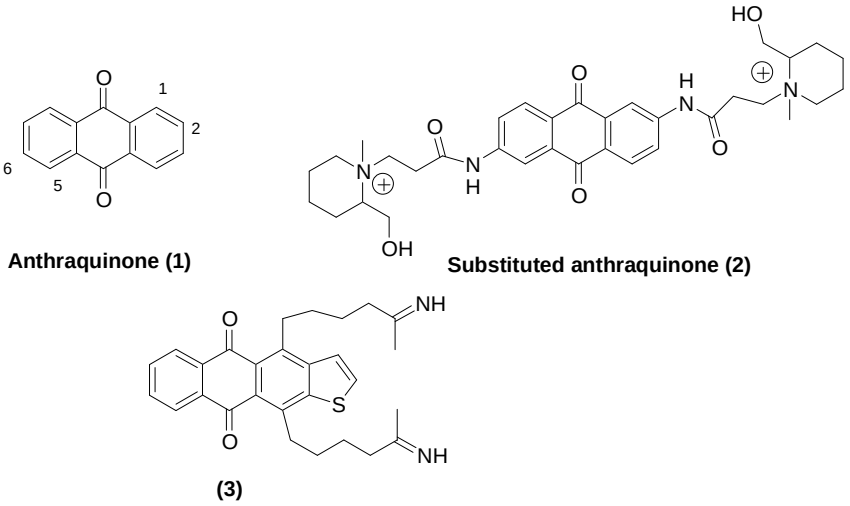

Figure 1.10. G-quadruplex ligands: Anthraquinone derivatives.

Quindoline: Anthraquinone derivatives (Figure 1.11) were reported to be better telomerase inhibitors than quindolines due to the presence of protonated side chains.[110] The solution structure of G-quadruplex-quindoline complex indicated that the binding is driven by end-stacking and electrostatic interactions.[111] The inclusion of an electron donating group at the 11 position of quindoline enhanced the electron density of N-5 nitrogen, resulting in protonation at physiological pH. Accordingly, substituted quindoline derivatives (**6**) were shown to bind induce G-quadruplex structures and inhibit telomerase in low micromolar range.[112-114] Quindoline derivative 2J (**5**) (Figure 1.11) was also reported decrease down regulation of transcription of c-Myc[81] and bcl-2 genes[115] by stabilizing G-quadruplex structures. However, further studies by Boddupally and coworkers suggested that quindoline-

mediated c-myc regulation was not due to the stabilization of G-quaduplexes, but via some other and unknown mechanism.[116] No fluorescence-based studies were reported for these quindoline derivatives.

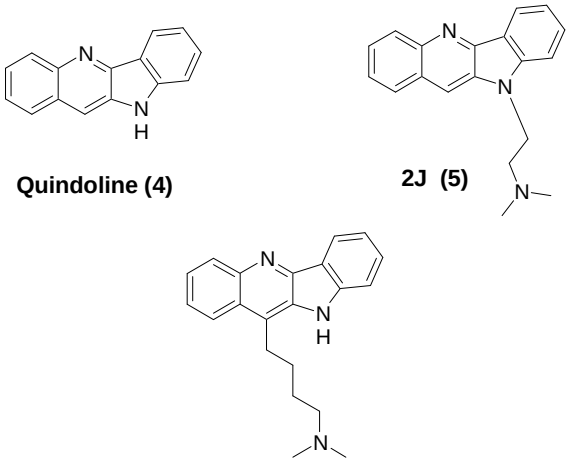

Figure 1.11. G-quadruplex ligands: quindoline derivatives.

Quinacridine: Crescent shaped quinacridine molecules (Boq1 (**8**)) were reported to bind to anti-parallel G-quadruplexes with 10-fold selectively duplex DNA. Boq1 end-stacks on G-tetrads and its cyclic framework disfavors intercalation into the double-stranded DNA.[117] A platinum-quinacridine hybrid, Pt-MPQ (**9**) was reported to interact with quadruplex DNA via a dual binding mode, targeting preferentially guanines of G-tetrads, thereby giving the possibility of irreversibly trapping G-quadruplex conformations.[118, 119] (Figure 1.12) The fluorescence properties associated with G-quadruplex binding were not reported for quinacridine based derivatives.

Perylene: The polycyclic molecule PIPER (**10**) (Figure 1.13) containing a perylene scaffold was reported to be an effective telomerase inhibitor in the low μM range. In addition, PIPER was also reported to induce G-quadruplex folding from duplex DNA of the c-Myc promoter.[120] NMR structures reveal that depending on the type of sequence, PIPER binds to G-quadruplex structures with variable stoichiometries.[121]

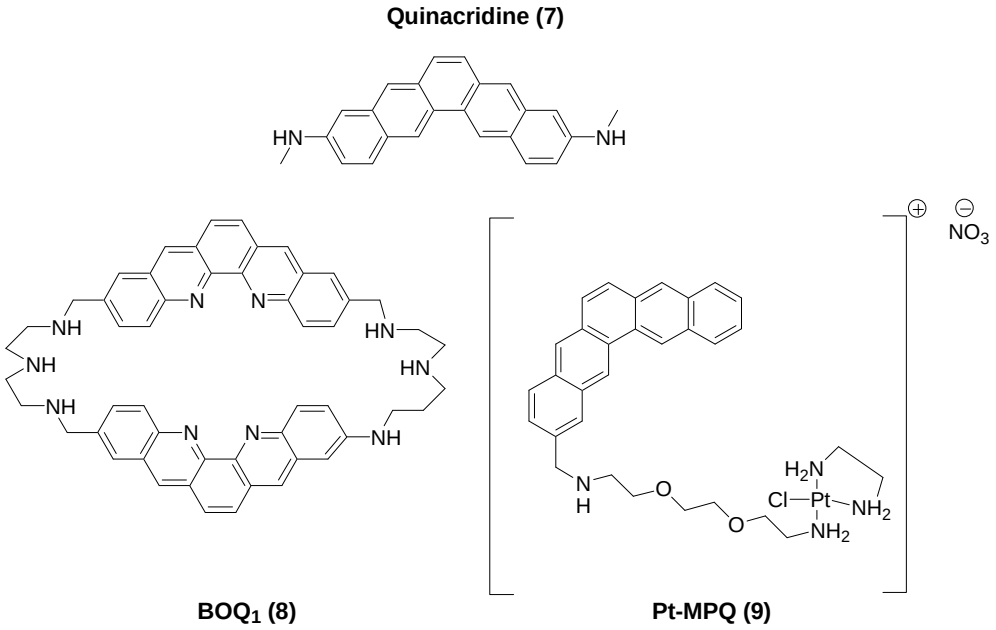

Figure 1.12. G-quadruplex ligands: quinacridine derivatives.

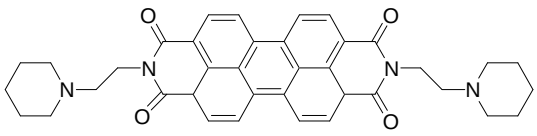

Figure 1.13. Structure of PIPER.

Berberines: Berberines (**11**) are natural alkaloids derived from Chinese herbs. Berberine moieties were reported to intercalate preferentially in intermolecular G-quadruplexes as compared to intermolecular G-quadruplexes.[122] UV-visible absorbance titrations revealed that G-quadruplex binding of berberine causes red shift (10-12 nm) and hypochromatic (34-40%) changes in absorbance.[123] 9-N-substituted berberine (**12**) was shown to bind c-Myc G-quadruplex DNA and down-regulate c-Myc expression[124] whereas a derivative of 9-O substituted berberine (**13**) showed improved binding affinity for telomeric DNA, and telomerase inhibition (Figure 1.14).[125]

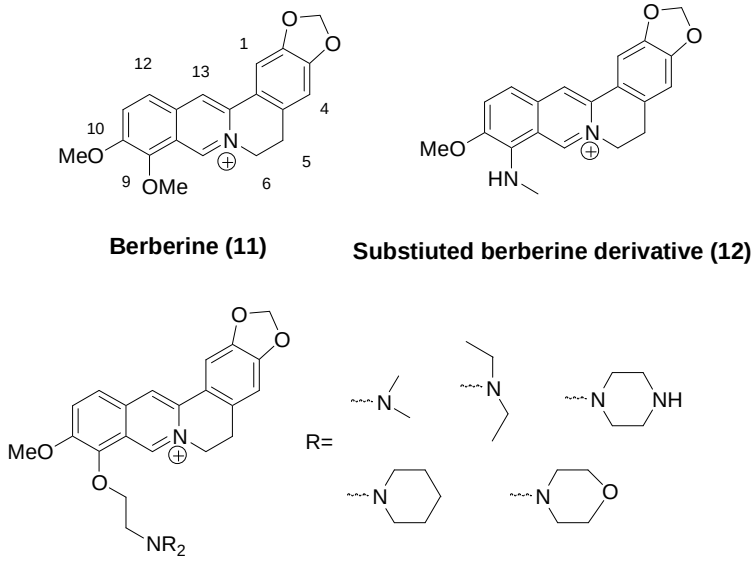

Figure 1.14. G-quadruplex ligands: berberine derivatives.

Acridine derivatives: Acridine derivatives such as proflavine, acridine orange and 9-aminoacridine (**14**) bind to duplex DNA with modest affinity ($K_d \approx 1 – 100$ μM),[126, 127] and exhibit very little structure selectivity.[128] Interestingly, acriflavine and proflavine have recently been reported to act as templates for the formation of G-quadruplex structures from cyclic diguanylate, but the resulting complexes exhibit quenched fluorescence.[129]

Neidle and coworkers synthesized and evaluated a series of 3,6,9-trisubstituted acridines (**15**) for telomerase inhibition.[130] One particular derivative, BRACO-19, binds to G-quadruplex with K_d of 32 nM and to duplex DNA with K_d of 1 μM.[131] A co-crystal structure with a bimolecular human telomeric G-quadruplex revealed that BRACO-19 asymmetrically stacks on G-tetrads, resulting in π-π overlap with two guanine bases (Figure 1).[132] Unfortunately, no fluorescence properties have been reported for BRACO-19.

Eritja and coworkers prepared oligomers of acridine (**16**) via solid phase synthesis and reported modest G-quadruplex affinities ranging from 0.16 – 22 μM that depend on the type of G-quadruplex used.[133] Contrary to the fluorescence quenching typically reported for acridines,[103, 104, 129] small increases in fluorescence intensity for the acridine oligomers (**16**) were observed at 440 nm upon addition of G-quadruplex DNA.[133] The reported increases were probably a result of decreased acridine-acridine self quenching when the samples were

excited at 360 nm,[126] or from DNA-acridine energy transfer when the samples were excited 252 nm.

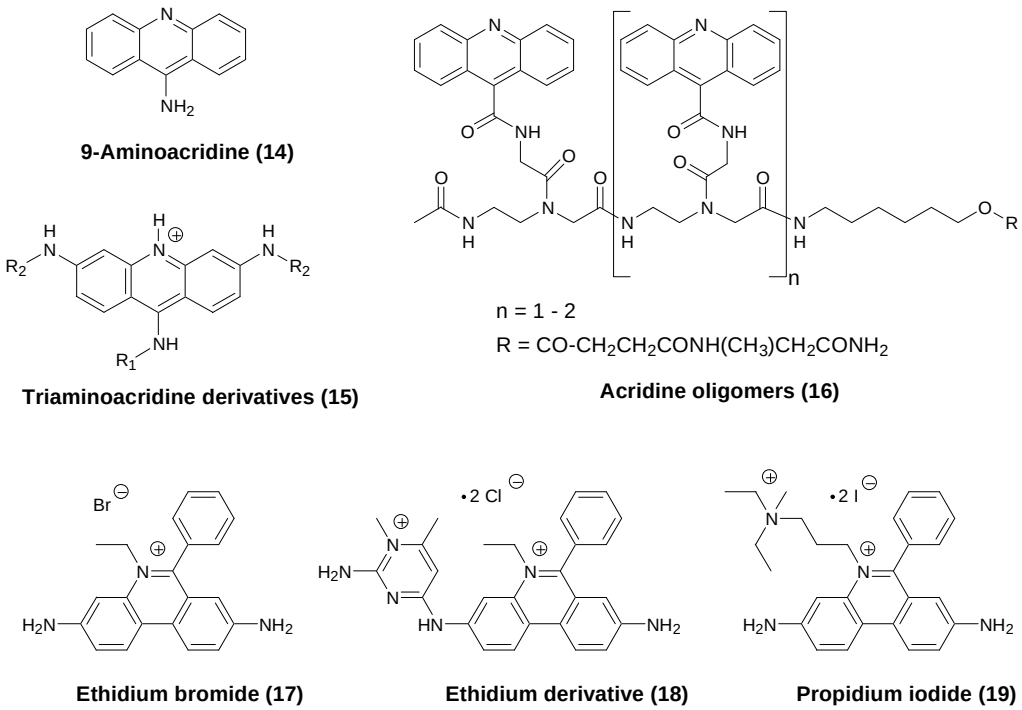

Figure 1.15. Intercalating agents : acridine and ethidium bromide

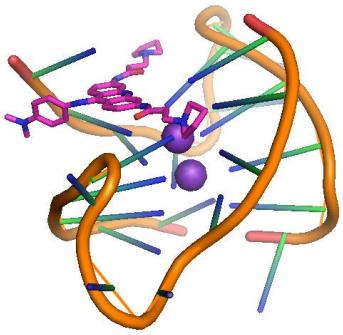

Figure 1.16. Crystal structure of BRACO-19 (**15**) bound to a human telomeric G-quadruplex (PDB accession code 3CE5).[132]

Ethidium derivatives: Depending on the exact sequence used, ethidium bromide (**17**) binds to duplex DNA with a broad range of different affinities (K_d = 0.3 – 130 μM).[134, 135] Fluorescence and calorimetric studies indicate that ethidium bromide exhibits similar binding affinities for G-quadruplex and duplex DNA,[102] while equilibrium dialysis experiments

suggested a large preference for duplex DNA.[115] The differences between the methods are likely a result of differences in stoichiometry that are typically not accounted for in affinity assessments. Interestingly, upon binding Poly d(G) - Poly d(C) ethidium's fluorescence is almost entirely quenched,[84] while binding d(GC) - Poly d(GC) and AT-rich duplexes results in a 30-fold enhancement in fluorescence.[136] For short oligonucleotides having similar compositions, the fluorescence enhancements observed for ethidium are highly dependent on DNA conformation, where: G-quadruplex < triplex < duplex.[137] Taken together, these properties make ethidium bromide a very poor probe for G-quadruplex DNA.

To improve upon the G-quadruplex affinity and specificity of ethidium, Mergny and co-workers prepared four known derivatives and discovered that ethidium derivative (**18**) bound to anti-parallel intramolecular G-quadruplexes with K_d values ranging from 90 – 120 nM.[138] This represents an approximate 10-fold selectivity as compared to duplex DNA (K_d = 1.1 μM).[138] Interestingly, the quantum yield of the ethidium derivative (**18**) increased from 0.04 to 0.2 upon G-quadruplex binding, and DNA-to-probe energy transfer reactions were also observed – consistent with the presence of stacking interactions between compound **18** and guanine residues. Experiments conducted in D_2O suggested that the fluorescence enhancements were a result of dye desolvation upon DNA binding.[138] Unfortunately, no staining of whole cells has been reported for ethidium derivative (**18**), possibly due to poor cellular uptake. Indeed, other dicationic ethidium derivatives, like propidium iodide (**19**), are known to be impermeable to cellular membranes and therefore used to selectively stain DNA of dead cells.

1.3.1.1. Cationic macrocycles

The large, nearly planar surface areas of G-tetrads provide good receptors for macrocyclic fluorophores having similar molecular dimensions.[45, 91, 96, 97, 139, 140] Compounds that stack onto the terminal G-tetrads of G-quadruplex structures typically exhibit 1:1 or 2:1 ligand:G-quadruplex binding stochiometries with K_d values ranging in the low nM to low μM range. These compounds can be grouped into basic categories according to their charges: cationic, anionic, and neutral macrocycles.

TmPyP4: The cationic porphyrin tetra-(N-methyl-4-pyridyl)porphine or "TMPyP4" (**20**) is probably the most widely-studied G-quadruplex ligand to date.[141-148] Early studies demonstrated that telomerase inhibition by TMPyP4 is relatively insensitive to the identity of

the metal ion coordinated within TMPyP4, but is highly dependent on the substituents at the meso positions.[142] Extensive substitution of the meso positions with groups other than pyridinium failed to generate compounds with improved inhibitory activities, but the resulting structure-activity relationships suggested that base stacking and charge-charge interactions are important for porphyrin-DNA binding.[142] Some caution must be exercised when interpreting such inhibitory data, however, since the reported trends in telomerase inhibition do not necessarily correlate with the G-quadruplex binding affinities of small molecules.[149]

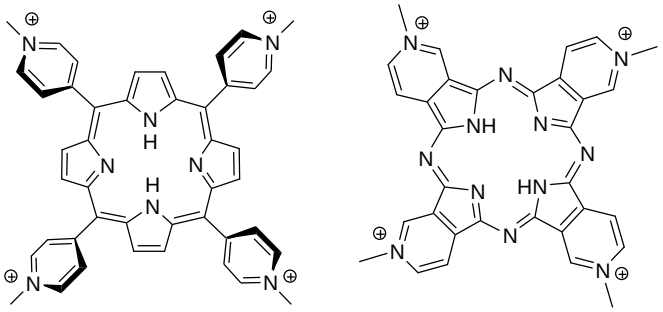

TMPyP4 (20)

3,4-TMPyPz (21)
(mixture of regioisomers)

Figure 1.17. Cationic macrocycles: TMPyP4, 3,4-TMPyPz.

X-ray crystallography and NMR studies demonstrated that TMPyP4 (**20**) can bind to G-quadruplex DNA at many different sites, including the terminal G-tetrads,[143] as well as the loops, grooves, and phosphodiester backbone (Figure 2).[144] TMPyP4 binds to duplex, triplex, G-quadruplex, single-stranded, and bulk genomic DNA with similar affinities ($K_d \approx$ 200 nM),[128, 145] and is therefore not a structure-specific ligand. Upon addition to whole cells, the uniform nuclear localization of TMPyP4 suggests preferential staining of duplex DNA.[146, 150]

TmPyP4 is a modestly fluorescent compound in water ($\Phi = 0.04$),[151] but is quenched upon G-quadruplex binding by photon-induced electron transfer from guanine residues.[147, 152] TMPyP4 can, however, exhibit a 2-fold higher quantum yield ($\Phi = 0.08$) when it is bound to AT-rich duplex DNA.[148, 152] This photophysical selectivity for duplex DNA can be partially overcome by monitoring energy transfer reactions from G-quadruplexes to TMPyP4 resulting from photoexcitation of the DNA at 260 nm.[98] At the present time, however, this type of approach is not compatible with cellular imaging experiments, due to the practical limitations of photoexcitation and autofluoresence in the UV range.

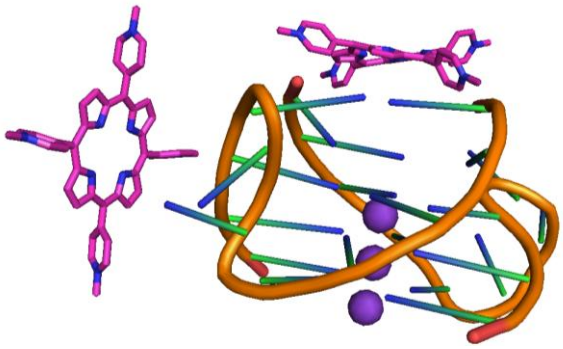

Figure 1.18. Crystal structure of TmPyP4 (**20**) bound to a human telomeric G-quadruplex (PDB accession code 2HRI).[144]

Tetramethylpyridiniumporphyrazines: According to computational modeling, phthalocyanines have especially good shape complementarity with stacked G-tetrads that constitute G-quadruplex DNA.[153, 154] Tetrapyridino porphyrazines are aza analogues of phthalocyanines where the four benzene units in the macrocycle are replaced by pyridine moieties. Balasubramanian and coworkers reported that tetramethylpyridiniumporphyrazine "3,4-TMPyPz" (**21**) binds to G-quadruplex DNA with K_d values ranging from 170 – 200 nM, while exhibiting 30-fold lower affinity to duplex DNA.[139] While 3,4-TMPyPz (**21**) is a weakly fluorescent compound, its fluorescence is quenched by both G-quadruplex and duplex DNA, and is therefore not suitable as a G-quadruplex fluorescent probe.[155]

1.3.1.2. Anionic macrocyclic G-quadruplex ligands

NMM: N-methyl mesoporphyrin (NMM) (**22**) is commercially available as a mixture of four N-methyl-pyrrole regioisomers. N-Alkylation causes a large distortion of the porphyrin macrocycle from planarity,[156] thereby decreasing self-association and increasing water solubility. NMM is a transition-state analog for iron insertion and potent inhibitor of ferrochelatase.[157] During the development of NMM-specific DNA aptamers as deoxyribozymes,[158] Sen and co-workers isolated NMM aptamers capable of adopting G-quadruplex structures that bind to NMM with good affinity (K_d = 0.5 – 1.0 μM).[159] These results provided the first reported examples of structure-selective G-quadruplex-ligand binding interactions.[159] Subsequent studies using equilibrium dialysis demonstrated that NMM is highly specific for G-quadruplexes as compared to other common DNA structures,[101] but NMM generally exhibits low-to-modest G-quadruplex affinity ($K_d \approx 10$ μM) and is selective for the parallel form of the human telomeric G-quadruplex.[160] NMM

also exhibits relatively weak fluorescence emissions that are enhanced 2 to 10-fold upon G-quadruplex binding.[148, 161] No reports about use of NMM as a fluorescent probe in cells are currently available, but strong protein-NMM binding interactions may dominate its cellular localization and bioavailability.[157, 161] Despite these potential limitations, the addition of NMM to single-celled organisms can impact functions associated G-quadruplex-forming DNA sequences such as telomere capping in cdc13-deficient *Saccharomyces cerevisiae,*[53] and recombination in *Neisseria gonorrhoeae*.[69]

Protoporphyrin IX (PPIX): Due to its potent inhibition of ferrochelatase,[157] the addition of NMM (**22**) to living cells causes the accumulation of protoporphyrin IX (PPIX, **23**).[162] PPIX is a ubiquitous heme precursor that is reported to be a G-quadruplex-selective fluorescent probe *in vitro*.[163] In DMSO, PPIX exists as a monomer with a good quantum yield for fluorescence (Φ = 0.16), while in water, self quenching is observed due to the formation PPIX micelles.[164] Fluorescence enhancements can therefore be observed upon addition of biomolecules that bind to and solubilize PPIX.[165] The addition of G-quadruplex DNA to PPIX results in a 16-fold increase in fluorescence. [163] According to these changes, PPIX was reported to selectively bind parallel G-quadruplex DNA with good affinity ($K_d \approx 30 - 120$ nM), while exhibiting much lower affinities for duplex and anti-parallel G-quadruplex DNA ($K_d > 50$ μM). [163] According to FRET-based melting assays, however, little or no thermal stabilization of the parallel human telomeric G-quadruplex was observed by PPIX when applied at 1 μM.[160] While the basis of these conflicting reports is not entirely clear, early studies using DNAzyme aptamers also support only modest binding interactions between PPIX and G-quadruplexes (K_M = 12.3 μM) in the presence of detergents (Triton X-100) and DMSO as co-solvents.[158]

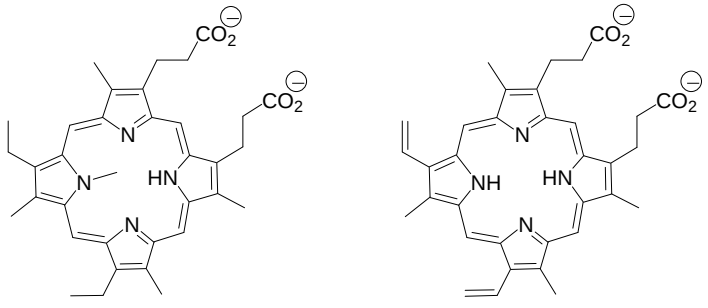

NMM (22)
(mixture of regioisomers)

PPIX (23)

Figure 1.19. Anionic macrocycles: NMM and PPIX.

The complex interplay between NMM, PPIX, and endogenous heme biosynthetic pathways may limit the usefulness of these compounds as fluorescent probes *in vivo*, but the potential ability of PPIX to bind G-quadruplexes involved in the regulation of tetrapyrrole biosynthesis presents an intriguing possibility for the hypothetical existence of a "deoxyriboswitch" in early evolution. Given the potential abilities of NMM and PPIX to bind to genomic G-quadruplexes that impact transcriptional control,[11] one can imagine a negative feedback loop where PPIX accumulation causes transcriptional deactivation of the same genes responsible for its biosynthesis. While similar regulatory mechanisms might be present in the insulin-linked polymorphic region (ILPR),[166] it is not clear how differential gene expression in diverse tissue types could be efficiently regulated by simple DNA – metabolite binding interactions in higher animals. A similar argument could explain why direct metabolite-RNA regulatory interactions or "riboswitches" are a common feature in bacteria, fungi and plants, [167] yet are very rare or possibly absent in mammals. [168]

1.3.3.3. Neutral macrocyclic G-quadruplex ligands

Telomestatin and L1BOD-7OTD: Telomestatin (SOT-095) (**24**) is natural product isolated from *Streptomyces anulatus* that binds to various G-quadruplexes with high affinity ($K_d \approx 30$ nM).[169, 170] Telomestatin also exhibits good selectivity for intra- versus inter-molecular G-quadruplex structures,[171] and it exhibits a 70-fold lower affinity for duplex DNA.[171] Synthetic analogs of telomestatin containing six or seven oxazole units have also been shown to exhibit good G-quadruplex affinity and selectivity,[172-174] but, like for the natural product, they also lack inherent fluorescence properties.[175] Nagasawa and coworkers therefore synthesized a macrocyclic heptazole (L1BOD-7OTD) containing a BODIPY fluorophore (**25**).[175] This conjugate exhibits excellent G-quadruplex affinity ($K_d \approx 0.2 – 80$ nM) and specificity *in vitro*, as well as sensitive G-quadruplex detection in native gels.[175] In an attempt to stain G-quadruplexes in cells, 0.5 μM of L1BOD-7OTD was incubated with HeLa cells for 18 hours, followed by fixation and permeabilization of the cells. Fluorescence was observed mostly in the nuclei and nucleoli of cells.[175] While this staining may reveal the presence of rDNA G-quadruplexes,[58] caution must again be exercised when interpreting these data, because common fixation and permeabilization methods can cause DNA conformational changes and redistribution of DNA ligands within cells.[53, 176] To date, no live-cell imaging has been reported for this promising probe.

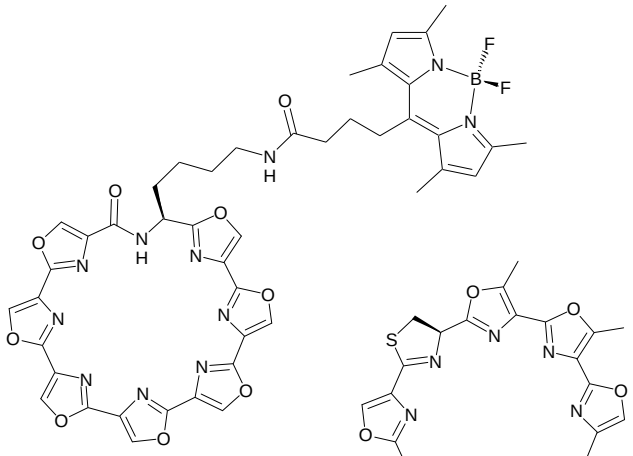

Figure 1.20. Neutral macrocycles: L1BOD-7OTD and Telomestatin.

Luminescent metal complexes: Transition metal complexes encompass a large family of G-quadruplex ligands,[177] with the attractive potential for time-resolved phosphorescent imaging.[178] In some cases, metal ions restrict a multidentate metal ligand into a co-planar conformation capable of end-stacking onto G-tetrads. For example, Vilar and co-workers reported a Nickel salphen complex (**26**) with 50-fold selectivity for G-quadruplexes as compared to duplex DNA, but no luminescence properties were reported for this complex.[179] Inspired by these results, Che and co-workers prepared a series of platinum-coordinated salphens and observed that one derivative, "Pt L3" (**27**) binds to c-Myc G-quadruplex with a K_d of 10 μM and exhibits a 10-fold lower affinity for duplex DNA.[166,180] This complex exhibits a low quantum yield for photoluminescence (Φ = 0.01) that increases approximately 8-fold upon DNA binding. Although the exact mechanism for this increase remains unknown,[180] relatively long lifetimes (= 1.40– 4.60 μs) indicate the presence of emissive triplet excited state(s).Che and coworkers synthesized a series of platinum (II) complexes containing a 2,6-bis-(benzimidazol-2-yl)pyridine (bzimpy) ligand.[181] These compounds exhibit a 10-fold or larger selectivity for binding G-quadruplex as compared to duplex DNA. One particular derivative "Pt-bzimpy" (**28**) exhibited a 38-fold increase in luminescence upon G-quadruplex binding, but only a 4-fold increase upon saturation with calf thymus DNA. Pt-bzimpy exhibited very mild cytotoxicity, but no cellular staining experiments were reported for this complex.

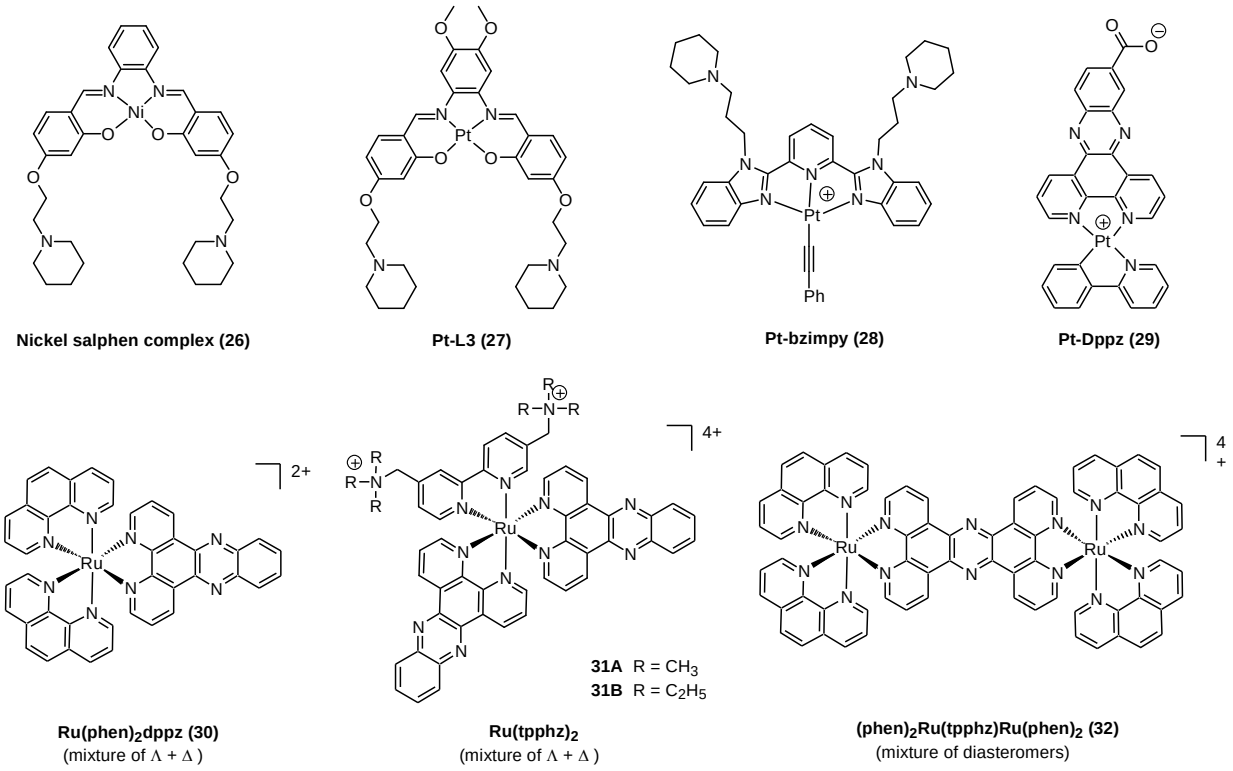

Figure 1.21. Luminescent metal complexes

Ma and coworkers synthesized a series of Pt complexes and found that a platinum-dipyridophenazine complex "Pt-Dppz" (**29**) exhibited a 293-fold increase in photoluminescence upon G-quadruplex binding.[182] The authors suggested that decreased water-mediated quenching of an emissive Pt→π* metal-to-ligand charge transfer was responsible for the fluorescence enhancement. Pt-Dppz exhibited good G-quadruplex affinity (K_d = 0.1 μM), and good G-quadruplex selectivity according to equilibrium dialysis and gel staining experiments. The limited water solubility of Pt-Dppz, however, required the addition of 5% DMF as a co-solvent in these experiments. Pt-Dppz was reported to exhibit modest cytotoxicity, but no cellular staining experiments were reported for this complex.

Octahedral ruthenium complexes containing intercalating moieties constitute a large family of DNA binders with interesting photophysical and electrochemical properties.[183] Shi and coworkers recently reported that Ru(phen)$_2$dppz (**30**) exhibits a 5-fold higher luminescence when bound to G-quadruplex versus i-motif DNA.[184] The same authors reported that the same complex containing bipyridine instead of phenanthroline ligands, Ru(bpy)$_2$dppz could differentially bind variable G-quadruplex topologies.[185] Mao and Ji synthesized two new tetracationic metal complexes **31A** and **31B** each containing two tppz ligands coordinated to

ruthenium. **31A** and 3**1B** bind to G-quadruplex DNA with a K_d of ~0.01 μM. Upon binding to G-quadruplex DNA, luminescence increased approximately 5- and 8-fold for **31A** and **31B**, respectively.[186] However, no cell based studies were reported for any of these ruthenium complexes.

The poor membrane permeability of metal complexes can greatly limit their cellular uptake.[178] While cationic metal complexes derived from porphyrins and phthalocyanines can provide exceptions to this rule,[187] octahedral ruthenium complexes typically exhibit poor uptake.[183] In 2009, Thomas and coworkers reported a dinuclear ruthenium complex containing a bridging tetrapyridophenazine ligand "tpphz" (**32**) selectively stains the nuclei of MCF-7 cells upon addition to live cells at 500 μM.[188] Experiments using endocyctosis inhibitors suggested that entry of these complexes into cells occurred via a non-endocytotic route. *In vitro* studies demonstrated that **32** binds to quadruplexes with affinities ($K_d \approx 0.23$ μM) very similar to duplex DNA ($K_d \approx 0.32$ μM).[189] The photoluminescent properties of **32** are highly sensitive to folded state of the DNA. Upon G-quadruplex binding, a 150-fold increase in luminescence was observed, while the addition of duplex DNA resulted in only a 50-fold increase.[190] The enhancements in luminescence were ascribed to the shielding of nitrogen atom of phenazine rings of **32** from water molecules. Most importantly, cells stained with **32** exhibited multiple emission profiles thought to originate from different DNA structures. Intense, uniform nuclear staining at 680 nm was attributed to duplex DNA, while punctate staining within the nucleus emitting at 630 nm was suggested to represent alternative DNA structures like the G-quadruplexes.[188] The emission profiles collected from the nuclei of stained cells did not exactly match those of standard samples prepared and analyzed *in vitro*.[190] Given the abilities of dinuclear ruthenium complexes to mediate direct photocleavage of DNA,[191] it is possible that the intra-nuclear targets of these interesting dinuclear complexes (**20**) can be further investigated using photocleavage and DNA sequencing.[192]

Pyrene-based derivatives: Pyrene exhibits bright fluorescence in water ($\Phi = 0.69$, $\varepsilon = 35'000$ $cm^{-1}M^{-1}$) that is quenched by molecular oxygen.[193] In 1999, Ren and Chaires evaluated pyrene methylamine (**33**) for its nucleic acid selectivity using competition dialysis, having the expectation that the large planar surface of pyrene would selectively bind triplex and/or G-quadruplex polymers.[101] Surprisingly, a preference for poly(dAdT) duplex DNA was

discovered and subsequently confirmed using fluorescence titration experiments.[101] The reversal of self-quenching upon DNA binding is an important mode of fluorescence enhancement for many of the fluorescent probes highlighted here (ex. acridine orange, DIGP, PPIX, etc).[126, 153, 163, 194] In contrast, pyrene-pyrene self association gives rise to emissive excimers that emit photons at ~480 nm. Pyrene excimer formation can provide a means to differentiate between alternative DNA conformations. For example, Yoon and co-workers synthesized an imidazolium pyrene derivative "JY-1" (**34**) that generates excimer emissions in the presence of $d(G)_3$ but not duplex DNA. The apparent affinity for $d(G)_3$ was only modest ($K_d \approx 2$ μM) and no cell-based studies have been reported,[195] but NMR and CD experiments suggested that JY-1 is able to induce G-quadruplex folding from single strands by binding interactions in the groove regions of the DNA.[195] This preference for groove binding may explain pyrene's selectivity for poly(dAdT) duplex DNA.[128]

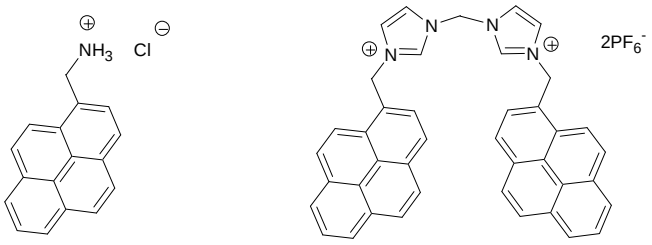

Pyrene methylamine (33) **JY-1 (34)**

Figure 1.22. Pyrene-containing derivatives.

Classic groove binders: The quantum yields of unfused aromatic polycyclic dyes like DAPI, Hoechst 33258, and cyanines depend strongly on the rotational motions between the unfused aryl groups. Upon photoexcitation, the free dyes typically exhibit rapid non-radiative relaxation via internal rotational diffusion. Upon DNA binding, the loss of these rotary motions causes a dramatic increase in quantum yield.[196] This same mechanism may account for the fluorescence enhancements reported for many other unfused aromatic compounds upon DNA binding.

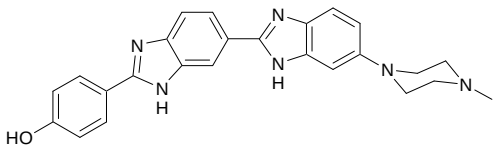

Hoechst 33258 (35)

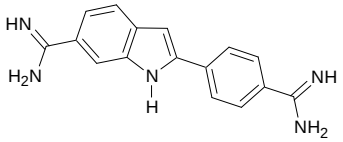

DAPI (36)

Figure 1.23. "Classic" minor groove binders: Hoeschst 33258 and DAPI.

Minor groove DNA binders are typically cationic, crescent shaped molecules. For example, Hoechst 33258 (**35**) is a commonly used cell-permeable probe that binds selectively to AT rich duplex DNA with K_d values ranging from 10 – 100 nM.[197] Although Hoechst 33258 exhibits useful fluorescence properties, it exhibits no G-quadruplex selectivity, with K_d values ranging from 0.1 – 1 μM.[198, 199] Other classic groove binders such as Distamycin, Netropsin, and DAPI (**36**) also exhibit selectivity for A/T-rich duplexes and lower affinities for G-quadruplex DNA.[101, 200, 201]

Cyanines: In 1996, Shafer and coworkers reported that the carbocyanine dye "DODC" (**37**) binds to a dimeric hairpin G-quadruplex *in vitro*.[202] The binding affinity ($K_d \approx 1$ μM) and selectivity were only modest (5-fold versus duplex DNA), but this interaction resulted in unique spectrophotometric signatures present in the dye-G-quadruplex complex which were absent for duplex and single-stranded DNA. Most notably, efficient DNA to DODC energy transfer reactions allowed for the detection of hairpin G-quadruplex structures in the presence of excess single strands and Watson-Crick duplexes. The resulting energy transfer emissions from DODC, however, were limited by its fluorescence quenching by the hairpin G-quadruplex.[202] To improve upon these properties, Tang and coworkers synthesized the cyanine derivative "ETC" (**38**) that exhibits a 70-fold fluorescence enhancement upon addition of parallel G-quadruplexes.[194] The mechanism for fluorescence enhancement was reported to be liberation of fluorescent monomers from non-fluorescent "J"-type aggregates. While no affinities or selectivity ratios were reported, no detectable fluorescence enhancements were observed upon addition of duplex DNA to ETC.

Kotlyar and coworkers screened a collection of known DNA-binding cyanine dyes to identify candidates that could exhibit structure-specific fluorescence properties.[99] The trimethine cyanine derivative "Cyan 2" (**39**) bound to G-quadruplex "wires" with high affinity that was accompanied by large increases in fluorescence intensity when the titrations were conducted in the absence of potassium ions.[99] In the presence of potassium ions, however, no increases in fluorescence intensity were observed. The authors suggested that Cyan 2 is able to intercalate into ion-G-wires in the absence of potassium ions. In the presence of potassium ions, however, Cyan 2 is thought to favor an external, groove binding mode.[99] Similar results have also been reported for TMPyP4 (**7**),[100] and thiazole orange (**40**).[100]

In the presence of sodium and potassium ions, the common fluorescent stain "thiazole orange" (**40**) exhibits similar affinity for G-quadruplex and duplex DNA (0.3 – 3.0 μM).[203, 204] DNA binding is accompanied by a very large (100 to 1000-fold) increase in quantum yield (Φ = 0.1 – 0.4) for **40**.[203] To improve G-quadruplex selectivity of thiazole orange while maintaining its useful fluorescence properties, Teulade-Fichou and co-workers synthesized a "hybrid" derivative "PDC-M-TO" (**41**). This compound contains a highly selective pyridocarboxamide G-quadruplex ligand fused to thiazole orange.[205] PDC-M-TO exhibits excellent selectivity and gives much larger fluorescence enhancements upon binding G-quadruplexes as compared to duplex DNA. PDC-M-TO can be used to selectively stain G-quadruplexes in gels, but no cell-based data have been reported for this promising probe. Following a similar strategy, Wong and coworkers fused a natural product benzofuroquinolinium moiety with thiazole orange to give a "Benzofuroquinolonium-benzathiazole hybrid" (**42**).[206] This compound also exhibited very impressive G-quadruplex selectivity and fluorescence enhancements as compared to duplex DNA. When applied to fixed cells, **42** gave intense staining of nucleoli. While the authors suggested that this staining may reveal the presence of rDNA G-quadruplexes,[206] common cross-linking and fixation methods can cause a dramatic redistribution of DNA ligands within cells.[176] Special caution must therefore be exercised when interpreting data collected using fixed cells.

Due its bright fluorescence when bound to G-quadruplexes, thiazole orange can be used as an energy acceptor from a second, non-covalent fluorescent probe in close proximity. As a fluorescent donor, Teulaude-Fischou and co-workers used the macrocyclic bis(quinacridine) derivative BOQ_1.[207] G-quadruplex structures were found to be capable of simultaneously hosting both molecules, allowing FRET to occur between them.[208] The addition of human

telomeric G-quadruplex to a mixture of dyes caused a 3-fold increase in thiazole orange fluorescence when BOQ1 was photoexcited. In contrast, no FRET was observed upon addition of duplex DNA. While this general strategy provides an attractive possibility for cellular imaging, no examples of such G-quadruplex FRET pairs have been reported in cell-based experiments.

A powerful two-step strategy to visualize G-quadruplex ligands bound to cellular DNA has recently been reported by Balasubramanian and co-workers.[209] According to this approach, the highly selective G-quadruplex ligand "Pyridostatin" was modified with a terminal alkyne group. The resulting non-fluorescent conjugate (**43**) was added to fixed cells and subsequently visualized by copper-catalyzed azide-alkyne "click" reactions with fluorescent azides. The nuclear distribution of **43** was found to be contained within nucleoli and many other foci located throughout the nucleus. Interestingly, co-staining experiments with TRF1 antibodies revealed that most of the **43**-containing foci were not associated with telomeric ends. Co-localization was instead observed with a GFP fusion protein of the DNA helicase "Pif1." This helicase is capable of binding to and resolving G-quadruplexes during DNA replication.[210, 211] Inhibition of such helicase activities by Pyridostatin was proposed to cause DNA damage and cell cycle arrest through DNA-damage checkpoint activation. Indeed, chromatin immunoprecipitation sequencing analysis of the DNA damage marker γ-H2AX revealed that pyridostatin was associated with clusters of DNA sequences having a high propensity for G-quadruplex formation. The DNA damage at these foci was proposed to result from both replication- and transcription-dependent processes.[209] Taken together, these results provide convincing evidence that endogenous "G4 resolvase activities" are important aspects of genome maintenance in human cells, and illustrate how site-selective probes for G-quadruplexes can be used to make fundamental biological discoveries.

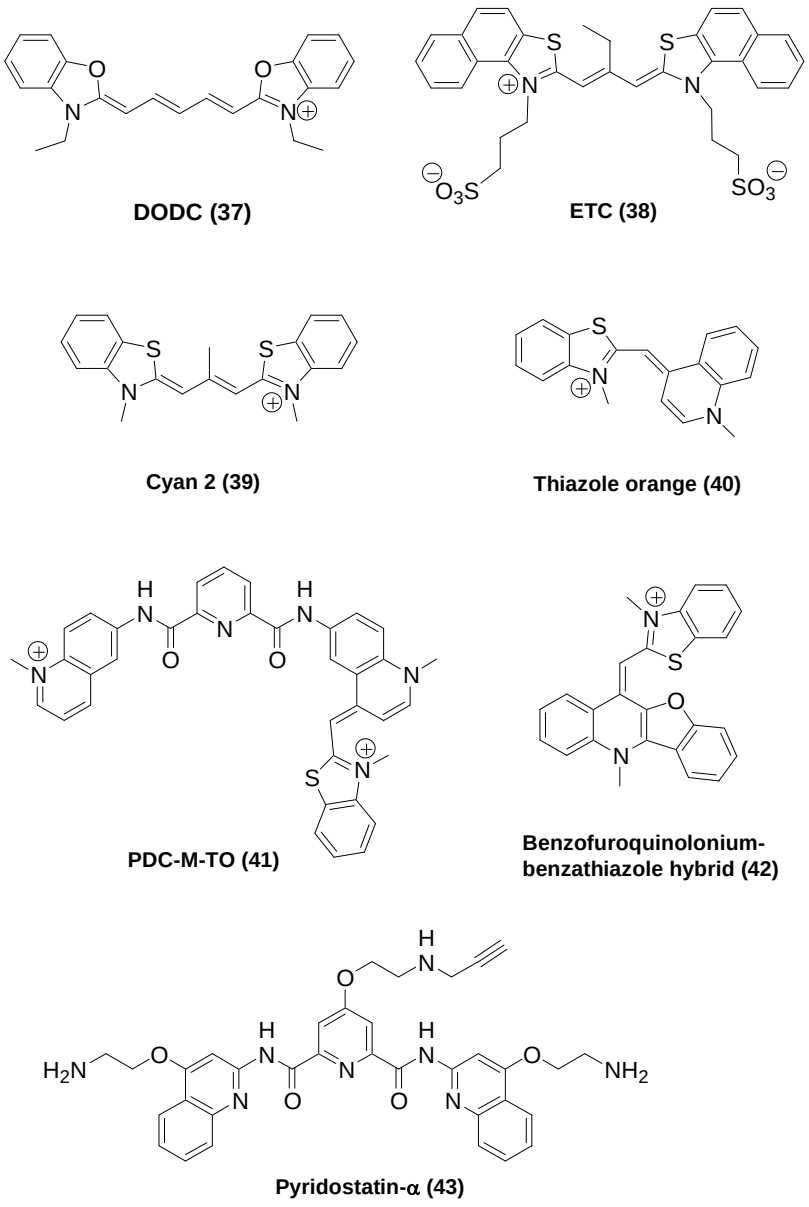

Figure 1.24. Cyanine-based derivatives and related compounds.

Triphenylmethane and tetraphenylethene dyes: Bhasikuttan and coworkers reported the well-known dye Malachite green (**44**) as a G-quadruplex fluorescent probe.[212] Upon photoexcitation, unbound Malachite green exhibits rapid non-radiative relaxation via internal rotational diffusion. Upon DNA binding, the loss of these rotary motions causes a dramatic increase in quantum yield. Although its binding affinities to G-quadruplex and duplex DNA are very similar ($K_d \approx 2 - 35$ μM), Malachite green exhibits up to a 100-fold increase in fluorescence upon addition of high concentrations (100 μM) of $d(G_2T)_{13}G$.[212] Given the potential for aggregation-induced fluorescence of these compounds,[213] it is unclear if this

100-fold increase was a result of DNA-dye aggregation or the formation of discrete complexes.

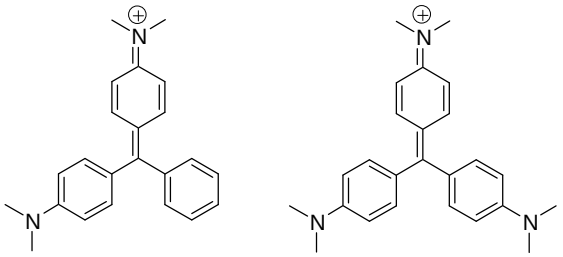

Malchite green (44) Crystal violet (45)

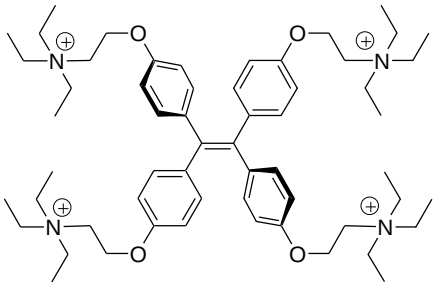

TTAPE (46)

Figure 1.25. Triphenylmethane and tetraphenylethene derivatives.

Kong and coworkers conducted a systematic comparison of Malachite green (**44**) and Crystal violet (**45**) for G-quadruplex selectivity and fluorescence enhancements.[214] The authors demonstrated that the fluorescence intensity of Crystal violet was consistently higher in the presence of diverse G-quadruplexes (6-fold increase) as compared to single-stranded and duplex DNA (3-fold increase).[214] Malachite green (**44**) was shown to give less consistent results than Crystal violet (**45**) in terms of its ability to differentiate G-quadruplex from duplex DNA structures. The reported binding affinity of Crystal violet for various G-quadruplexes, single-stranded and duplex DNA were all very similar ($K_d \approx 20 – 40$ μM), but the fluorescence intensities observed from anti-parallel G-quadruplexes were more intense than those from parallel G-quadruplex complexes.[214] However, the maximal changes in Crystal violet fluorescence intensity (60 to 100-fold) were much smaller than those used to detect Malachite green fluorescence changes in cells (1’000 to 18’000-fold) by a protein-based sensor.[215] These results suggest that **44** and **45** will probably not provide a practical means to detect G-quadruplex structures in cellular environments.

Reversal of self-quenching upon DNA binding is an important mode of fluorescence enhancement for many of the probes presented here. In contrast, 1,1,2,2-Tetrakis[4-(2-

bromoethoxy)-phenyl]ethene "TTAPE" (**46**) exhibits aggregation-induced emission enhancements upon DNA binding.[213] Unbound TTAPE in aqueous solutions is essentially non-luminescent due to intramolecular rotational diffusion, but the addition of organic solvents that cause a loss of TTAPE solubility or alternatively, cause increases in solvent viscosity result increased luminescence at 472 nm. TTAPE binds to G-rich single-stranded DNA to give 4-fold increases in emissions at 470 nm in a potassium-dependent manor. TTAPE binds to G-quadruplex DNA with a modest apparent affinity (K_d = 4 μM). The resulting aggregation present in these complexes was reversible, as the addition of the C-rich complementary DNA released non-emissive TTAPE due to the formation of duplex DNA. [213]

Carbazoles: Dicationic carbazole derivatives are known to bind selectively to the minor groove of AT-rich duplex DNA.[190,216] Chang and his colleagues reported that a novel carbazole derivative: 3,6-bis(1-methyl-4-vinyl pyridinium) carbazole diiodide "BMVC" (**47**) exhibits large (10 to 100-fold) increases in fluorescence intensity upon binding G-quadruplex and duplex DNA.[217] While its affinities to duplex and G-quadruplex DNAs are very similar, a shift in BMVC emission wavelength from 550 nm to 575 nm was observed in the case of the G-quadruplex binding.[217] Interestingly, the addition of BMVC to metaphase spreads resulted in uniform chromosomal staining, but with slightly higher emissions at ~580 nm near the telomeric ends.[218] To provide better signal-to-noise, two-photon excitation fluorescence lifetime imaging microscopy was conducted. This approach was aimed at utilizing the slightly longer fluorescence lifetime of BMVC when bound to G-quadruplexes (2.2 ns) as compared to duplexes (1.5 ns). The resulting time-resolved emissions from BMVC in metaphase spreads appeared, to some extent, localized at the ends of chromosomes.[219] While the differences were interpreted in terms of G-quadruplex structures, the staining patterns have not yet been independently validated using orthogonal means such as co-localization with telomere binding proteins.

In a related study, Teulade-Fichou and coworkers synthesized a small family of N-Phenyl carbazoles. One such derivative "Cbz-2Py" (**48**) exhibited bright fluorescence upon DNA binding ($\Phi \approx 0.58$, $\varepsilon \approx 22{,}000$ $cm^{-1}M^{-1}$) as well as a very good two-photon absorption cross-section ($\delta \approx 200$ GM), but similar binding affinities ($K_d \approx 1$ μM) were observed for G-

quadruplex and AT-rich duplex DNA.[220] Two-photon imaging of Cbz-2Py (**48**) in fixed cells suggested uniform staining of double stranded DNA.

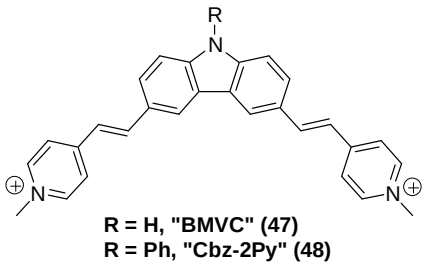

Figure 1.26. Carbazole derivatives: BMVC and CBZ-2Py.

1.4. Aims

The existence of G-quadruplex DNA structures and their potential role(s) in normal mammalian biology remain unclear. To address these fundamental questions, powerful probes for characterizing conformational dynamics of nucleic acids *in vivo* are needed. Fluorescent probes capable of structure-specific binding reporting of G-quadruplexes *in vivo* will provide much needed tools for basic biological research and the continued exploration of G-quadruplex DNA as a potential drug target. The objective of this thesis is to evaluate the guanidinium- and ammonium-containing phthalocyanines for probing G-quadruplex structures that may be present in the promoter regions of mammalian genes.

1.5. Reference

[1] F. H. Crick, *Symp Soc Exp Biol* **1958**, *12*, 138.
[2] F. Miescher, *Medicinisch-chemische Untersuchungen* **1871**, *4*, 441–460.
[3] J. D. Watson, F. H. Crick, *Nature* **1953**, *171*, 737.
[4] N. B. Ulyanov, W. R. Bauer, T. L. James, *J Biomol NMR* **2002**, *22*, 265.
[5] M. J. van Dongen, J. F. Doreleijers, G. A. van der Marel, J. H. van Boom, C. W. Hilbers, S. S. Wijmenga, *Nat Struct Biol* **1999**, *6*, 854.
[6] A. T. Phan, M. Gueron, J. L. Leroy, *J Mol Biol* **2000**, *299*, 123.
[7] Y. Wang, D. J. Patel, *Structure* **1993**, *1*, 263.
[8] I. Bang, *Biochem Z* **1910**, *26*, 293.
[9] M. Gellert, M. N. Lipsett, D. R. Davies, *Proc Natl Acad Sci U S A* **1962**, *48*, 2013.
[10] R. H. Shafer, I. Smirnov, *Biopolymers* **2000**, *56*, 209.
[11] A. Risitano, K. R. Fox, *Biochemistry* **2003**, *42*, 6507.
[12] A. T. Phan, Y. S. Modi, D. J. Patel, *J Am Chem Soc* **2004**, *126*, 8710.
[13] M. Marusic, P. Sket, L. Bauer, V. Viglasky, J. Plavec, *Nucleic Acids Res* **2012**, *40*, 6946.
[14] S. Arnott, R. Chandrasekaran, C. M. Marttila, *Biochem J* **1974**, *141*, 537.
[15] P. Hazel, J. Huppert, S. Balasubramanian, S. Neidle, *J Am Chem Soc* **2004**, *126*, 16405.

[16] A. Bugaut, S. Balasubramanian, *Biochemistry* **2008**, *47*, 689.
[17] A. Guedin, A. De Cian, J. Gros, L. Lacroix, J. L. Mergny, *Biochimie* **2008**, *90*, 686.
[18] P. A. Rachwal, T. Brown, K. R. Fox, *FEBS Lett* **2007**, *581*, 1657.
[19] J. L. Leroy, M. Gueron, J. L. Mergny, C. Helene, *Nucleic Acids Res* **1994**, *22*, 1600.
[20] T. Simonsson, M. Pribylova, M. Vorlickova, *Biochem Biophys Res Commun* **2000**, *278*, 158.
[21] Y. Xu, H. Sugiyama, *Nucleic Acids Res* **2006**, *34*, 949.
[22] K. Guo, A. Pourpak, K. Beetz-Rogers, V. Gokhale, D. Sun, L. H. Hurley, *J Am Chem Soc* **2007**, *129*, 10220.
[23] K. Guo, V. Gokhale, L. H. Hurley, D. Sun, *Nucleic Acids Res* **2008**, *36*, 4598.
[24] S. Kendrick, Y. Akiyama, S. M. Hecht, L. H. Hurley, *J Am Chem Soc* **2009**, *131*, 17667.
[25] P. Bucek, J. Jaumot, A. Avino, R. Eritja, R. Gargallo, *Chemistry* **2009**, *15*, 12663.
[26] A. T. Phan, J. L. Mergny, *Nucleic Acids Res* **2002**, *30*, 4618.
[27] M. Fry, *Front Biosci* **2007**, *12*, 4336.
[28] E. Baldrich, C. K. O'Sullivan, *Anal Biochem* **2005**, *341*, 194.
[29] P. Armas, S. Nasif, N. B. Calcaterra, *J Cell Biochem* **2008**, *103*, 1013.
[30] D. Sun, K. Guo, J. J. Rusche, L. H. Hurley, *Nucleic Acids Res* **2005**, *33*, 6070.
[31] D. Miyoshi, S. Matsumura, S. Nakano, N. Sugimoto, *J Am Chem Soc* **2004**, *126*, 165.
[32] A. K. Shukla, K. B. Roy, *J Biochem* **2006**, *139*, 35.
[33] F. Kouzine, D. Levens, *Front Biosci* **2007**, *12*, 4409.
[34] F. Kouzine, S. Sanford, Z. Elisha-Feil, D. Levens, *Nat Struct Mol Biol* **2008**, *15*, 146.
[35] N. Kumar, S. Maiti, *Nucleic Acids Res* **2008**, *36*, 5610.
[36] P. Rawal, V. B. Kummarasetti, J. Ravindran, N. Kumar, K. Halder, R. Sharma, M. Mukerji, S. K. Das, S. Chowdhury, *Genome Res* **2006**, *16*, 644.
[37] H. J. Lipps, D. Rhodes, *Trends Cell Biol* **2009**, *19*, 414.
[38] J. E. Johnson, J. S. Smith, M. L. Kozak, F. B. Johnson, *Biochimie* **2008**, *90*, 1250.
[39] J. L. Huppert, S. Balasubramanian, *Nucleic Acids Res* **2005**, *33*, 2908.
[40] A. J. Cesare, R. R. Reddel, *Nat Rev Genet* **2010**, *11*, 319.
[41] F. E. Pryde, E. J. Louis, *Biochemistry (Mosc)* **1997**, *62*, 1232.
[42] C. Krafft, J. M. Benevides, G. J. Thomas, Jr., *Nucleic Acids Res* **2002**, *30*, 3981.
[43] E. J. Richards, F. M. Ausubel, *Cell* **1988**, *53*, 127.
[44] G. N. Parkinson, M. P. Lee, S. Neidle, *Nature* **2002**, *417*, 876.
[45] S. Burge, G. N. Parkinson, P. Hazel, A. K. Todd, S. Neidle, *Nucleic Acids Res* **2006**, *34*, 5402.
[46] D. Sen, W. Gilbert, *Nature* **1988**, *334*, 364.
[47] C. Schaffitzel, I. Berger, J. Postberg, J. Hanes, H. J. Lipps, A. Pluckthun, *Proc Natl Acad Sci U S A* **2001**, *98*, 8572.
[48] K. Paeschke, T. Simonsson, J. Postberg, D. Rhodes, H. J. Lipps, *Nat Struct Mol Biol* **2005**, *12*, 847.
[49] J. Dai, M. Carver, D. Yang, *Biochimie* **2008**, *90*, 1172.
[50] A. J. Zaug, E. R. Podell, T. R. Cech, *Proc Natl Acad Sci U S A* **2005**, *102*, 10864.
[51] G. Biffi, D. Tannahill, J. Mccafferty, S. Balasubramanian, *Nature Chemistry* **2013**.
[52] M. L. Zhang, X. J. Tong, X. H. Fu, B. O. Zhou, J. Wang, X. H. Liao, Q. J. Li, N. Shen, J. Ding, J. Q. Zhou, *Nat Struct Mol Biol* **2010**, *17*, 202.
[53] J. S. Smith, Q. Chen, L. A. Yatsunyk, J. M. Nicoludis, M. S. Garcia, R. Kranaster, S. Balasubramanian, D. Monchaud, M. P. Teulade-Fichou, L. Abramowitz, D. C. Schultz, F. B. Johnson, *Nat Struct Mol Biol* **2011**, *18*, 478.
[54] T. Tauchi, K. Shin-ya, G. Sashida, M. Sumi, S. Okabe, J. H. Ohyashiki, K. Ohyashiki, *Oncogene* **2006**, *25*, 5719.

[55] D. Gomez, T. Wenner, B. Brassart, C. Douarre, M. F. O'Donohue, V. El Khoury, K. Shin-Ya, H. Morjani, C. Trentesaux, J. F. Riou, *J Biol Chem* **2006**, *281*, 38721.
[56] A. De Cian, G. Cristofari, P. Reichenbach, E. De Lemos, D. Monchaud, M. P. Teulade-Fichou, K. Shin-Ya, L. Lacroix, J. Lingner, J. L. Mergny, *Proc Natl Acad Sci U S A* **2007**, *104*, 17347.
[57] I. Grummt, *Prog Nucleic Acid Res Mol Biol* **1999**, *62*, 109.
[58] L. A. Hanakahi, H. Sun, N. Maizels, *J Biol Chem* **1999**, *274*, 15908.
[59] V. Gonzalez, K. Guo, L. Hurley, D. Sun, *J Biol Chem* **2009**, *284*, 23622.
[60] M. L. Duquette, P. Handa, J. A. Vincent, A. F. Taylor, N. Maizels, *Genes Dev* **2004**, *18*, 1618.
[61] M. Fry, L. A. Loeb, *J Biol Chem* **1999**, *274*, 12797.
[62] P. M. Grierson, K. Lillard, G. K. Behbehani, K. A. Combs, S. Bhattacharyya, S. Acharya, J. Groden, *Hum Mol Genet* **2011**, *21*, 1172.
[63] R. A. Marciniak, D. B. Lombard, F. B. Johnson, L. Guarente, *Proc Natl Acad Sci U S A* **1998**, *95*, 6887.
[64] M. Shiratori, T. Suzuki, C. Itoh, M. Goto, Y. Furuichi, T. Matsumoto, *Oncogene* **2002**, *21*, 2447.
[65] D. Drygin, A. Siddiqui-Jain, S. O'Brien, M. Schwaebe, A. Lin, J. Bliesath, C. B. Ho, C. Proffitt, K. Trent, J. P. Whitten, J. K. Lim, D. Von Hoff, K. Anderes, W. G. Rice, *Cancer Res* **2009**, *69*, 7653.
[66] K. Yu, F. Chedin, C. L. Hsieh, T. E. Wilson, M. R. Lieber, *Nat Immunol* **2003**, *4*, 442.
[67] K. J. Neaves, J. L. Huppert, R. M. Henderson, J. M. Edwardson, *Nucleic Acids Res* **2009**, *37*, 6269.
[68] E. D. Larson, M. L. Duquette, W. J. Cummings, R. J. Streiff, N. Maizels, *Curr Biol* **2005**, *15*, 470.
[69] L. A. Cahoon, H. S. Seifert, *Science* **2009**, *325*, 764.
[70] J. L. Huppert, S. Balasubramanian, *Nucleic Acids Res* **2007**, *35*, 406.
[71] J. Eddy, N. Maizels, *Nucleic Acids Res* **2008**, *36*, 1321.
[72] A. Siddiqui-Jain, C. L. Grand, D. J. Bearss, L. H. Hurley, *Proc Natl Acad Sci U S A* **2002**, *99*, 11593.
[73] M. M. Mason, J. A. Grasso, O. Gavrilova, M. Reitman, *J Biol Chem* **1996**, *271*, 25459.
[74] S. P. Clark, C. D. Lewis, G. Felsenfeld, *Nucleic Acids Res* **1990**, *18*, 5119.
[75] S. T. Hsu, P. Varnai, A. Bugaut, A. P. Reszka, S. Neidle, S. Balasubramanian, *J Am Chem Soc* **2009**, *131*, 13399.
[76] Y. Qin, E. M. Rezler, V. Gokhale, D. Sun, L. H. Hurley, *Nucleic Acids Res* **2007**, *35*, 7698.
[77] X. Tong, W. Lan, X. Zhang, H. Wu, M. Liu, C. Cao, *Nucleic Acids Res*, *39*, 6753.
[78] D. Yang, L. H. Hurley, *Nucleosides Nucleotides Nucleic Acids* **2006**, *25*, 951.
[79] T. A. Brooks, L. H. Hurley, *Nat Rev Cancer* **2009**, *9*, 849.
[80] T. S. Dexheimer, S. S. Carey, S. Zuohe, V. M. Gokhale, X. Hu, L. B. Murata, E. M. Maes, A. Weichsel, D. Sun, E. J. Meuillet, W. R. Montfort, L. H. Hurley, *Mol Cancer Ther* **2009**, *8*, 1363.
[81] T. M. Ou, Y. J. Lu, C. Zhang, Z. S. Huang, X. D. Wang, J. H. Tan, Y. Chen, D. L. Ma, K. Y. Wong, J. C. Tang, A. S. Chan, L. Q. Gu, *J Med Chem* **2007**, *50*, 1465.
[82] H. J. Kang, H. J. Park, *Biochemistry* **2009**, *48*, 7392.
[83] S. G. Hershman, Q. Chen, J. Y. Lee, M. L. Kozak, P. Yue, L. S. Wang, F. B. Johnson, *Nucleic Acids Res* **2008**, *36*, 144.
[84] A. Verma, V. K. Yadav, R. Basundra, A. Kumar, S. Chowdhury, *Nucleic Acids Res* **2009**, *37*, 4194.

[85] D. Hanahan, R. A. Weinberg, *Cell* **2000**, *100*, 57.
[86] A. M. Zahler, J. R. Williamson, T. R. Cech, D. M. Prescott, *Nature* **1991**, *350*, 718.
[87] S. Balasubramanian, L. H. Hurley, S. Neidle, *Nat Rev Drug Discov* **2011**, *10*, 261.
[88] T. M. Ou, Y. J. Lu, J. H. Tan, Z. S. Huang, K. Y. Wong, L. Q. Gu, *ChemMedChem* **2008**, *3*, 690.
[89] A. De Cian, L. Lacroix, C. Douarre, N. Temime-Smaali, C. Trentesaux, J. F. Riou, J. L. Mergny, *Biochimie* **2008**, *90*, 131.
[90] Y. Xu, *Chem Soc Rev* **2011**, *40*, 2719.
[91] D. Monchaud, M. P. Teulade-Fichou, *Org Biomol Chem* **2008**, *6*, 627.
[92] N. Luedtke, *Chimia* **2009**, *63*, 134.
[93] S. Neidle, G. N. Parkinson, *Biochimie* **2008**, *90*, 1184.
[94] E. Largy, A. Granzhan, F. Hamon, D. Verga, M. P. Teulade-Fichou, *Top Curr Chem* **2012**.
[95] L. S. Lerman, *J Mol Biol* **1961**, *3*, 18.
[96] S. Neidle, *Curr Opin Struct Biol* **2009**, *19*, 239.
[97] Y. Qin, L. H. Hurley, *Biochimie* **2008**, *90*, 1149.
[98] I. Lubitz, N. Borovok, A. Kotlyar, *Biochemistry* **2007**, *46*, 12925.
[99] V. B. Kovalska, M. Y. Losytskyy, S. M. Yarmoluk, I. Lubitz, A. B. Kotlyar, *J Fluoresc* **2011**, *21*, 223.
[100] I. Lubitz, D. Zikich, A. Kotlyar, *Biochemistry* **2010**, *49*, 3567.
[101] J. Ren, J. B. Chaires, *Biochemistry* **1999**, *38*, 16067.
[102] Q. Guo, M. Lu, L. A. Marky, N. R. Kallenbach, *Biochemistry* **1992**, *31*, 2451.
[103] J. P. Schreiber, M. P. Duane, *J Mol Biol* **1974**, *83*, 487.
[104] Y. Kubota, Y. Motoda, *Biochemistry* **1980**, *19*, 4189.
[105] D. Sun, B. Thompson, B. E. Cathers, M. Salazar, S. M. Kerwin, J. O. Trent, T. C. Jenkins, S. Neidle, L. H. Hurley, *J Med Chem* **1997**, *40*, 2113.
[106] H. S. Huang, I. B. Chen, K. F. Huang, W. C. Lu, F. Y. Shieh, Y. Y. Huang, F. C. Huang, J. J. Lin, *Chem Pharm Bull (Tokyo)* **2007**, *55*, 284.
[107] H. S. Huang, K. F. Huang, C. L. Li, Y. Y. Huang, Y. H. Chiang, F. C. Huang, J. J. Lin, *Bioorg Med Chem* **2008**, *16*, 6976.
[108] G. Zagotto, C. Sissi, L. Lucatello, C. Pivetta, S. A. Cadamuro, K. R. Fox, S. Neidle, M. Palumbo, *J Med Chem* **2008**, *51*, 5566.
[109] D. Kaluzhny, N. Ilyinsky, A. Shchekotikhin, Y. Sinkevich, P. O. Tsvetkov, V. Tsvetkov, A. Veselovsky, M. Livshits, O. Borisova, A. Shtil, A. Shchyolkina, *PLoS One* **2011**, *6*, e27151.
[110] V. Caprio, B. Guyen, Y. Opoku-Boahen, J. Mann, S. M. Gowan, L. M. Kelland, M. A. Read, S. Neidle, *Bioorg Med Chem Lett* **2000**, *10*, 2063.
[111] J. Dai, M. Carver, L. H. Hurley, D. Yang, *J Am Chem Soc*, *133*, 17673.
[112] Y. J. Lu, T. M. Ou, J. H. Tan, J. Q. Hou, W. Y. Shao, D. Peng, N. Sun, X. D. Wang, W. B. Wu, X. Z. Bu, Z. S. Huang, D. L. Ma, K. Y. Wong, L. Q. Gu, *J Med Chem* **2008**, *51*, 6381.
[113] W. Xu, J. H. Tan, S. B. Chen, J. Q. Hou, D. Li, Z. S. Huang, L. Q. Gu, *Biochem Biophys Res Commun*, *406*, 454.
[114] J. L. Zhou, Y. J. Lu, T. M. Ou, J. M. Zhou, Z. S. Huang, X. F. Zhu, C. J. Du, X. Z. Bu, L. Ma, L. Q. Gu, Y. M. Li, A. S. Chan, *J Med Chem* **2005**, *48*, 7315.
[115] X. D. Wang, T. M. Ou, Y. J. Lu, Z. Li, Z. Xu, C. Xi, J. H. Tan, S. L. Huang, L. K. An, D. Li, L. Q. Gu, Z. S. Huang, *J Med Chem*, *53*, 4390.
[116] P. V. Boddupally, S. Hahn, C. Beman, B. De, T. A. Brooks, V. Gokhale, L. H. Hurley, *J Med Chem* **2012**, *55*, 6076.

[117] M. P. Teulade-Fichou, C. Carrasco, L. Guittat, C. Bailly, P. Alberti, J. L. Mergny, A. David, J. M. Lehn, W. D. Wilson, *J Am Chem Soc* **2003**, *125*, 4732.
[118] H. Bertrand, S. Bombard, D. Monchaud, M. P. Teulade-Fichou, *Nucleic Acids Symp Ser (Oxf)* **2008**, 163.
[119] H. Bertrand, S. Bombard, D. Monchaud, M. P. Teulade-Fichou, *J Biol Inorg Chem* **2007**, *12*, 1003.
[120] A. Rangan, O. Y. Fedoroff, L. H. Hurley, *J Biol Chem* **2001**, *276*, 4640.
[121] O. Y. Fedoroff, M. Salazar, H. Han, V. V. Chemeris, S. M. Kerwin, L. H. Hurley, *Biochemistry* **1998**, *37*, 12367.
[122] M. Franceschin, L. Rossetti, A. D'Ambrosio, S. Schirripa, A. Bianco, G. Ortaggi, M. Savino, C. Schultes, S. Neidle, *Bioorg Med Chem Lett* **2006**, *16*, 1707.
[123] A. Arora, C. Balasubramanian, N. Kumar, S. Agrawal, R. P. Ojha, S. Maiti, *Febs J* **2008**, *275*, 3971.
[124] Y. Ma, T. M. Ou, J. Q. Hou, Y. J. Lu, J. H. Tan, L. Q. Gu, Z. S. Huang, *Bioorg Med Chem* **2008**, *16*, 7582.
[125] Y. Ma, T. M. Ou, J. H. Tan, J. Q. Hou, S. L. Huang, L. Q. Gu, Z. S. Huang, *Bioorg Med Chem Lett* **2009**, *19*, 3414.
[126] J. Kapuscinski, Z. Darzynkiewicz, M. R. Melamed, *Biochem Pharmacol* **1983**, *32*, 3679.
[127] K. Yamaoka, M. Masujima, *Biopolymers* **1978**, *17*, 2485.
[128] J. Ren, J. B. Chaires, *Methods in Enzymology, Drug-nucleic acids interaction, Vol. 340*, Academic Press, **2001**.
[129] S. Nakayama, I. Kelsey, J. Wang, H. O. Sintim, *Chem Commun (Camb)* **2011**, *47*, 4766.
[130] R. J. Harrison, S. M. Gowan, L. R. Kelland, S. Neidle, *Bioorg Med Chem Lett* **1999**, *9*, 2463.
[131] M. J. Moore, C. M. Schultes, J. Cuesta, F. Cuenca, M. Gunaratnam, F. A. Tanious, W. D. Wilson, S. Neidle, *J Med Chem* **2006**, *49*, 582.
[132] N. H. Campbell, G. N. Parkinson, A. P. Reszka, S. Neidle, *J Am Chem Soc* **2008**, *130*, 6722.
[133] R. Ferreira, A. Avino, R. Perez-Tomas, R. Gargallo, R. Eritja, *J Nucleic Acids* **2010**, *2010*.
[134] J. L. Bresloff, D. M. Crothers, *Biochemistry* **1981**, *20*, 3547.
[135] N. W. Luedtke, J. S. Hwang, E. Nava, D. Gut, M. Kol, Y. Tor, *Nucleic Acids Res* **2003**, *31*, 5732.
[136] L. J. Latimer, J. S. Lee, *J Biol Chem* **1991**, *266*, 13849.
[137] X. G. Sun, E. H. Cao, J. He, Q. J. F., *Science in China series B-Chemistry* **1999**, *42*.
[138] F. Koeppel, J. F. Riou, A. Laoui, P. Mailliet, P. B. Arimondo, D. Labit, O. Petitgenet, C. Helene, J. L. Mergny, *Nucleic Acids Res* **2001**, *29*, 1087.
[139] D. J. Patel, A. T. Phan, V. Kuryavyi, *Nucleic Acids Res* **2007**, *35*, 7429.
[140] M. C. Miller, H. T. Le, W. L. Dean, P. A. Holt, J. B. Chaires, J. O. Trent, *Org Biomol Chem* **2011**, *9*, 7633.
[141] R. T. Wheelhouse, D. Sun, H. Han, F. X. Han, L. H. Hurley, *J. Am. Chem. Soc.* **1998**, *120*, 3261.
[142] D. F. Shi, R. T. Wheelhouse, D. Sun, L. H. Hurley, *J Med Chem* **2001**, *44*, 4509.
[143] A. T. Phan, V. Kuryavyi, H. Y. Gaw, D. J. Patel, *Nat Chem Biol* **2005**, *1*, 167.
[144] G. N. Parkinson, R. Ghosh, S. Neidle, *Biochemistry* **2007**, *46*, 2390.
[145] M. W. Freyer, R. Buscaglia, K. Kaplan, D. Cashman, L. H. Hurley, E. A. Lewis, *Biophys J* **2007**, *92*, 2007.

[146] G. N. Georgiou, M. T. Ahmet, A. Houlton, J. Silver, R. J. Cherry, *Photochem Photobiol* **1994**, *59*, 419.
[147] H. Zhang, X. Xiao, P. Wang, S. Pang, F. Qu, X. Ai, J. Zhang, *Spectrochim Acta A Mol Biomol Spectrosc* **2009**, *74*, 243.
[148] H. Arthanari, S. Basu, T. L. Kawano, P. H. Bolton, *Nucleic Acids Res* **1998**, *26*, 3724.
[149] C. Y. Chen, Q. Wang, J. Q. Liu, Y. H. Hao, Z. Tan, *J Am Chem Soc* **2011**, *133*, 15036.
[150] J. W. Snyder, J. D. Lambert, P. R. Ogilby, *Photochem Photobiol* **2006**, *82*, 177.
[151] V. Chirvony, *Journal of Porphyrins and Phthalocyanines* **2003**, *7*, 766.
[152] H. Zhang, X. Wang, P. Wang, S. Pang, X. Ai, J. Zhang, *Science in China Series B: Chemistry* **2008**, *51*, 452.
[153] J. Alzeer, N. W. Luedtke, *Biochemistry* **2010**, *49*, 4339.
[154] D. P. Goncalves, R. Rodriguez, S. Balasubramanian, J. K. Sanders, *Chem Commun (Camb)* **2006**, 4685.
[155] J. Alzeer, N. W. Luedtke, *Unpublished results* **2012**.
[156] M. O. Senge, W. W. Kalish, Runge S., *Liebigs Annalen-Recueil* **1997**, 1345.
[157] F. De Matteis, A. H. Gibbs, A. G. Smith, *Biochem J* **1980**, *189*, 645.
[158] Y. Li, D. Sen, *Biochemistry* **1997**, *36*, 5589.
[159] Y. Li, C. R. Geyer, D. Sen, *Biochemistry* **1996**, *35*, 6911.
[160] J. M. Nicoludis, S. P. Barrett, J. L. Mergny, L. A. Yatsunyk, *Nucleic Acids Res* **2012**, *40*, 5432.
[161] J. Ren, H. Qin, J. Wang, N. W. Luedtke, E. Wang, *Anal Bioanal Chem* **2011**, *399*, 2763.
[162] S. I. Beale, N. C. Chen, *Plant Physiol* **1983**, *71*, 263.
[163] T. Li, E. Wang, S. Dong, *Anal Chem* **2010**, *82*, 7576.
[164] H. Takino, C. Li, S. Hu, T. T. Kuo, E. Geissinger, H. K. Muller-Hermelink, B. Kim, S. H. Swerdlow, H. Inagaki, *Mod Pathol* **2008**, *21*, 1517.
[165] L. Brancaleon, H. Moseley, *Biophys Chem* **2002**, *96*, 77.
[166] J. D. Schonhoft, A. Das, F. Achamyeleh, S. Samdani, A. Sewell, H. Mao, S. Basu, *Biopolymers* **2009**, *93*, 21.
[167] R. R. Breaker, *Mol Cell* **2011**, *43*, 867.
[168] P. S. Ray, J. Jia, P. Yao, M. Majumder, M. Hatzoglou, P. L. Fox, *Nature* **2009**, *457*, 915.
[169] K. Shin-ya, K. Wierzba, K. Matsuo, T. Ohtani, Y. Yamada, K. Furihata, Y. Hayakawa, H. Seto, *J Am Chem Soc* **2001**, *123*, 1262.
[170] M. Y. Kim, H. Vankayalapati, K. Shin-Ya, K. Wierzba, L. H. Hurley, *J Am Chem Soc* **2002**, *124*, 2098.
[171] M. Y. Kim, M. Gleason-Guzman, E. Izbicka, D. Nishioka, L. H. Hurley, *Cancer Res* **2003**, *63*, 3247.
[172] G. S. Minhas, D. S. Pilch, J. E. Kerrigan, E. J. LaVoie, J. E. Rice, *Bioorg Med Chem Lett* **2006**, *16*, 3891.
[173] D. S. Pilch, C. M. Barbieri, S. G. Rzuczek, E. J. Lavoie, J. E. Rice, *Biochimie* **2008**, *90*, 1233.
[174] M. Tera, H. Ishizuka, M. Takagi, M. Suganuma, K. Shin-ya, K. Nagasawa, *Angew Chem Int Ed Engl* **2008**, *47*, 5557.
[175] M. Tera, K. Iida, K. Ikebukuro, H. Seimiya, K. Shin-Ya, K. Nagasawa, *Org Biomol Chem* **2010**, *8*, 2749.
[176] J. M. Belitsky, S. J. Leslie, P. S. Arora, T. A. Beerman, P. B. Dervan, *Bioorg Med Chem* **2002**, *10*, 3313.

[177] S. N. Georgiades, N. H. Abd Karim, K. Suntharalingam, R. Vilar, *Angew Chem Int Ed Engl* **2010**, *49*, 4020.
[178] Q. Zhao, C. Huang, F. Li, *Chem Soc Rev* **2011**, *40*, 2508.
[179] J. E. Reed, A. A. Arnal, S. Neidle, R. Vilar, *J Am Chem Soc* **2006**, *128*, 5992.
[180] P. Wu, D. L. Ma, C. H. Leung, S. C. Yan, N. Zhu, R. Abagyan, C. M. Che, *Chemistry* **2009**, *15*, 13008.
[181] P. Wang, C. H. Leung, D. L. Ma, S. C. Yan, C. M. Che, *Chemistry* **2010**, *16*, 6900.
[182] D. L. Ma, C. M. Che, S. C. Yan, *J Am Chem Soc* **2009**, *131*, 1835.
[183] B. M. Zeglis, V. C. Pierre, J. K. Barton, *Chem Commun (Camb)* **2007**, 4565.
[184] S. Shi, J. Zhao, X. Geng, T. Yao, H. Huang, T. Liu, L. Zheng, Z. Li, D. Yang, L. Ji, *Dalton Trans* **2010**, *39*, 2490.
[185] S. Shi, X. Geng, J. Zhao, T. Yao, C. Wang, D. Yang, L. Zheng, L. Ji, *Biochimie* **2010**, *92*, 370.
[186] J. Sun, Y. An, L. Zhang, H. Y. Chen, Y. Han, Y. J. Wang, Z. W. Mao, L. N. Ji, *J Inorg Biochem* **2011**, *105*, 149.
[187] J. Alzeer, B. R. Vummidi, P. J. Roth, N. W. Luedtke, *Angew Chem Int Ed Engl* **2009**, *48*, 9362.
[188] M. R. Gill, J. Garcia-Lara, S. J. Foster, C. Smythe, G. Battaglia, J. A. Thomas, *Nat Chem* **2009**, *1*, 662.
[189] C. Rajput, R. Rutkaite, L. Swanson, I. Haq, J. A. Thomas, *Chemistry* **2006**, *12*, 4611.
[190] T. Wilson, M. P. Williamson, J. A. Thomas, *Org Biomol Chem* **2010**, *8*, 2617.
[191] A. Bouskila, E. Amouyal, C. Verchere-Beaur, I. Sasaki, A. Gaudemer, *J Photochem Photobiol B* **2004**, *76*, 69.
[192] K. W. Zheng, D. Zhang, L. X. Zhang, Y. H. Hao, X. Zhou, Z. Tan, *J Am Chem Soc* **2011**, *133*, 1475.
[193] F. P. Schwarz, S. P. Wasik, *Anal Chem* **1976**, *48*, 524.
[194] Q. Yang, J. Xiang, S. Yang, Q. Zhou, Q. Li, Y. Tang, G. Xu, *Chem Commun (Camb)* **2009**, 1103.
[195] H. N. Kim, E.-H. Lee, Z. Xu, H.-E. Kim, H.-S. Lee, J.-H. Lee, J. Yoon, *Biomaterials* **2012**, *33*.
[196] J. Kapuscinski, B. Skoczylas, *Nucl. Acids Res.* **1978**, *5*, 3775.
[197] K. E. Rao, K. Krowicki, G. Burckhardt, C. Zimmer, J. W. Lown, *Chem Res Toxicol* **1991**, *4*, 241.
[198] A. K. Jain, S. Bhattacharya, *Bioconjug Chem* **2011**, *22*, 2355.
[199] S. Maiti, N. K. Chaudhury, S. Chowdhury, *Biochem Biophys Res Commun* **2003**, *310*, 505.
[200] J. H. Moon, S. K. Kim, U. Sehlstedt, A. Rodger, B. Norden, *Biopolymers* **1996**, *38*, 593.
[201] K. Jansen, P. Lincoln, B. Norden, *Biochemistry* **1993**, *32*, 6605.
[202] Q. Chen, I. D. Kuntz, R. H. Shafer, *Proc Natl Acad Sci U S A* **1996**, *93*, 2635.
[203] J. Nygren, N. Svanvik, M. Kubista, *Biopolymers* **1998**, *46*, 39.
[204] D. Monchaud, C. Allain, M. P. Teulade-Fichou, *Nucleosides Nucleotides Nucleic Acids* **2007**, *26*, 1585.
[205] P. Yang, A. De Cian, M. P. Teulade-Fichou, J. L. Mergny, D. Monchaud, *Angew Chem Int Ed Engl* **2009**, *48*, 2188.
[206] Y. J. Lu, S. C. Yan, F. Y. Chan, L. Zou, W. H. Chung, W. L. Wong, B. Qiu, N. Sun, P. H. Chan, Z. S. Huang, L. Q. Gu, K. Y. Wong, *Chem Commun (Camb)* **2011**, *47*, 4971.

[207] M. P. Teulade-Fichou, C. Hounsou, L. Guittat, J. L. Mergny, P. Alberti, C. Carrasco, C. Bailly, J. M. Lehn, W. D. Wilson, *Nucleosides Nucleotides Nucleic Acids* **2003**, *22*, 1483.
[208] C. Allain, D. Monchaud, M. P. Teulade-Fichou, *J Am Chem Soc* **2006**, *128*, 11890.
[209] R. Rodriguez, K. M. Miller, J. V. Forment, C. R. Bradshaw, M. Nikan, S. Britton, T. Oelschlaegel, B. Xhemalce, S. Balasubramanian, S. P. Jackson, *Nat Chem Biol* **2012**, *8*, 301.
[210] C. M. Sanders, *Biochem J* **2010**, *430*, 119.
[211] K. Paeschke, J. A. Capra, V. A. Zakian, *Cell* **2011**, *145*, 678.
[212] A. C. Bhasikuttan, J. Mohanty, H. Pal, *Angew Chem Int Ed Engl* **2007**, *46*, 9305.
[213] Y. Hong, M. Haussler, J. W. Lam, Z. Li, K. K. Sin, Y. Dong, H. Tong, J. Liu, A. Qin, R. Renneberg, B. Z. Tang, *Chemistry* **2008**, *14*, 6428.
[214] D. M. Kong, Y. E. Ma, J. Wu, H. X. Shen, *Chemistry* **2009**, *15*, 901.
[215] C. Szent-Gyorgyi, B. F. Schmidt, Y. Creeger, G. W. Fisher, K. L. Zakel, S. Adler, J. A. Fitzpatrick, C. A. Woolford, Q. Yan, K. V. Vasilev, P. B. Berget, M. P. Bruchez, J. W. Jarvik, A. Waggoner, *Nat Biotechnol* **2008**, *26*, 235.
[216] F. A. Tanious, D. Ding, D. A. Patrick, C. Bailly, R. R. Tidwell, W. D. Wilson, *Biochemistry* **2000**, *39*, 12091.
[217] C. C. Chang, J. Y. Wu, C. W. Chien, W. S. Wu, H. Liu, C. C. Kang, L. J. Yu, T. C. Chang, *Anal Chem* **2003**, *75*, 6177.
[218] C. C. Chang, I. C. Kuo, I. F. Ling, C. T. Chen, H. C. Chen, P. J. Lou, J. J. Lin, T. C. Chang, *Anal Chem* **2004**, *76*, 4490.
[219] C. C. Chang, J. F. Chu, F. J. Kao, Y. C. Chiu, P. J. Lou, H. C. Chen, T. C. Chang, *Anal Chem* **2006**, *78*, 2810.
[220] B. Dumat, G. Bordeau, E. Faurel-Paul, F. Mahuteau-Betzer, N. Saettel, M. Bombled, G. Metge, F. Charra, C. Fiorini-Debuisschert, M. P. Teulade-Fichou, *Biochimie* **2011**, *93*, 1209.

Chapter 2. Cationic phthalocyanines as G-quadruplex probes

2.1. Introduction

After being discovered as impurities in 1907,[1] phthalocyanines (Pcs) have been widely utilized as materials in diverse fields. Pcs are heteroaromatic, symmetric molecules containing four isoindole units linked with nitrogen atoms. Due to their interesting photophysical properties, Pcs have range of applications as dyes, catalysts, chemical sensors and in data storage devices. *In vivo* applications of phthalocyanines include tattoo inks and as photosensitizers in photodynamic therapy.[2] Though Pcs are structurally related to porphyrins, Pcs are strictly synthetic as they do not occur naturally. According to computational modeling, phthalocyanines have especially good shape complementarity with G-tetrads that constitute G-quadruplex DNA (Figure 2.1).[3] We were interested in developing cationic phthalocyanines with guanidinium groups because the cellular uptake and DNA/RNA affinity is typically better for guanidinium-containing molecules than analogous molecules containing ammonium[4, 5] We therefore synthesized a small family of guanidinium-containing phthalocyanines (Figure 2.2).[2, 6]

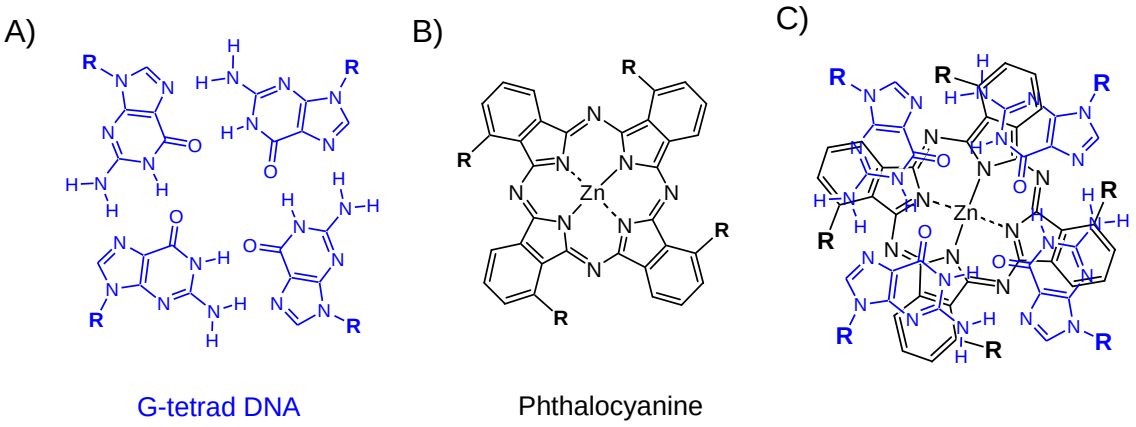

Figure 2.1. Structure of G-tetrad present in the G-quadruplex DNA (A) and phthalocyanine scaffold (B). Overlay of G-tetrad and phthalocyanine, illustrating similarities in molecular dimensions (C).

2.2. Results and Discussion

2.2.1. Synthesis of guanidino phthalocyanines

Tetrakis-(diisopropyl-guanidine) zinc phthalocyanine "Zn-DIGP" were synthesized according to Figure 2.2. Phthalic anhydride was reacted with zinc chloride and ammonium molybdate at 185 ºC to give the Zinc-containing macrocycle (**2**) in 98% yield. **2** was then reduced by sodium sulfide to give **3**. Tetraamino zinc phthalocyanine (**3**) was then heated with diisopropyl carbodiimide in the presence of pyridine-HCl at 120 ºC to yield a demetallated guanidinium-containing phthalocyanine (**4**) in 83% isolated yield. Heating **4** in the presence of zinc chloride provides zinc-diisopropyl guanidino phthalocyanines (**5**) in 79% isolated yield.

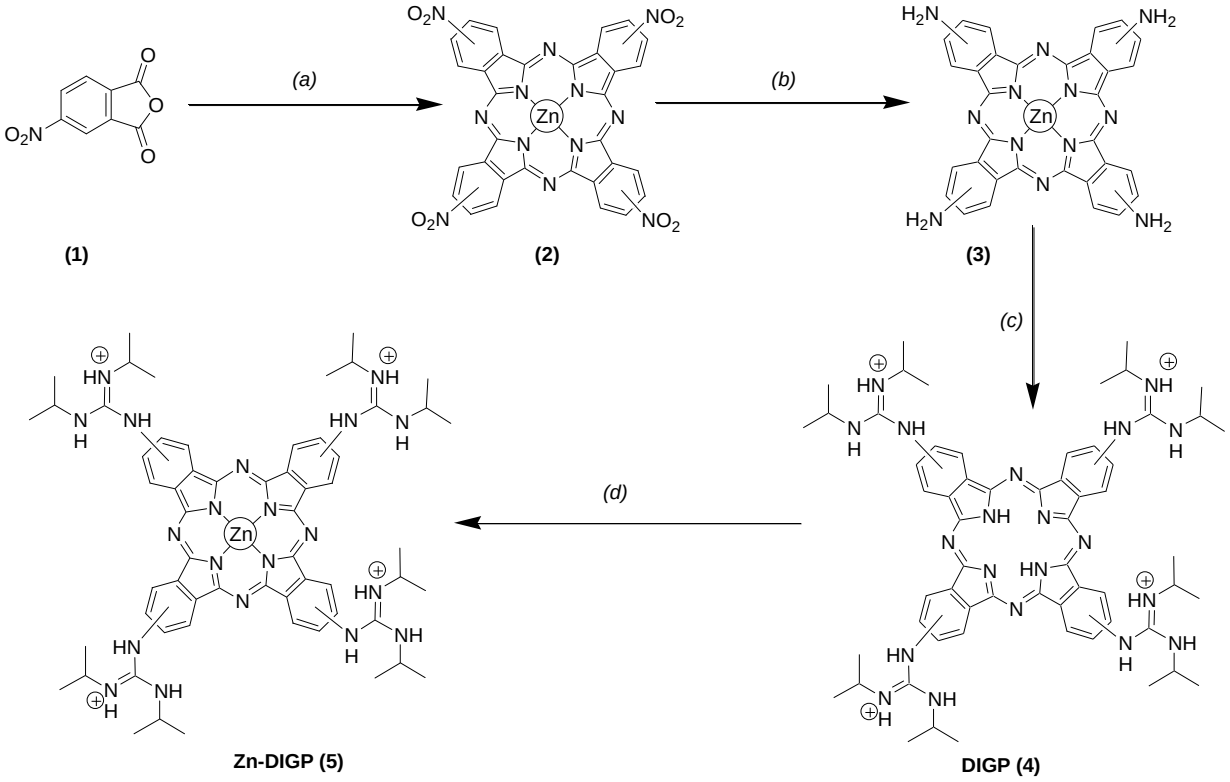

Figure 2.2. Synthesis and structures of guanidino zinc phthalocyanines **6** – **8**.[13,15] Reagents and conditions: (a) zinc chloride (0.25 equiv), ammonium molybdate (0.1 mol %), nitrobenzene, 185 ^{o}C, 4 h, 98%; (b) sodium sulfide (12 eq), DMF, 60 ^{o}C, 1.5 h, 75%; (c) diisopropyl carbodiimide (20 – 50 equiv), pyridine/pyridinium-HCl, 120 ^{o}C, 20 h; (d) trifluoroacetic acid (TFA) / water (e) zinc chloride, sodium acetate / acetic acid, 120 ^{o}C, 1 – 4 h; TFA / water.[13,15]

2.2.2. Absorption spectra of Zn-DIGP and DIGP

Zn-DIGP and DIGP exhibit intense bands in their absorption spectra. The strongest absorption band is the Q-band which originates from π-π* transitions. Zn-DIGP exhibits a single Q-band is in the range of 650-680 nm whereas DIGP shows a split Q-band in the same range due to the loss of molecular symmetry.[7, 8] In the metal free derivative, two of the isoindole nitrogen carries hydrogen atoms and the other two are iminic type nitrogens that cause loss of molecular and therefore electronic symmetry.

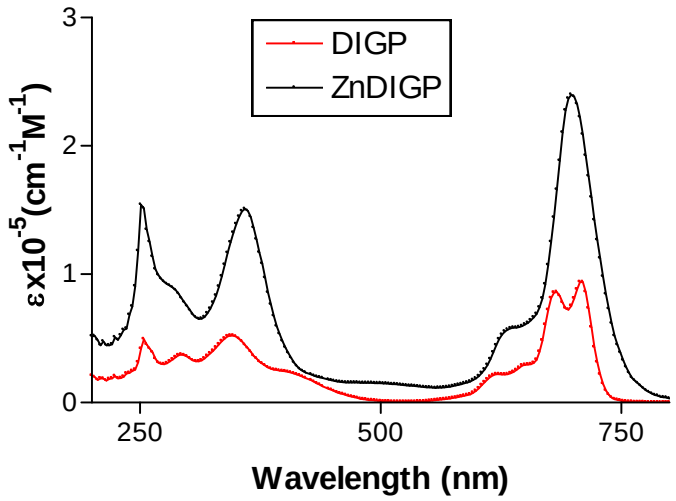

Figure 2.3. Absorption spectra of Zn-DIGP and DIGP in DMSO.

Both Zn-DIGP and DIGP exhibit excellent solubility and obeys beer's law over the concentration of 0.3 – 1 μM in DMSO. The fluorescence quantum yield in DMSO was determined to be 0.28 and 0.25 for Zn-DIGP and DIGP respectively. In water, however, these compounds exhibit quenched fluorescence ($\Phi < 0.001$) as a result of strong self-association.[9]

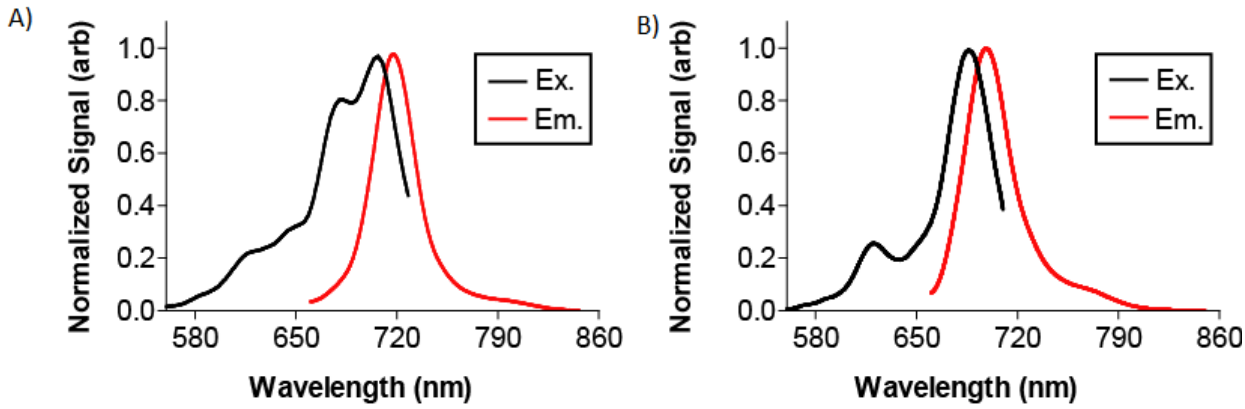

Figure 2.4. (A) Excitation spectra (λ_{em} = 770 nm) and emission spectra (λ_{ex} = 600 nm) of DIGP (B) Excitation spectra (λ_{em} = 750 nm) and emission spectra (λ_{ex} = 600 nm) of Zn-DIGP in DMSO.

2.2.3. Binding studies

For DNA binding studies, G-quadruplex-forming sequences from the promoter region of c-myc and human telomeric sequence ("Htelo") were used. Both of these sequences are reported to form intramolecular G-quadruplexes *in vitro*.[10-12] To evaluate G-quadruplex specificity, a mutated human telomeric sequence in which guanine was replaced by adenine ("Htelo-Mut"), as well as C-rich complement strands of c-Myc ("c-Myc-C") and Htelo ("Htelo-C") was used. According to circular dichroism, "Htelo-Mut" does not form a stable G-quadruplex structure.

Name	Sequence (5`-3`)
c-Myc	TGAGGGTGGGGAGGGTGGGGAA
Htelo	GTTA$(GGGTTA)_4$GG
Htelo-mut	GTTA$(GAGTTA)_4$GG
Htelo-C	CC$(TAACCC)_4$TAAC
c-Myc-C	$(C)_4A(C)_2TT(C)_4A(C)_3T(C)_4A(C)_3T(C)_4$

Table 2.1. Sequences used in the binding studies.

The stoichiometries of Zn-DIGP-G-quadruplex DNA binding were determined by monitoring the absorbance spectrum of 1 μM of Zn-DIGP upon addition of variable equivalents of c-Myc, Htelo and Htelo-C DNA. With the addition of DNA, increase in the extinction coefficient at 690 nm was observed (Figure 2.5). The addition of 0.25 equivalents of c-Myc caused a 50% increase in the extinction coefficient. This suggests that two equivalents of Zn-

DIGP bind to one equivalent c-Myc G-quadruplex. Similarly, Zn-DIGP was found to bind Htelo and Htelo-mut with stoichiometries of 1:1 and 4:1, respectively (Figure 2.5).

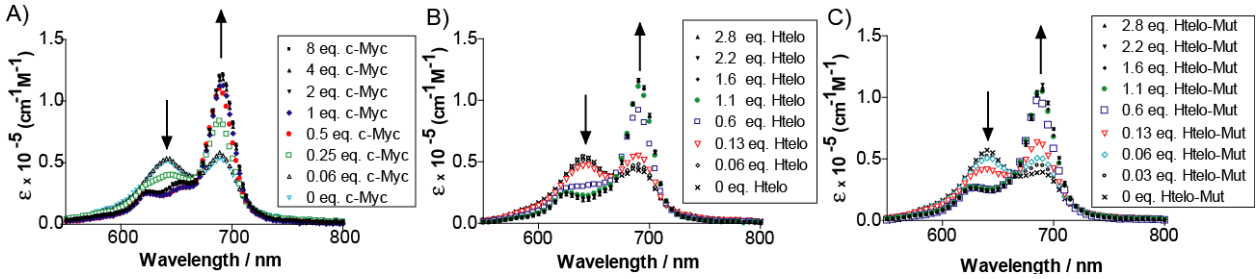

Figure 2.5. Absorption spectra of 1 µM of Zn-DIGP upon titration with c-Myc (A), Htelo (B) and Htelo mutant (C).

To evaluate the DNA affinity of Zn-DIGP, two types of binding assays were performed. The first assay monitors Zn-DIGP fluorescence upon addition of DNA. Upon binding DNA, Zn-DIGP exhibits a large increase in fluorescence that can be monitored using excitation at 620 nm and emission at 705 nm (Figure 2.6). The origin of this fluorescence enhancement is the reversal of Zn-DIGP self quenching in water by DNA binding (Figure 2.6).[9]

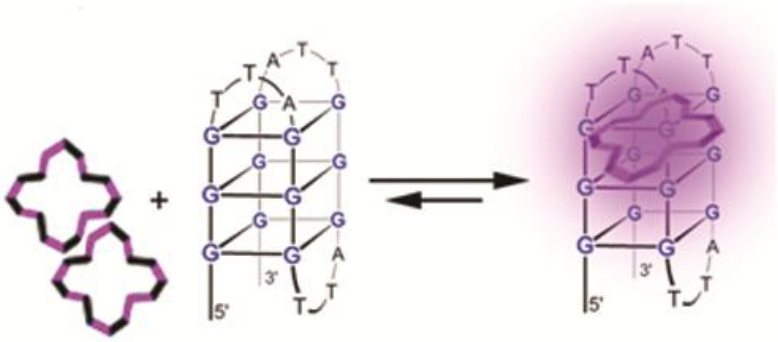

Figure 2.6. Schematic of "turn-on" fluorescence of Zn-DIGP.[9]

To measure DNA affinity, variable concentrations of nucleic acids were added to a fixed concentration (10 nM) of Zn-DIGP and fluorescence was monitored. As shown in Figure 2.7, a dramatic increase in Zn-DIGP fluorescence was observed upon adding nucleic acids to give highly fluorescent complexes ($\Phi = 0.06 \pm 0.002$). Figure 2.7 A) presents the data fitted with one phase exponential association and B) presents sigmoidal dose response curve fits. Zn-DIGP binds to c-Myc and Htelo G-quadruplex structure at a very low concentration as compared to Htelo-Mut, c-Myc-C and tRNA mix. The trend of Zn-DIGP affinity was found to be c-Myc G-quadruplex > Htelo > Htelo-Mut > tRNA > calf thymus duplex DNA > c-

Myc-C. By using 2:1 binding model, the analysis of these data revealed K_d of $\leq$ 2nM to c-Myc G-quadruplex. A limit must be reported since the probe concentration used for direct detection was higher than the apparent K_d values, and Zn-DIGP aggregation might cause an underestimated DNA binding affinity. Compared to other nucleic acids structures, such as calf thymus duplex DNA (CT-DNA) and tRNA, Zn-DIGP shows at least 1000-fold and 100-fold G-quadruplex selectivity, respectively (Figure 2.7B).

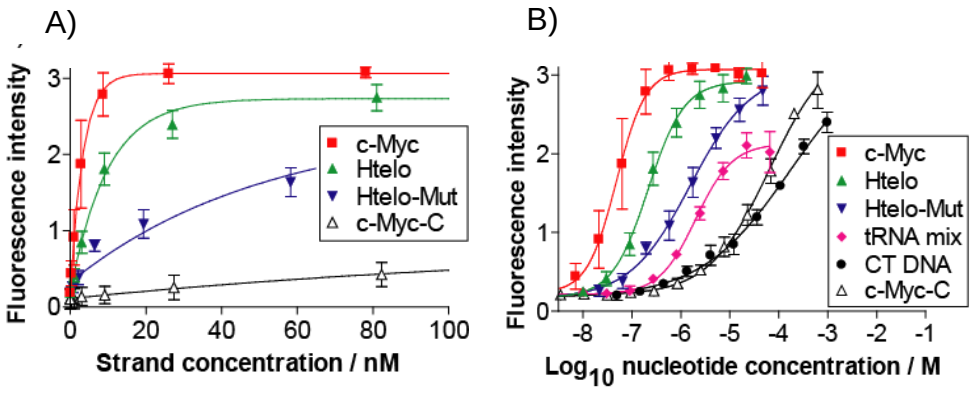

Figure 2.7. Fluorescence enhancement studies of 10 nM of Zn-DIGP upon addition of different nucleic acids.

By means of fluorescence enhancement assays, it was not possible to test the selectivity of Zn-DIGP for G-quadruplex DNA in the presence of competitor DNA. To evaluate the selectivity of Zn-DIGP for G-quadruplex DNA in the presence of other nucleic acid structures, a fluorescence quenching assay was performed (Figure 2.8).

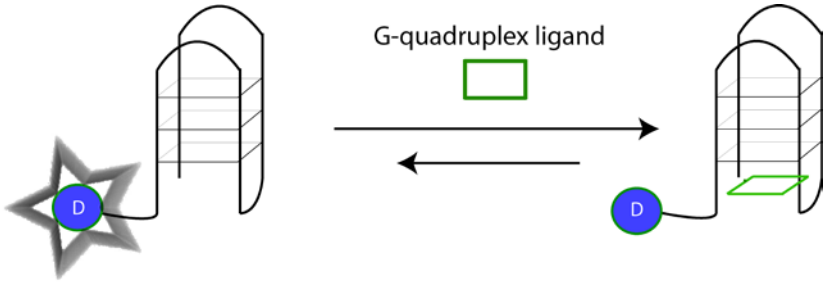

Figure 2.8. Schematic of fluorescence quenching assays.

The impressive G-quadruplex affinity and specificity of Zn-DIGP was confirmed by monitoring the fluorescence quenching of a 5'-fluorescein-labeled c-Myc DNA upon titration of Zn-DIGP in the presence or absence of a 1,000-fold nucleotide excess of CT-DNA (Figure 2.9). The likely reason for fluorescence quenching was attributed to environmental changes of fluroescein upon binding of Zn-DIGP to c-Myc DNA. As a control, the known cationic

porphyrin Zn-TMPyP4 (**20**, Chapter 1) was also evaluated. Consistent with its promiscuous binding of nucleic acids,[13] a 10-fold loss in the apparent binding affinity of Zn-TMPyP4 was observed in the presence of competitor CT-DNA (Figure 2.9A), while a high apparent affinity ($K_d \leq 2$ nM) between Zn-DIGP and c-Myc was measured even in the presence of a 1,000-fold excess of CT-DNA. The metal free derivative DIGP exhibited similar G-quadruplex affinity but somewhat lower selectivity (Figure 2.9B).

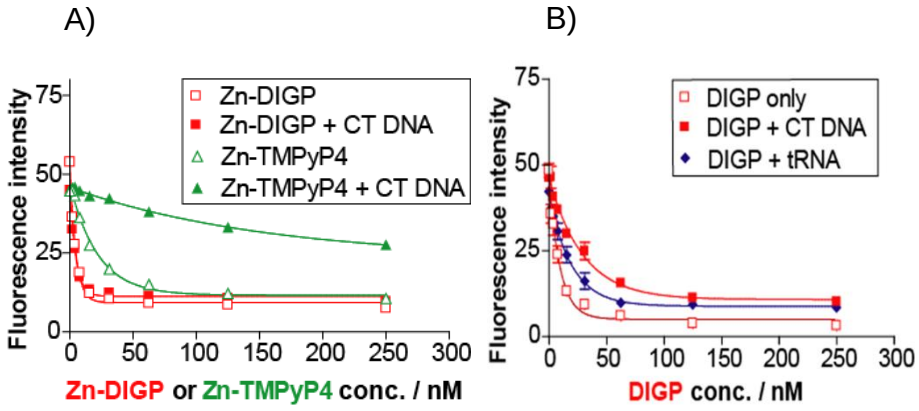

Figure 2.9. Fluorescence quenching of 10 nM solutions of the 5`-fluroescein-labeled c-Myc DNA (Ex: 495 nm, Em: 520 nm) with Zn-DIGP (A), Zn-TMPyP4 (A) or DIGP (B) in the presence of a 1000-fold excess of calf thymus DNA or 100-fold excess of tRNA.

2.2.4. Cytotoxicity studies

To determine a suitable concentration limit of Zn-DIGP and DIGP for cell-based studies, it is important to know the effective concentration at which 50% of treated cells die (EC_{50}). EC_{50} values for Zn-DIGP and DIGP were measured using resazurin reduction assays. Resazurin is a non-fluorescent dye which is reduced by mitochondrial enzymes to give fluorescent resofurin (Figure 2.10). The fluorescent resofurin can be quantified using an excitation and emission wavelength of 560 nm and 590 nm in spectrophotometer.

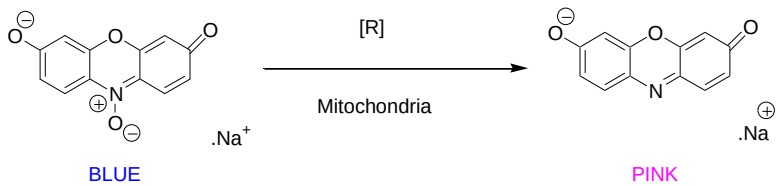

Figure 2.10. Reduction of resazurin to resofurin by mitochondrial enzymes.

Variable concentrations of Zn-DIGP and DIGP were titrated into B16F10, SKMEL-28, Macrophage or MCF-7 cell cultures. After incubation for 24 hours, resazurin was added and

incubated for an additional 2-3 hours. Measured fluorescence data was fit using a sigmoidal dose response curve to calculate EC_{50} values (Figure 2.11). A summary of EC_{50} values of Zn-DIGP and DIGP for various cell lines is given in Table 2.2.

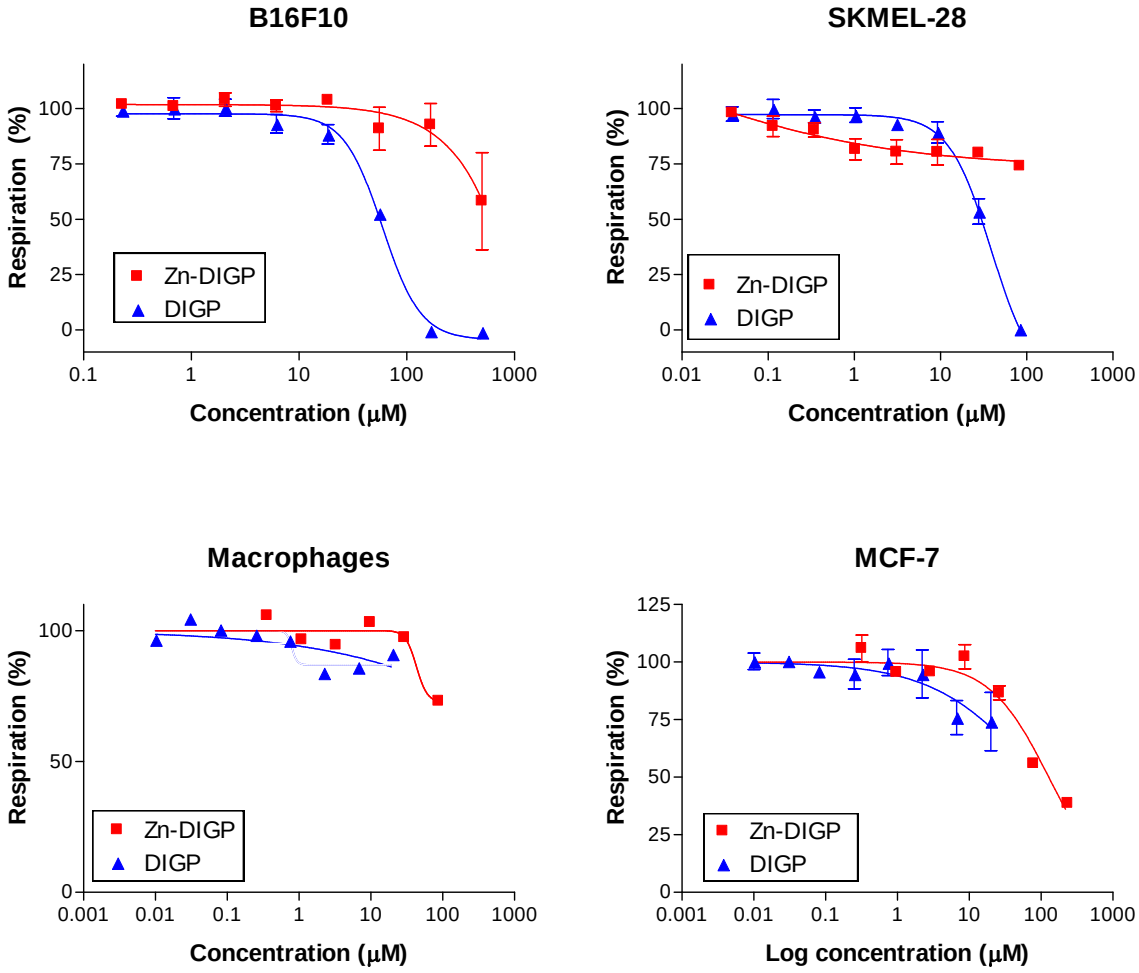

Figure 2.11. Cellular respiration of cell cultures treated with variable concentrations of Zn-DIGP and DIGP for 24 hours.

Cell lines	Type	Origin	EC_{50} (µM)	
			Zn-DIGP	DIGP
B16F10	Melanoma	Mouse	>80	41 ± 8
SKMEL-28	Melanoma	Human	>80	39 ± 6
MCF-7	Breast carcinoma	Human	>80	>20
Macrophages	Leukemia	Human	>80	>20

Table 2.2. Summary of cytotoxicity values after Zn-DIGP- and DIGP- treatment in different cell lines for 24 hours.

It is possible that these molecules could exhibit genotoxicity and prevent cell divisions upon prolonged treatment; hence we decided to evaluate long-term cytotoxicity. For these studies, the seeding number of cells was reduced to 5'000 instead of 10'000. As shown in Figure 2.12, the time-dependent inhibition of respiration is very similar. These results demonstrate that longer incubation periods of Zn-DIGP and DIGP have no significant effect of the EC_{50} values for B16F10 cells. Microscopic examination of cells treated with 5 µM of Zn-DIGP did not show any change in morphology or growth rate even after 10 days.

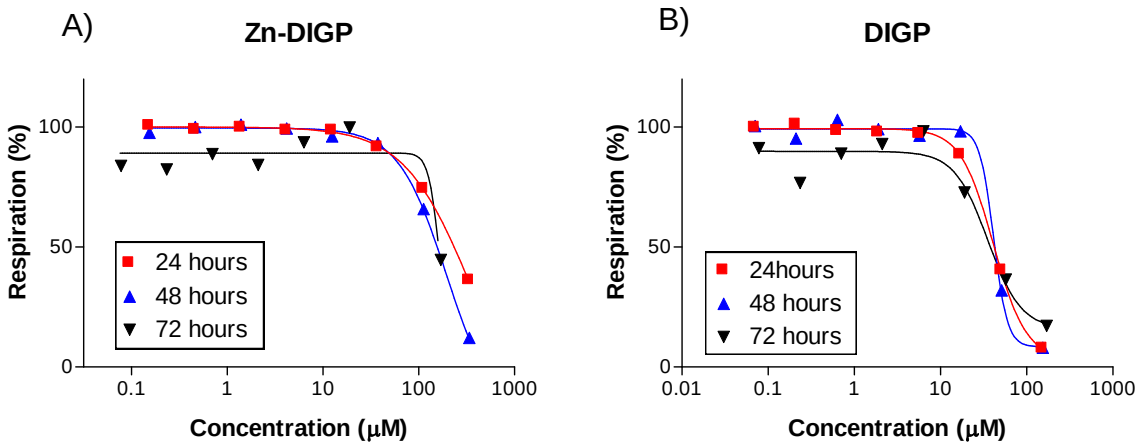

Figure 2.12. Cellular respiration of B16F10 cells after treatment with Zn-DIGP (A) and DIGP (B) for 24-72 hours.

2.2.5. Cellular localization

Since Zn-DIGP and DIGP were not toxic in the low micromolar range, we decided to use 5 µM to probe for G-quadruplex DNA in cells. SKMEL-28 cells were initially chosen because of their excellent morphology and easy handling. Utilizing its pro-fluorescent properties, Zn-DIGP and DIGP can be added to cells and directly imaged using fluorescence microscopy. Initial studies with living SKMEL-28 cells reveal that Zn-DIGP stains the peri-nuclear regions of the living cells. DIGP exhibits weak fluorescence localized in cytoplasm and peri-nuclear regions (Figure 2.13). These compounds were tested in different cell lines including Hela, SKMEL-28, B16F10 and SHSY5Y, and in all cases their uptake was observed with similar staining patterns in living cells (Figure 2.14). Unfortunately, Zn-DIGP did not stain in the nucleus of living cells making it difficult to probe for G-quadruplex structures.

Based upon its localization in live cells, we speculated that Zn-DIGP can be endocytosed and trapped in lysozomes. To evaluate this possibility 60 nM of lysotracker was added to living cells followed by 5 µM of Zn-DIGP or DIGP. As shown in Figure 2.15, Zn-DIGP co-

localizes with lysotracker demonstrating that Zn-DIGP is taken up in the lysozomes of living cells. Interestingly, live-cell fluorescence imaging of Zn-DIGP can cause changes in morphology and dye distribution during data collection due to its potent phototoxicity (Chapter 3).

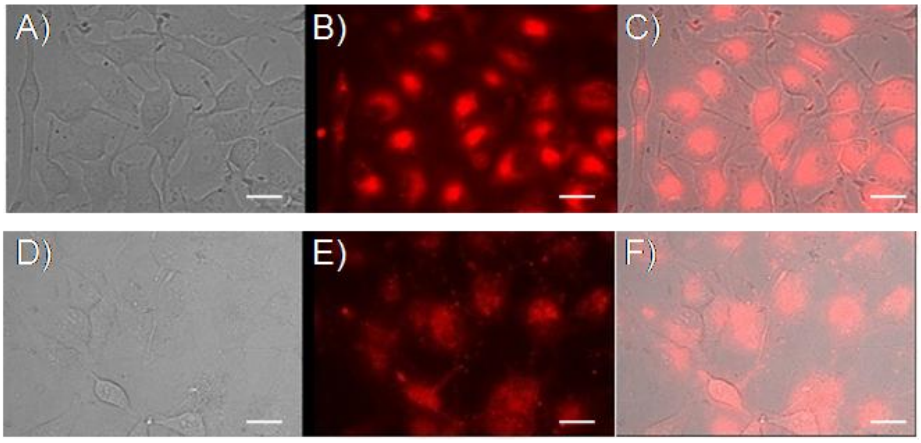

Figure 2.13. Live SKMEL-28 cells stained with 3 μM of Zn-DIGP or DIGP for 3 hours. **A) & D)** Brightfield image. **B)** Zn-DIGP fluorescence (Ex = 620 nm, Em = 700 nm). **E)** DIGP fluorescence (Ex = 620 nm, Em = 700 nm). **C)** Composite image of A) – B). **F)** Composite image of D) -E). Scale bars represent 15 μm.

One possibility for achieving better imaging results is to use fixed cells. Cell fixation is a popular method to identify the localization of probes while the cells are supposedly maintained in a static state. Although cellular dynamics are compromised, the precise localization of molecules can reveal cellular targets. Cells were therefore fixed using para-formaldehyde (PFA) and then treated with DIGP or Zn-DIGP.

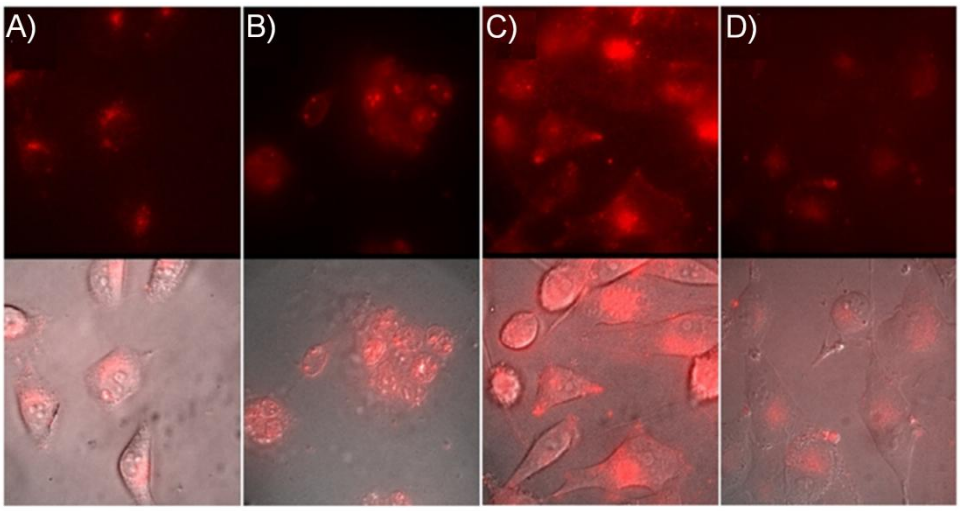

Figure 2.14. Wide-field fluorescence microscopy images of living A) HeLa, B) MCF7, C) SKMEL-28 cells treated with 3 µM of Zn-DIGP in PBS for 2 hours. D) SKMEL-28 cells treated with 10 µM of Zn-DIGP in supplemented RPMI media for 2 hours.

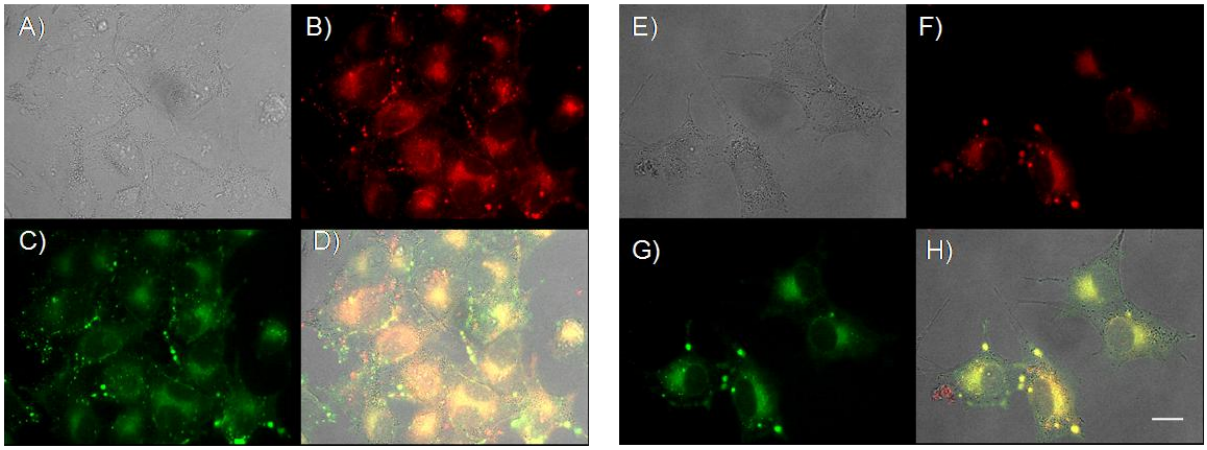

Figure 2.15. Live cell images of SKMEL-28 cells treated with Zn-DIGP (A-D) or DIGP (E-F). Initial incubation with 60 nM of lysotracker (Ex = 490 nm, Em = 520 nm) (C & G) for 90 minutes and Zn-DIGP or DIGP (Ex = 620 nm, Em = 700 nm) (B & F) for 3 hours. A) and E) are bright-filed images. D) and H) provide overlays. Images taken in wide field microscope. Scale bars represent 30 µm.

The addition of Zn-DIGP to fixed cells results in staining of perinuclear and nuclear regions. DIGP, in contrast, specifically localizes to the nucleus of fixed cells (Figure 2.16). Binding of DIGP to double stranded DNA in these cells is indicated by a competition experiments where the fixed cells were first treated with DIGP for 3 hours followed by addition of duplex specific dye Hoechst 33342. As shown in Figure 2.17, the addition of Hoechst 33342 causes relocalization of DIGP to the nucleolus and cytoplasm. Such relocalization was not observed

for Zn-DIGP (Figure 2.18). Consistent with *in vitro* binding assays (Figure 2.9), these results demonstrate that DIGP binds to cellular duplex DNA while Zn-DIGP does not.

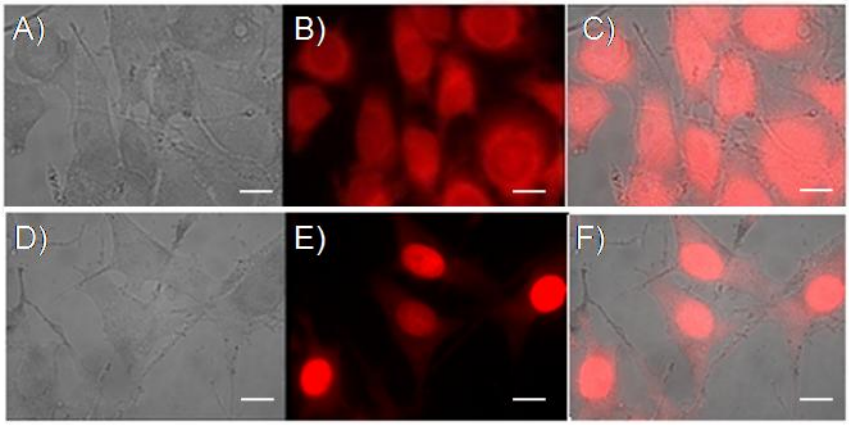

Figure 2.16. Fixed SKMEL-28 cells stained with 3 μM of DIGP or Zn-DIGP for 3 hours. A) & D) Bright field image. B) Zn-DIGP fluorescence (Ex = 620 nm, Em = 700 nm). E) DIGP fluorescence. C) Composite image of A) – B). F) Composite image of D) - E), Scale bars represent 30 μm.

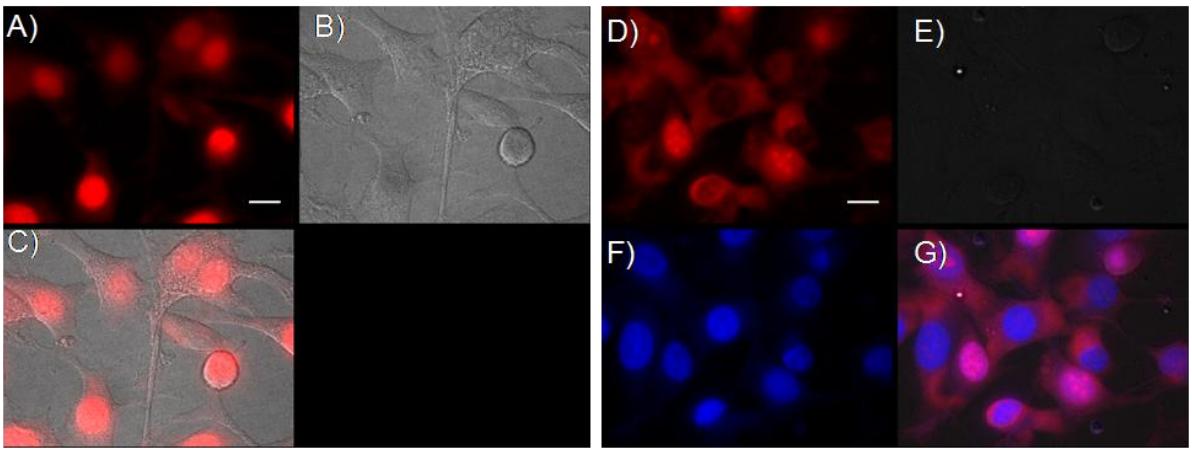

Figure 2.17. Fixed SKMEL-28 cells treated with 3 μM of DIGP for 3 hours before (A-C) and after addition of Hoechst 33342 (D-G). A) and D) Fluroescence of DIGP (Ex = 620 nm, Em = 700 nm); B) and E) Bright field-images F) Fluorescence of Hoechst 33342 (Ex = 360 nm, Em = 470 nm); C) and G) Composite images of bright-field and fluorescence. Scale bars represent 30 μm.

Zn-DIGP has much lower dissociation constant for binding G-quadruplex (K_d < 2 nM) than the concentrations used for these cell-staining experiments (3 μM). Fixed cells were therefore treated with variable concentrations (3 μM, 300 nM and 30 nM) of Zn-DIGP or DIGP and imaged using fluorescence microscopy. Consistent with initial studies, 3 μM of Zn-DIGP stains mostly the peri-nuclear region of fixed cells, but 300 nM caused staining of the nucleolus (Figure 2.19). Cells treated with 30 nM of Zn-DIGP exhibited weak fluorescent

staining, similar in magnitude to the auto-fluorescence of SKMEL-28 cells. Consistent with *in vitro* binding assays (Figure 2.9), DIGP can bind weakly to duplex DNA. When treated with 3 µM and 300 nM of DIGP, nuclear staining was observed (Figure 2.19 D-E). Cells treated with 30 nM of DIGP, in contrast, exhibited irregular staining of the cell surface (Figure 2.19 F).

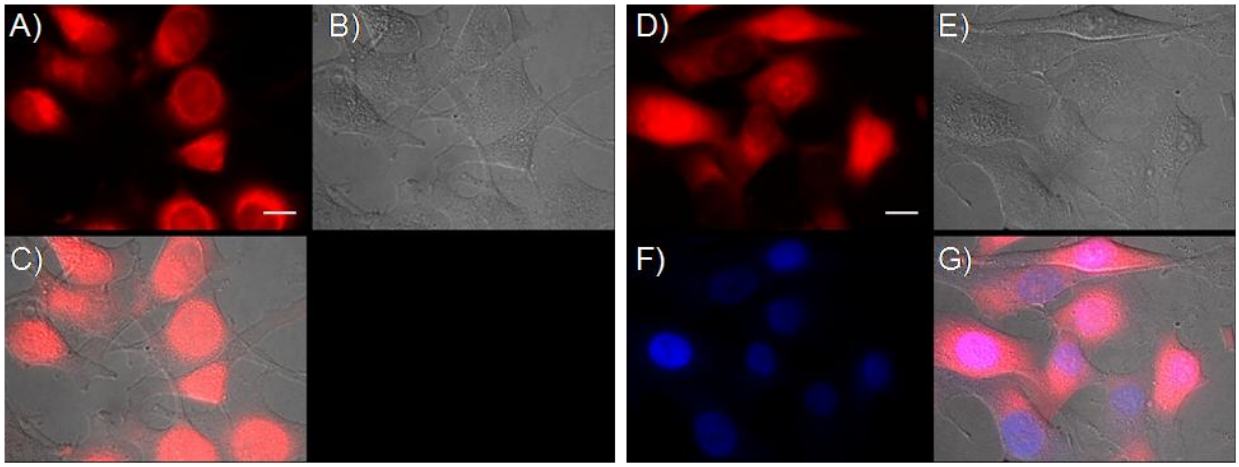

Figure 2.18. Fixed SKMEL-28 cells treated with 3 µM of Zn-DIGP for 3 hours, before (A-C) and after addition of Hoechst 33342 (D-G). A) and D) Fluorescence of Zn-DIGP (Ex = 620 nm, Em = 700 nm); B) and E) Bright field-images F) Fluorescence of Hoechst 33342 (Ex = 360 nm, Em = 470 nm); C) and G) Composite images of bright-field and fluorescence.

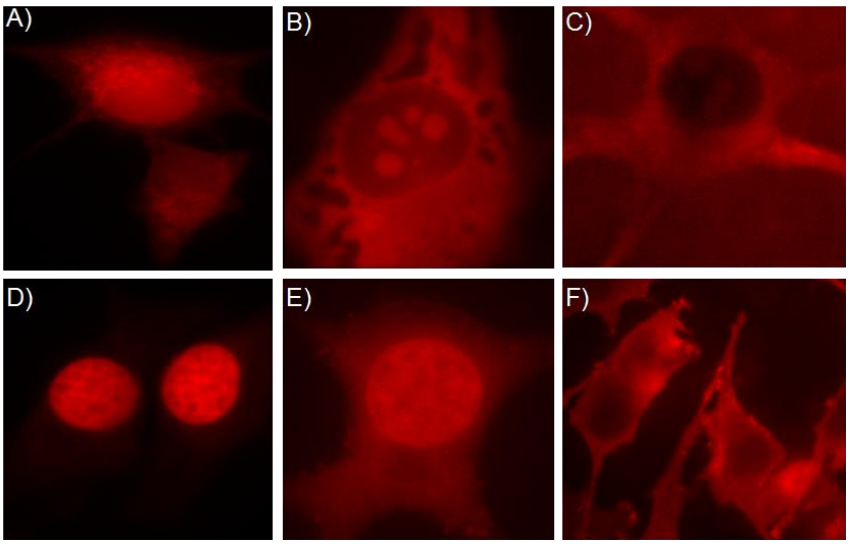

Figure 2.19. Wide-field fluorescence microscopy images of fixed SKMEL-28 cells treated with Zn-DIGP (3 µM (A), 300 nM (B), 30 nM (C)) or DIGP (3 µM (D), 300 nM (E), 30 nM (F)) for 3 hours.

2.2.6. Microarray analyses

As the cellular imaging studies did not provide direct evidence for the ability of Zn-DIGP or DIGP to specifically stain G-quadruplex DNA inside living cells, we used an indirect approach to test for the presence of G-quadruplexes in the promoter regions of genes. Prof. Hurley and coworkers previously reported that G-quadruplex sequences located in the promoter regions of oncogenes can be involved in gene regulation.[12] To provide a relatively unbiased approach for identifying the Zn-DIGP's ability to regulate global gene transcription, microarray analyses were performed. It was expected that the results from the microarray analyses could be correlated with the presence of putative G-quadruplexes in the promoter region of each gene.

Microarray analysis is already recognized as a powerful technique to identify the impact of genotoxic compounds. As previously reported for cisplatin,[14] experiments were conducted using B16F10 cells in media containing 2% fetal calf serum (FCS). mRNA was harvested from cells grown in the presence/absence of Zn-DIGP, DIGP, or cisplatin. Extracted mRNA was subjected cDNA synthesis using a Cy3- or Cy5- labeled primer (Table 2.3). The cDNA was then subjected to hybridization with Agilent whole-genome mouse arrays and fluorescence intensities were collected in a scanner.

A summary of microarray results are shown in Figure 2.20. Each dot in these graphs represents a single gene. The dots in the region of the diagonal line are the genes that show no changes in expression levels. The genes above and below the diagonal line represent upregulated genes and downregulated genes, respectively. The number of genes that exhibit changes in gene expression of 2-fold or more relative to untreated samples is provided in Table 2.3. As reported previously, cisplatin treatment causes 2-fold changes in expression for more than 750 genes, whereas Zn-DIGP affected the expression of only 40 genes. A second trial using primers with inversion of the Cy3/Cy5 used in cDNA synthesis revealed only 24 genes with 2-fold changes in expression upon Zn-DIGP addition. Among the two Zn-DIGP trials, only 2 genes were found to be consistent: Sqstm1 and CXCL10. Both of these genes lack G-quadruplex motifs in their promoter regions, 5`- and 3`-UTRs. In addition, database search for the presence of G-quadruplex forming motifs among all positive hits in both trials revealed no correlation between the presence of G-quadruplex forming sequences in the promoters and changes in gene expression.

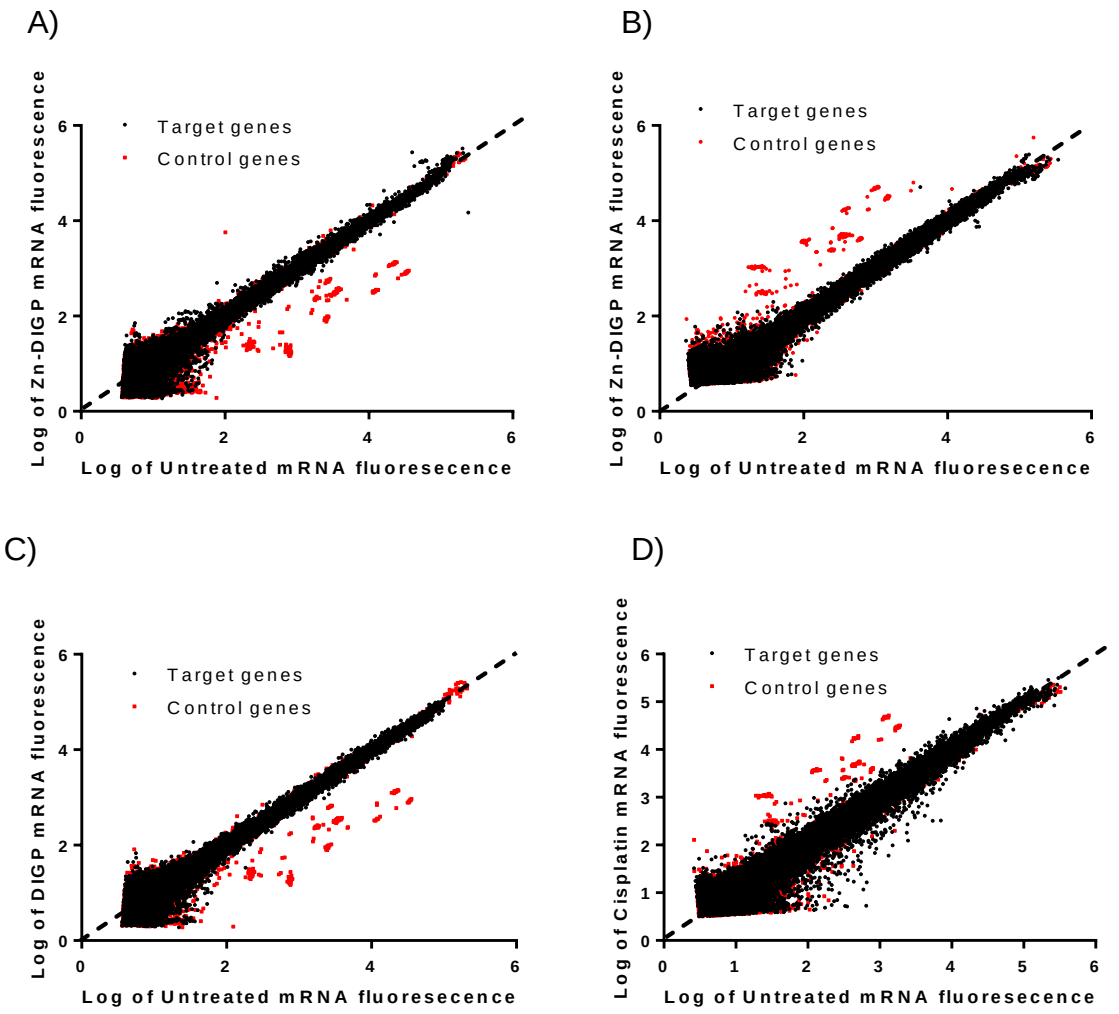

Figure 2.20. Dot plots of microarray analysis after (A and B) Zn-DIGP-, (C) DIGP- and (D) cisplatin-treatment of B16F10 cells for 24 hours.

Compounds	Cy 3	Cy 5	Total	Upregulated	Downregulated
Zn-DIGP -1	Untreated	Zn-DIGP	52	42	10
DIGP	Untreated	DIGP	24	14	10
Cisplatin	Cisplatin	Untreated	743	230	513
Zn-DIGP -2	Zn-DIGP	Untreated	28	10	18

Table 2.3. Summary of total number genes that show at least 2-fold changes in mRNA levels after treatment with Zn-DIGP, DIGP, or cisplatin in B16F10 cells.

2.2.6. qRT-PCR

The results of microarray analyses were further evaluated by quantitative real time PCR (qRT-PCR). These studies confirmed that Zn-DIGP causes 2-fold overexpression of CXCL10, but no change in SQSTM1.

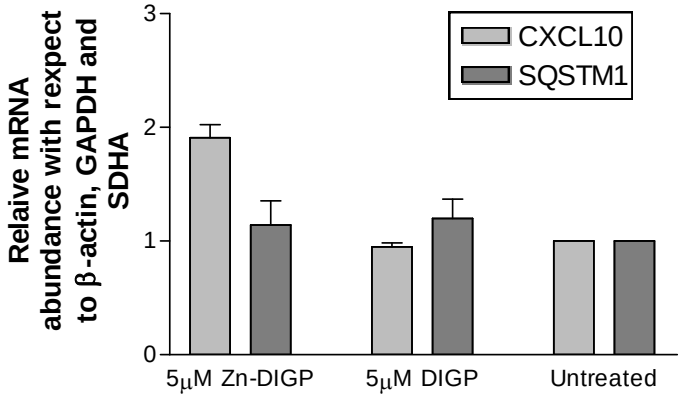

Figure 2.21. Relative mRNA expression levels of CXCL10 and SQSTM1 according to qRT-PCR in B16F10 cells treated with DIGP or Zn-DIGP for 24 hours.

Further qRT-PCR experiments revealed that Zn-DIGP-mediated changes of CXCL10 mRNA were both dose dependent and time dependent (Figure 2.22). The biological importance of this discovery is presented in Chapter 4.

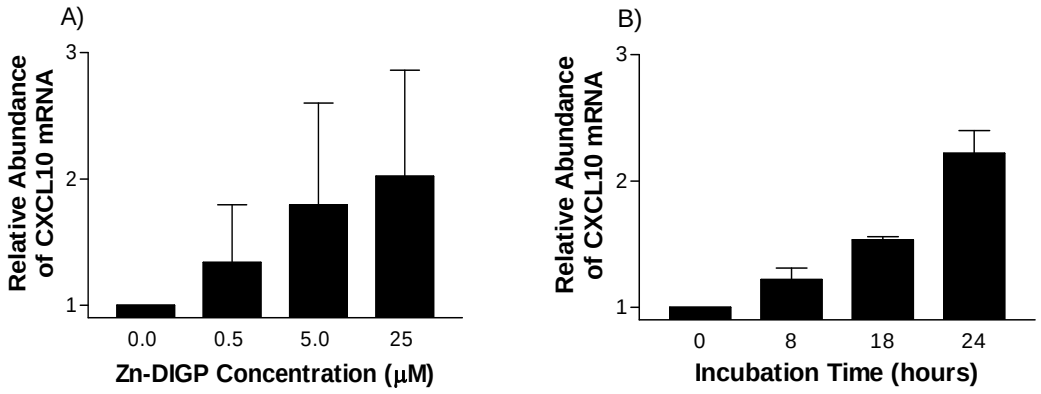

Figure 2.22. Changes in relative CXCL10 mRNA abundance according to qRT PCR. A) Zn-DIGP concentration-dependent changes after 24 hours of treatment. B) Time-dependent changes in mRNA abundance in the presence of 5 μM of Zn-DIGP. The results are with respect to untreated cells and normalized to two different housekeeping genes (β-actin and SDHA).

Having confirmed the microarray "hit" of CXCL10 for Zn-DIGP treated cells, the conspicuous absence of "hits" for genes reported to have functional G-quadruplex sequence

(PQS) in their promoter regions was tested next. Changes in the expression of selected genes such as MMP-2, MTA-1, RB1, VEGF and c-Myc (Table 2.4) were evaluated using qRT-PCR upon addition of variable concentrations of Zn-DIGP to B16F10 cells.

No	Gene	Gene location	TSS	TES	Sequence (5`-3`)
1.	MMP-2	Promoter	-68		GGGCGAGTAGGGGGGTGGGGCAGAG AGGGGCGGG
		Promoter	-40		CCCGAGTGCGCCCCCCGCCCCCAGCCCC
		3`UTR		-1009	CCCAGGCGCCCCTTCCCCCTCCAAT CCCACCAACCC
		3`UTR		-508	CCCGCTCAGCCCTCCCTGCCCCTCCC
2.	MTA-1	Promoter	-257		GGGGCACAGGGAGGGATCACCAGGG
		Promoter	-90		GGGAAGGGGCGCGCGGGCCGCG GGCGGCGCGGGG
		Promoter	-36		CCCGAGGCCCCTCCCCGCCGCCC
		3`UTR		-389	CCCCCCGCCCCTCGCCCG CCCACACGGCCCCTTCCCAG CCAGCCCGCCGCCCGCCCC
3.	RB1	Promoter	-530		CCCCACAGCTCCCTCCCTTCCTTTCCC
4.	VEGFA	Promoter	-388		CCCTCTCCCCACCCGTCCC
		Promtoter	-58		GGGGCGGGCCGGGGGCGGGGTCC CGGCGGGG
		3`UTR		-413	CCCTCCCCGATCCCCTGGCTCCCC

Table 2.4. Positions of putative G-quadruplex forming motifs and their sequences present in the promoter regions of different oncogenes. TSS: Transcription start site; TES: Transcription end site.

As shown in Figure 2.23, 5 μM of Zn-DIGP caused only small increases in MMP-2, MTA-1 and RB1 over expression of MMP-2, MTA-1, and RB-1. However, none of these changes were dose dependent. Since c-Myc is a well studied model system for G-quadruplex-dependent transcriptional regulation,[12] time dependent studies using various doses of Zn-DIGP and DIGP were performed in B16F10 cells. Addition of 25 μM of DIGP to B16F10 for 48 hours caused decreased c-Myc mRNA abundance. Since this concentration is close to the EC_{50} of DIGP (35 μM), we concluded the effect is probably G-quadruplex independent.[12]

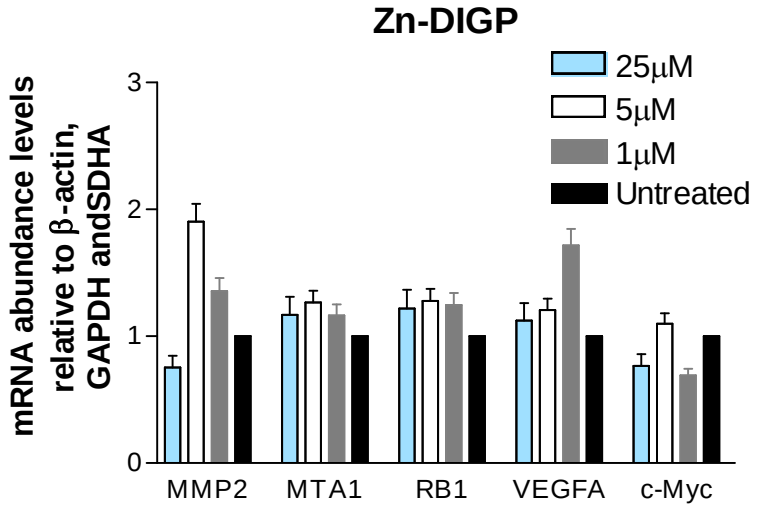

Figure 2.23. Changes in mRNA abundance of selected oncogenes according to qRT-PCR upon addition of various concentrations of Zn-DIGP for 24 hours in B16F10 cells.

To address the possibility of cell type-specific effects, dependency on cell lines, we decided to evaluate the ability of Zn-DIGP and DIGP to effect c-Myc gene expression in SKMEL-28 cells. As shown in Figure 2.25, Zn-DIGP and DIGP did not cause any significant changes in the c-Myc mRNA levels as compared to untreated samples.

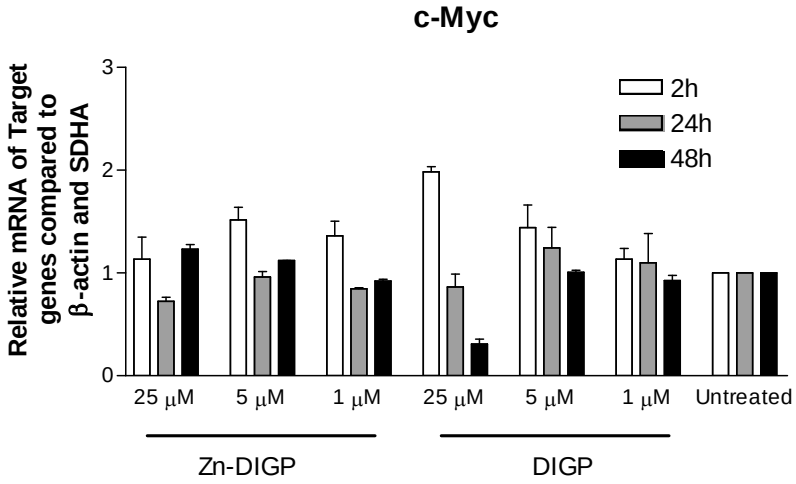

Figure 2.24. Relative levels of c-Myc mRNA according to qRT-PCR following addition of different concentrations of Zn-DIGP-/DIGP- to B16F10 cells for 2, 24 or 48 hours.

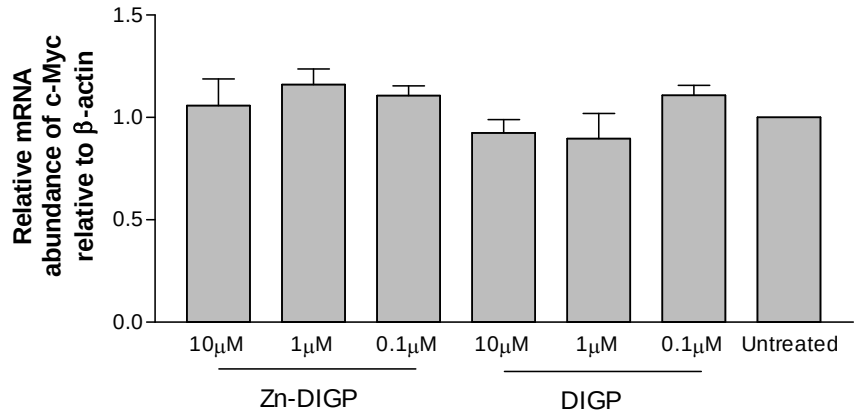

Figure 2.25. Relative levels of c-Myc mRNA according to qRT-PCR upon addition of Zn-DIGP-/DIGP- to SKMEL-28 cells for 24 hours.

2.3. Ammonium phthalocyanines

In contrast to previously-reported studies using TmPyP4 (**20,** Chapter 1),[15] Zn-DIGP and DIGP did not exhibit the ability to affect gene expression in a G-quadruplex-dependent fashion. However, the limited number of mRNA changes according to microarray analyses prevented any statistically-meaningful conclusion. Therefore, we decided to evaluate ammonium phthalocyanine derivatives (Figure 2.26). It has been previously reported that octa-ammonium phthalocyanines are G-quadruplex ligands (K_d = 120 nM).[16] These compounds can cause a G-quadruplex conformational change from anti-parallel to parallel structures and can induce G-quadruplex folding in the absence of potassium ions.[17] No cell-based studies of the octa-ammonium phthalocyanines were reported. Recently, Duan and coworkers reported "Zn-APc" (**9**) and showed it binds with duplex DNA with moderate affinity (K_a =1.33 x 10^5 M^{-1}).[14] However, no evaluation of its potential ability to selectively bind to G-quadruplex DNA was reported.

2.3.1. Synthesis

Tetra(trimethylammonio)phthalocyanato zinc tetratrifluoroacetate (Zn-APc, **9**) and tetra (trimethylammonio)phthalocyanato tetratrifluoroacetate (APc, **11**) were synthesized as illustrated in Figure 2.26. Macrocycle **7** was synthesized by molybdenum catalyzed macrocyclization. It was then reduced using Na_2S to give **8**. Methylation of each amino group was achieved using excess of CH_3I in DMF to give Zn-APc (**9**). This product was heated at

high temperature in pyridine HCl to give the metal-free product (**11**). Synthesis and purification of **9** and **11** were performed by Raul Pereira (Figure 2.26).

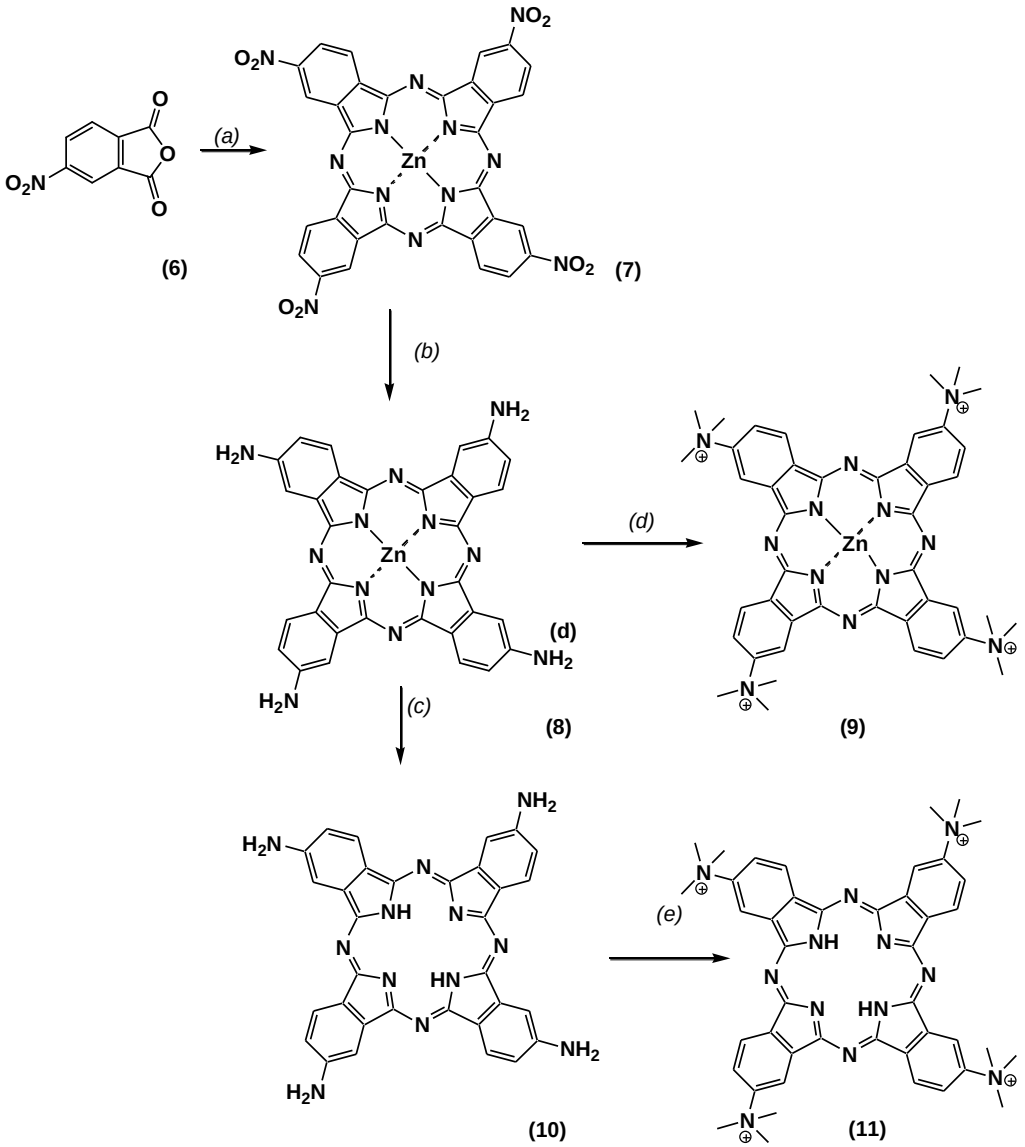

Figure 2.26. Synthetic route for the synthesis of zinc (Zn-APc) and zinc-free quaternary ammonium phthalocyanines (APc). Reagents and conditions: (a) zinc chloride (0.25 equiv), ammonium molybdate (0.1 mol %), nitrobenzene, 185 ^{o}C, 4 h, 98%; (b) sodium sulfide (12 eq), DMF, 60 ^{o}C, 1.5 h, 75%; (c) pyridine/pyridinium-HCl, 120 ^{o}C, 17 h; (d and e) excess of methyl iodide, DMF, 25 ^{o}C, 51h

2.3.2. Binding studies

Fluorescence-quenching assays were performed as described in Section 2.2.3 with Zn-APc and APc. Zn-APc displayed high affinity for G-quadruplex DNA (Figure 2.27). The binding isotherm was identical in the presence or absence of a 1'000-fold excess calf thymus DNA, suggesting excellent specificity of Zn-APc to G-quadruplex DNA. The addition of tRNA caused a small reduction in apparent G-quadruplex affinity. The dissociation constants are

summarized in Table 2.5. Together with the similar results obtained for Zn-DIGP (Figure 2.9), these data demonstrate that the substituents on the phthalocyanine scaffold do not have a dramatic influence on the G-quadruplex binding affinity or specificity *in vitro*.

Interestingly, APc displayed a 5-fold higher affinity for G-quadruplex DNA than DIGP (Figure 2.9). In addition, a smaller loss in apparent binding affinity was observed for APc in the presence of competitor nucleic acids (Figure 2.27 B) as compared to DIGP (Figure 2.9).

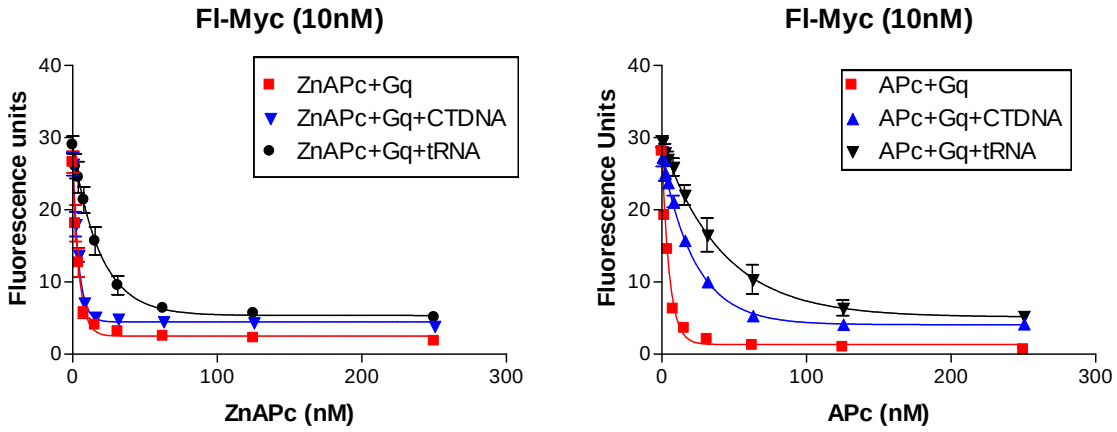

Figure 2.27. Fluorescence quenching of 10 nM solution of the 5`-fluroescein labeled c-Myc DNA by Zn-APc and APc in the presence of 1'000-fold excess of calf thymus DNA or 100-fold excess of tRNA.

S.No	Compound	K_d (nM)		
		c-Myc	c-Myc + CT DNA	c-Myc + tRNA
1	Zn-APc	< 2	< 2	21.3 ± 3
2.	APc	< 2	27 ± 2	53 ± 5

Table 2.5. Binding affinity and selectivity of Zn-APc and APc to c-Myc G-quadruplex in the presence of duplex DNA and tRNA.

2.3.3. Cytotoxicity studies

To identify suitable concentrations for cell-based studies, the toxicity of Zn-APc and APc was evaluated using resazurin-based cytotoxicity assays in B16F10 cells. The results demonstrate that Zn-APc and APc exhibited little or no toxicity upto 80 µM (Figure 2.28).

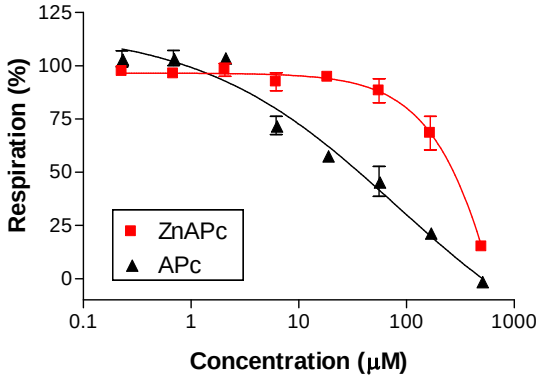

Figure 2.28. Cellular respiration of B16F10 cells upon treatment with Zn-APc and APc for 24 hours.

2.3.4. Cellular Localization

Since Zn-APc and APc were not toxic in the low-micromolar range, their ability to probe G-quadruplex DNA in cells was assayed using fluorescence microscopy. Similar to Zn-DIGP and DIGP, Zn-APc and APc were also pro-fluorescent and they could be simply added to cells and imaged directly. Depending on the concentration of the molecules and whether living or fixed cells were used, Zn-APc and APc show variable localization. In live cells, Zn-APc and APc did not reveal any detectable fluorescence in the cells (Figure 2.29 and Figure 2.30). Brief exposure of light (few seconds) from the microscope cause increased fluorescence, and longer exposure times caused the cells to undergo morphological changes consistent with phototoxicity. The reasons of morphological changes could be due to the ability of Zn-APc and APc to behave as photosensitiers.

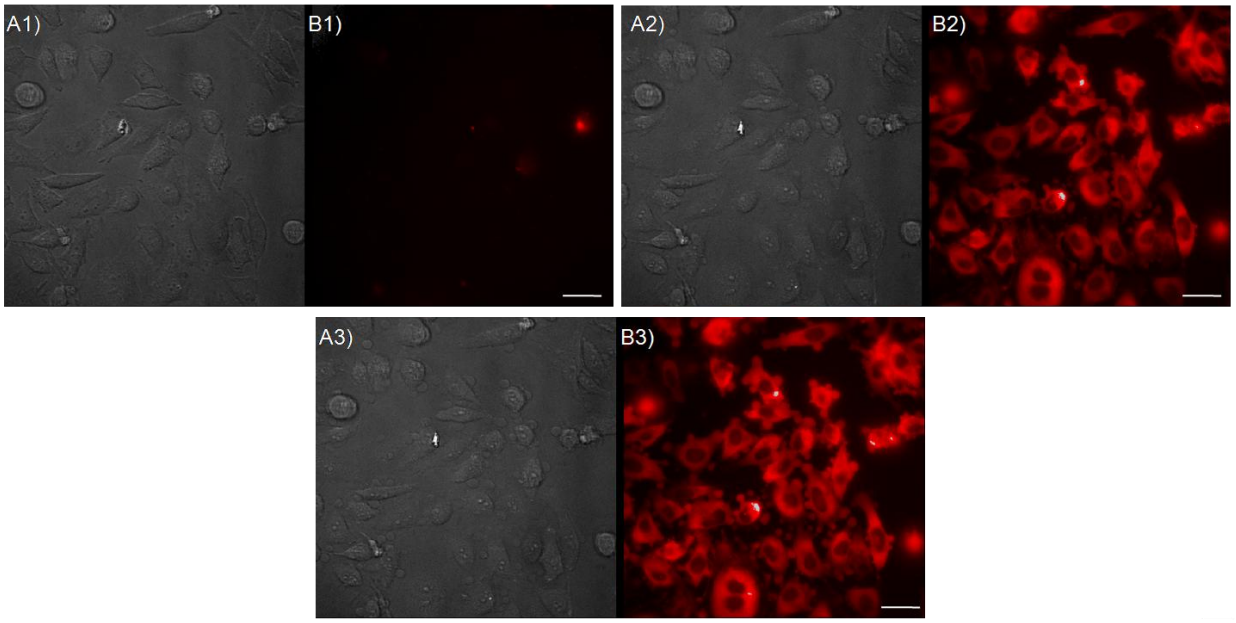

Figure 2.29. Imaging of live HeLa cells upon treatment with 3 μM of Zn-APc for 3 hours. A: Bright field images B: fluorescence images (Ex = 620 nm, Em = 700 nm). Images 1-3 demonstrate the effects of increasing light exposure from the microscope. Scale bars represent 30 μm.

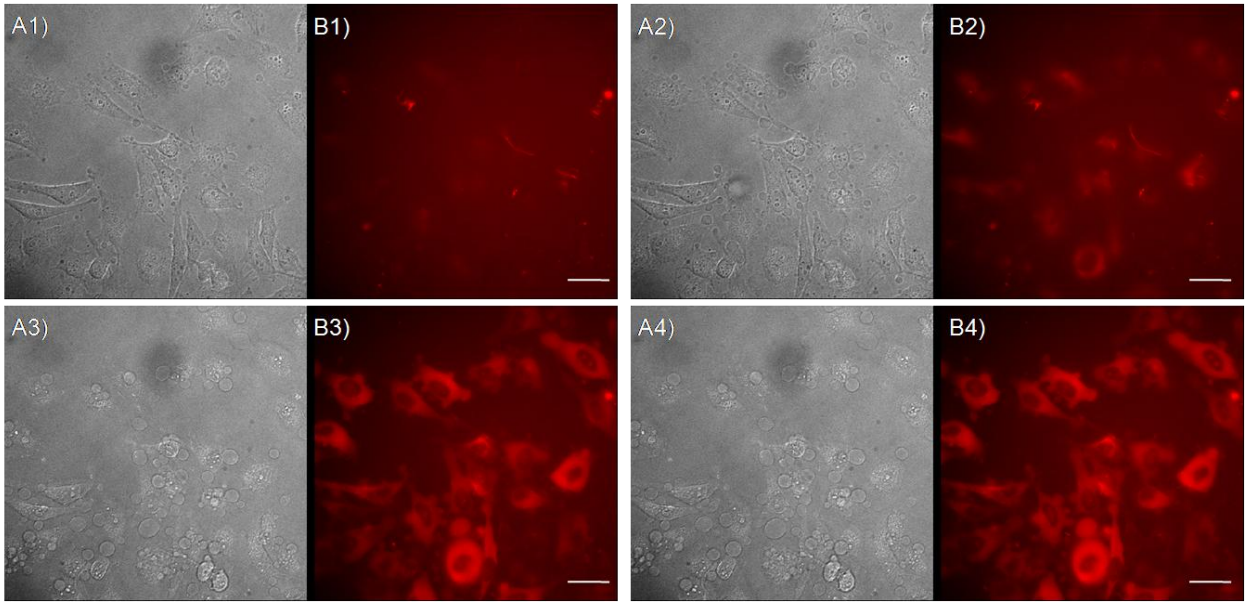

Figure 2.30. Imaging of live HeLa cells upon treatment with 3 μM of APc for 3 hours. A: Bright field images B: fluorescence images (Ex = 620 nm, Em = 700 nm). Images 1-4 demonstrate the effects of increasing light exposure from the microscope. Scale bars represent 30 μm.

The ability of Zn-APc and APc to behave as fluorescent probe was then evaluated in fixed SKMEL-28 cells. Interestingly, the addition of 3 μM, 300 nM and 30 nM of Zn-APc results

in nucleolar staining, while the addition of 3 μM and 300 nM of APc causes nuclear staining. At 30 nM, APc causes nucleolar staining (Figure 2.31).

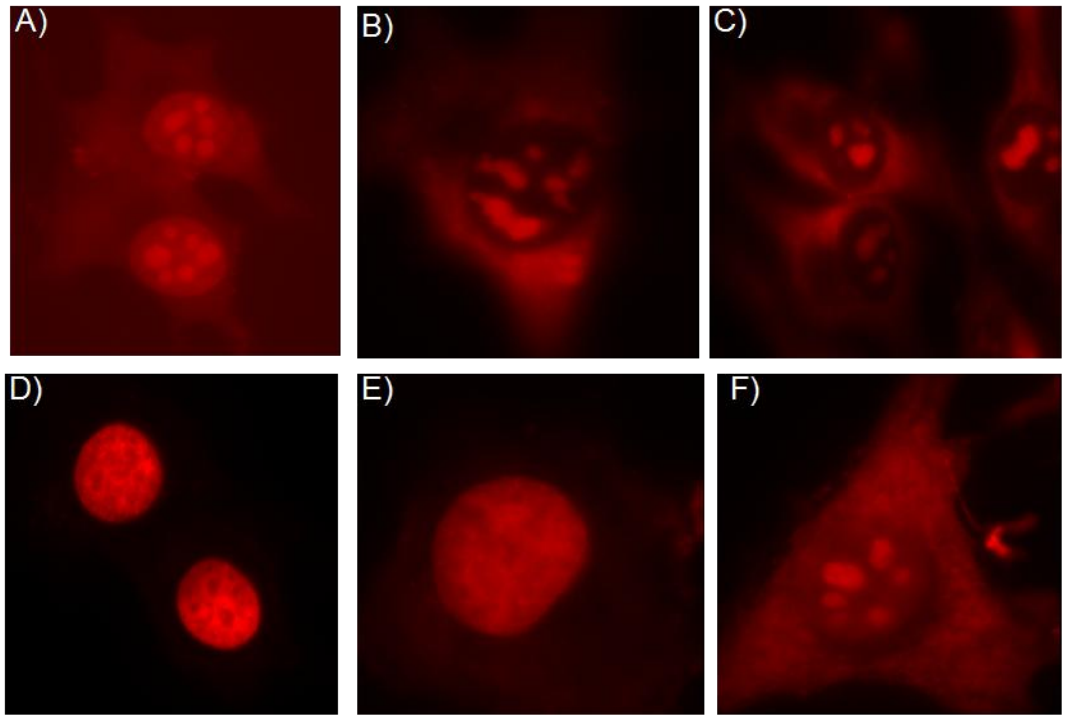

Figure 2.31. Wide field microscopy images of fixed SKMEL-28 cells treated with Zn-APc (3 μM (A), 300 nM (B), 30 nM (C)) or APc (3 μM (D), 300 nM (E), 30 nM (F)) for 3 hours. Images were collected using Ex = 620 nm, Em = 700 nm.

2.3.5. DNAse/RNAse digestion

Zn-APc was localized in nucleolus which is known to contain repetitive G-rich sequence.[18] In fixed cells, we speculated that Zn-APc may bind to G-quadruplex structures formed from the rDNA repeats. To test this hypothesis, fixed cells were subjected to DNAse and RNase treatment, followed by 30 nM of Zn-APc for 3 hours. As a control, the double stranded DNA specific dye Hoechst 33342 was also included. As expected, the DNase treated cells show diminished staining by Hoechst 33342 whereas RNase-treated cells still show strong nuclear staining by Hoechst 33342 (Figure 2.34; blue color). When Zn-APc was added to DNase treated cells, it was localized in nucleolus, similar to control cells. The addition of Zn-APc to RNAse-treated cells resulted in nuclear, not nucleolar, staining. These results suggest that Zn-APc prefers to bind RNA contained within the nucleolus in fixed SKMEL-28 cells (Figure 2.32).

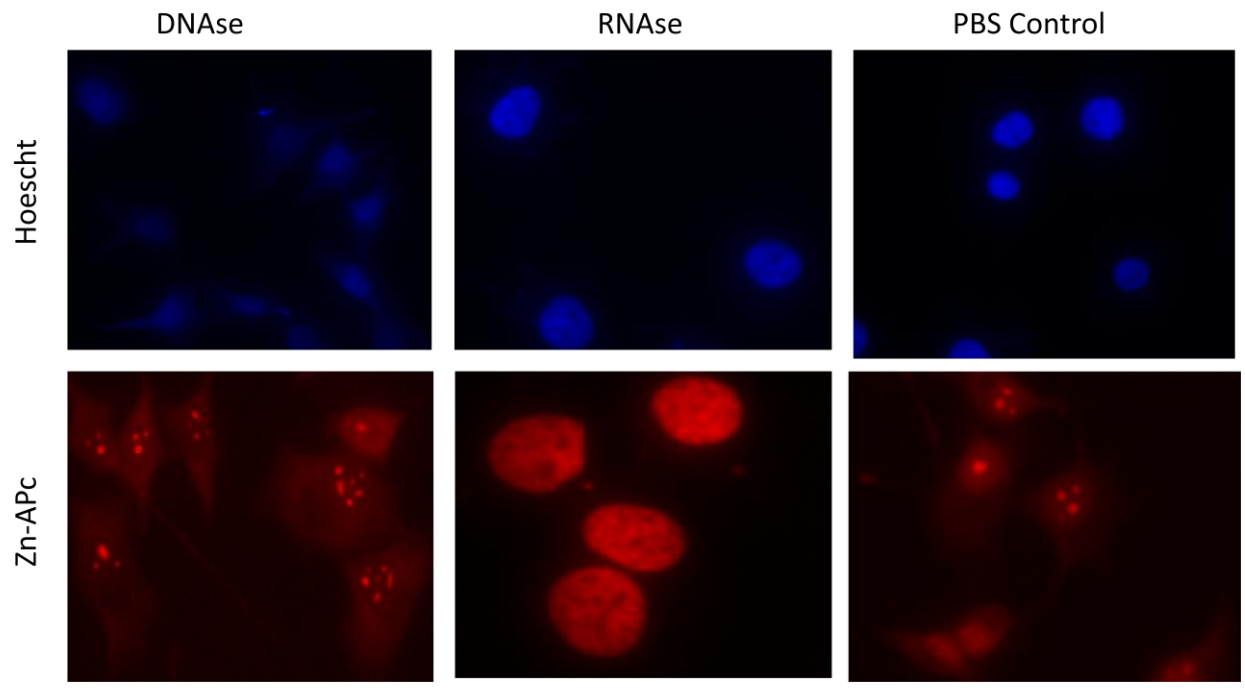

Figure 2.32. DNase and RNase digestion of fixed SKMEL-28 cells followed by addition 20 μM of Hoechst 33342 and 30 nM of Zn-APc for probing localization. Blue represents nucleus specific dye Hoechst 33342 (Ex = 360 nm, Em = 470 nm), Red represents Zn-APc (Ex = 620 nm, Em = 700 nm).

2.3.6. Microarray analyses

To probe promoter G-quadruplexes using Zn-APc and APc, we conducted global gene RNA expression analysis in B16F10 cells treated with 5 μM of Zn-APc or APc for 24 hours in media containing 2% FCS. The mRNA was extracted from treated and untreated samples, and subjected to cDNA synthesis using labeled primers (Table 2.6). The labeled cDNA samples were then allowed to hybridize to whole genome mouse arrays from agilent, and the fluorescence intensities of Cy3 and Cy5 were recorded with a scanner.

Cy 3	Cy 5
Zn-APc-1	Untreated 1
APc -1	Untreated 1
Zn-APc-2	Untreated 2
APc-2	Untreated 2

Table 2.6. cDNA labels used in microarray analyses.

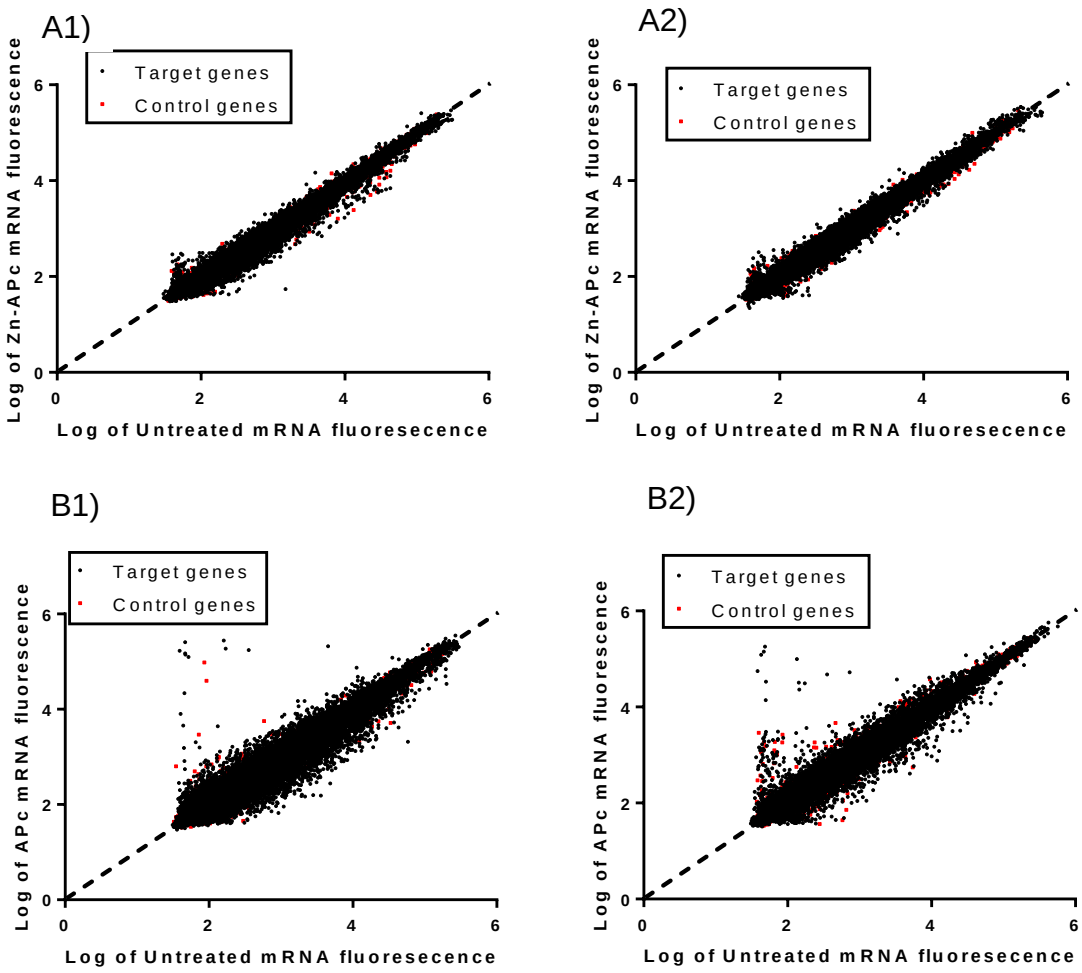

Figure 2.33. Microarray analyses of two different trials of Zn-APc (A1&A2) and APc (B1&B2) treated B16F10 cells.

A summary of these microarray analyses is depicted in Figure 2.33. Each dot represents one gene and the diagonal line represents no changes in RNA expression between treated and untreated samples. The genes above and below the diagonal line indicate higher or lower RNA quantities as compared to untreated samples, respectively. The dots further from the diagonal indicate larger changes that were observed mostly for APc-treated samples (Figure 2.33B). The number of genes that exhibited at least 2-fold changes in RNA expression upon addition of Zn-APc and APc addition are shown in Table 2.7. Only the genes that showed significant expression ($p < 0.001$) between both trials are included.

>2-fold	Up-regulated	Down-regulated	Total
Zn-APc	12	287	299
APc	798	1302	2102

Table 2.7. Results of microarray analyses summarizing the number of genes with 2-fold or larger changes in mRNA expression upon addition of Zn-APc or APc to B16F10 cells.

Genes that exhibited 2-fold or larger changes in mRNA expression were analyzed for the presence of PQSs in their promoter regions, 5`-UTR, 3`-UTR using the quadparser database. This database contains information on whether a particular gene has PQS present in promoter, 5`UTR, or 3`UTR. The putative PQS consensus used for this analysis was $G_{3+}N_{1-7}G_{3+}N_{1-7}G_{3+}N_{1-7}G_{3+}$. The results demonstrate that almost 50% of the genes affected by Zn-APc contain at least one G-quadruplex forming sequence either in promoter, 5`-UTR or 3`-UTR. Some of the genes were uncharacterized and therefore not available in quadparser database (Table 2.8).

Location	Number of putative G-quadruplexes		
	Total	Down-regulated	Up-regulated
Promoter	99 (39%)	96	3
5`-UTR	12 (4.8%)	12	0
3`-UTR	39 (15.7%)	35	4
No G-quadruplex	127 (51%)	122	5
Uncharacterized genes	51	48	3

Table 2.8. The number of genes that contain G-quadruplex motifs that exhibit at least 2-fold changes in mRNA quantities upon addition of 5 μM of Zn-APc.

The hits for the presence of at least one PQS in the promoter region were analyzed further. The PQS frequency near the promoter was plotted against the distance from transcription start site (up to 1’000 bp). As shown in Figure 2.34, the results demonstrate that a high frequency of G-quadruplex motifs were present within 200 bp of the transcription start site (TSS). A similar pattern was observed for all genes containing at least one PQS in the promoter.[19] The enrichment of PQS proximal to TSSs could possibly indicate quadruplexes that functions as switches of transcription.[12, 19] However, if this model was accurate, the addition of G-quadruplex binder should affect PQS-containing promoters more frequently than promoters lacking a PQS. This was not observed. Only 39% of the 299 genes affected by

Zn-APc addition contained at least one PQS near the promoter. This value significantly lower than the 42% of all genes that contain at least one PQS within 1'000 bp of the TSS. The results suggest that Zn-APc did not regulate gene expression according to the promoter PQS model previously proposed. [12, 19]

Next, PQS were searched in the 3'-UTR and 5'-UTR in Zn-APc targeted genes that showed 2-fold changes. Unexpectedly, only 4% and 12.2% of the positive hits possessed PQS in 5`-UTR and 3'-UTR respectively. These values are less than the 12% and 15.3% reported to be present in all genes. These results suggest that Zn-APc-targeted genes were independent of the presence of G-quadruplex sequence present in the promoter, 3`-UTR, or 5`-UTR.

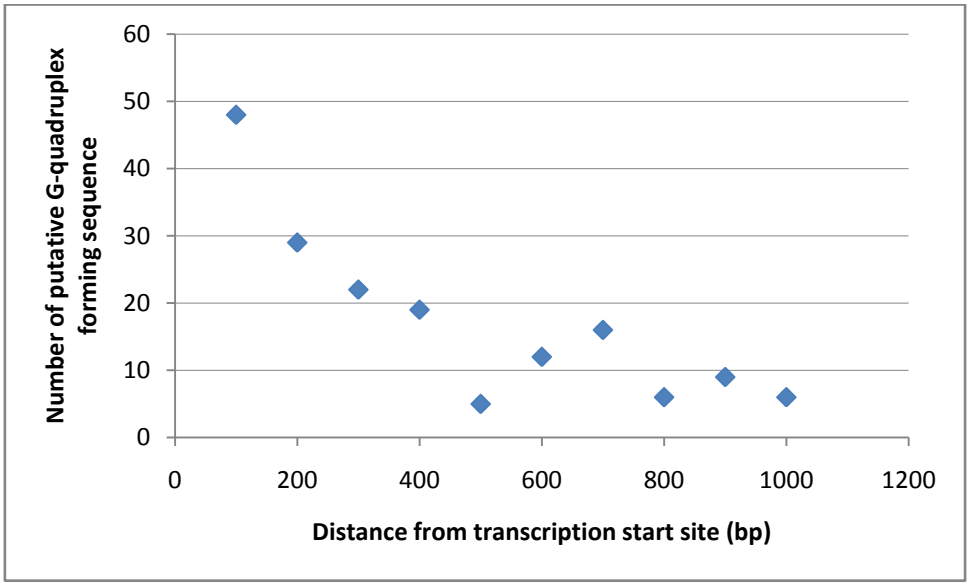

Figure 2.34. Graph showing the number of putative G-quadruplex motifs present in each of the 100 bp upstream of the transcription start site of 299 genes that exhibited 2-fold or larger changes in mRNA abundance upon addition of Zn-APc to B16F10 cells.

As shown in Figure 2.33, the addition of APc caused much larger changes in mRNA expression in B16F10 cells than Zn-APc. These results are summarized in Table 2.9 - 2.11. To make the data analysis more feasible, genes with a 3-fold or larger changes in mRNA abundance were analyzed for the presence of PQSs in their promoter regions, 5`-UTR and 3`-UTR using quadparser.

Results in Table 2.10 illustrate that out of 667 total genes, only 477 were characterized. Among the characterized genes, 188 genes have at least one "promoter" PQS within 1'000 bp upstream of the TSS (39%). This frequency was again lower than the overall frequency of

PQS from the TSS of all genes in the mouse genome.[20] A similar analysis of these 477 genes for PQS frequency in the 5`-UTR and 3`-UTR suggested that 5.6% and 13.4% of characterized genes affected by APc contain at least one PQS in 3`-UTR and 5`-UTR respectively. This frequency was again lower than the global frequency of all characterized genes containing at least one PQS in the promoter, 5`-UTR or 3`-UTR. Similar to Zn-APc, the results obtained with APc indicate that there is no correlation between the APc-targeted genes and PQS occurrence in the promoter, 3`-UTR, or 5`-UTR (Table 2.10).

Number of genes	Total	Down-regulated	Up-regulated
> 4-fold	172	102	70
> 3-fold	667	417	250
> 2-fold	2271	1404	867

Table 2.9. The total number of genes affected by 5 μM of APc in B16F10 cells according to microarray analyses.

Location	Number of genes		
	Total	Down-regulated	Up-regulated
Characterized genes	477	303	174
Promoter PQS	188 (39.4%)	134	54
5`-UTR PQS	28 (5.6%)	20	8
3`-UTR PQS	64 (13.3%)	11	53
No PQS	247 (51%)	140	107
Uncharacterized genes	190	114	76

Table 2.10. The number of genes that contain putative G-quadruplex motifs in the promoter regions that exhibit at least 3-fold changes in mRNA abundance upon addition of 5 μM of APc.

Location	Number of genes		
	Total	Down	Up
Characterized genes	125	77	48
Intron PQS	66 (52%)	46	20
Intron PQS – 1st 100 bp	22 (17.6%)	17	5
No PQS	59 (47.2%)	31	28
Uncharacterized genes	47	25	22

Table 2.11. The number of genes that contain putative G-quadruplex motifs in the introns that exhibit at least 4-fold changes in mRNA abundance upon addition of 5 μM of APc.

Previous studies have reported a 16% frequency of genes containing at least one PQS in the first 100 bp of the first intron. Maizels and coworkers proposed that G-quadruplex formation in these regions could potentially affect the completion of pre-mRNA transcription.[21] We therefore analyzed the genes affected by APc addition for PQS sequences present in the first intron (Table 2.11). Approximately 18% of the genes possess at least one PQS, this frequency is very similar to the genomic average (16%). So the addition of APc did not have bias on intron specific G-quadruplex mediated gene expression.

Among the APc affected genes, we speculated that the 39% of genes that possess a promoter PQS affected would be independent of 20% of genes that possess an intronic PQS. The genes that showed 4-fold changes in mRNA abundance were analyzed in this way. The genes that contain at least one promoter PQS, intronic and/or promoter PQS are represented by a Venn diagram. The results shown in Figure 2.35 demonstrate that no significant correlation was observed between APc targeted genes and their respective PQSs.

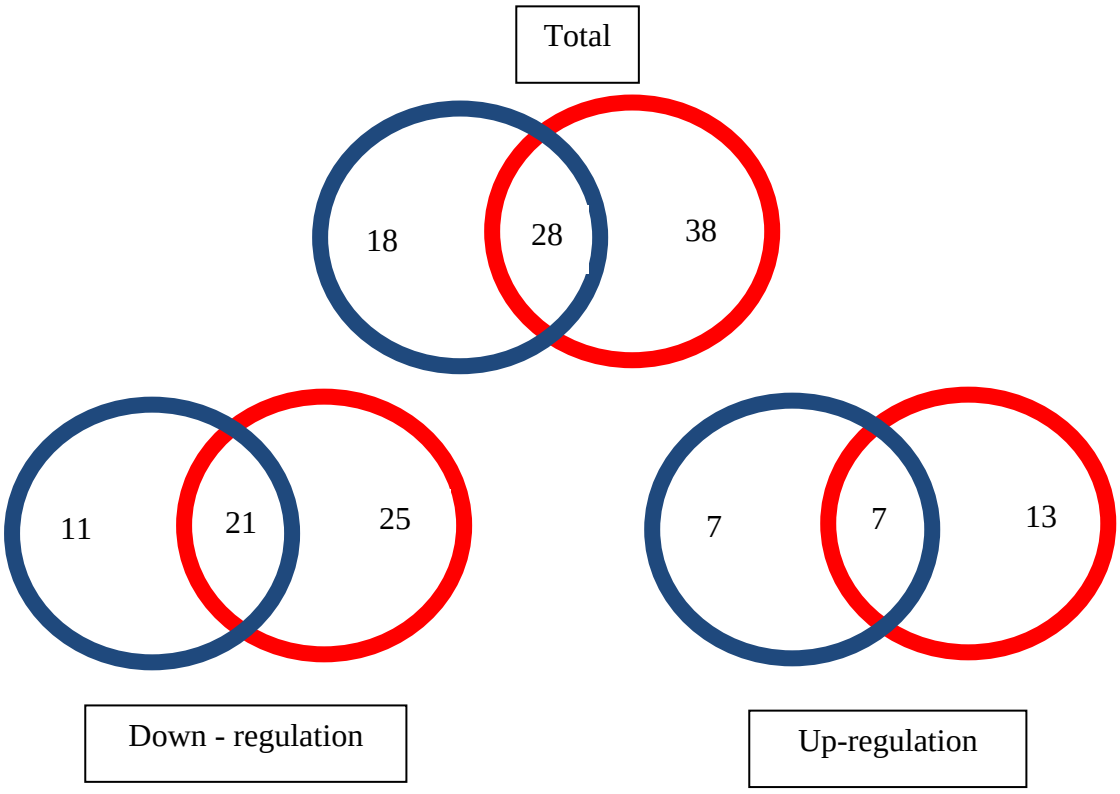

Figure 2.35. Venn diagram representing the number of genes affected by APc (> 4-fold) that have PQS in the promoter (Red), and first intron (Blue). Common genes are shown interjunction of two circles.

2.4. Conclusion

Zn-DIGP has favorable "turn-on" fluorescence properties. Zn-DIGP binds to G-quadruplex DNA with high affinity ($K_d \leq 2$ nM) and selectivity. DIGP is less selective than Zn-DIGP, as it binds to duplex DNA and tRNA. Zn-DIGP and DIGP are both capable of being taken up by living cells. Zn-DIGP was mostly localized in lysozomes of living cells, and in perinuclear regions of fixed cells. Microarray analyses were performed to identify the possible target genes of these compounds. Both Zn-DIGP and DIGP resulted in differential expression of only very few genes. Among which, only one gene: CXCL10 was consistently up regulated. No correlation was observed among the genes and putative G-quadruplex forming sequences in their promoters. The possible reasons for over expression of CXCL10 will be addressed in the Chapter 4.

Similar to Zn-DIGP and DIGP, Zn-APc and APc bind to G-quadruplex DNA with high affinity. They are also relatively non-toxic, cell permeable probes that localizes in peri-nuclear regions of living cells. In fixed cells, APc and Zn-APc stain RNA in the nucleolus. Microarray analyses resulted in as many as 299 genes for Zn-APc and 2'000 genes for APc that gave 2-fold or larger changes in mRNA expression. However, no correlation between the mRNA quantities and the presence of G-quadruplex forming motifs in promoter, intron, 5`UTR or 3`UTR was observed.

None of the four phthalocyanine molecules therefore provide evidence for G-quadruplexes as a regulatory element for gene expression in mammalian cells. These results call into question previous studies that have proposed G-quadruplex structures as gene regulators of mammalian cells.

2.5. Experimental Methods

2.5.1. Binding assays

DNA oligos (~30 μM) were heated in a "TKE" buffer containing 50 mM Tris-HCl (pH 7.4) 150 mM KCl, and 0.5 mM EDTA to 99 ^{o}C then slowly cooled to room temperature (over approximately 3 hrs) before use. tRNA Sigma Type X-SA was dissolved into TKE at room temperature and quantified using $\varepsilon = 9'640\ cm^{-1}\ M\ ntd^{-1}$ (25 ^{o}C). Type I, highly polymerized calf thymus DNA was dissolved into TKE at 37 ^{o}C overnight (12 hrs), centrifuged at 20'000 x g, and the supernatant diluted 2X into TKE buffer. The solution was then sonicated for 2 minutes in a TPC-15 bath sonicator from Telsonic Ultrasonics, and the solution quantified using $\varepsilon = 6'550\ cm^{-1}\ M\ ntd^{-1}$ (25 ^{o}C).

Oligo Name	Sequence	ε ($cm^{-1}M^{-1}$) (99 ^{o}C)	ε ($cm^{-1}M^{-1}$) (25 ^{o}C)
c-Myc	TGAGGGTGGGGAGGGTGGGGAA	229'900	160'900
Fl-cMyc	Flu-TGAGGGTGGGGAGGGTGGGGAA	262'400	193'400
Htelo	GTTA$(GGGTTA)_4$GG	306'900	276'200
Htelo-mut	GTTA$(GAGTTA)_4$GG	319'300	287'400
Htelo-C:	CC$(TAACCC)_4$TAAC	-	274'000
c-Myc-long:	$(G)_4A(G)_3T(G)_4A(G)_3T(G)_4AA(G)_2T(G)_4$	321'500	257'200
c-Myc-C:	$(C)_4A(C)_2TT(C)_4A(C)_3T(C)_4A(C)_3T(C)_4$	-	242'600

All titrations were conducted at room temperature in a "TKE" buffer containing 50 mM Tris-HCl (pH 7.4), 150 mM KCl, and 0.5 mM EDTA. Absorbance and emission spectra were collected using a SpectraMax MP5 spectrophotometer in Greiner Bio-one UV-Star 96-well plates (final volume = 200 μL). Fluorescence binding assays were conducted in Corning 384-well black polystyrene assay plates with non-binding surfaces (final volume = 80 μL). For absorbance and fluorescence enhancement experiments, a 2X solution of Zn-DIGP (2 μM or 20 nM) was added to the plate followed by one volume of DNA solution and mixed once by pipette. Plates were read multiple times to ensure equilibration was reached. Rapid equilibration of all binding interactions (after 30 minutes or less) was observed in all cases. For the fluorescence quenching experiments, color-free (natural) 1.7 mL polypropylene tubes (high clarity) obtained from Milian were used for making serial dilutions of each compound. An equal volume of Zn-DIGP and 20 nM solution of the fluorescein-containing DNA were mixed in a 384-well plate containing by pipetting exactly once. Measures had to be taken to circumvent some binding of Zn-DIGP to plastic tubes and pipette tips during their handling. This problem is most pronounced at concentrations below 100 nM and can be avoided by making two serial dilutions in the same plastic tubes. After incubating for one hour, the first dilutions were discarded and each tube kept for a second serial dilution. This pre-saturates each tube without increasing the concentration of Zn-DIGP. We have conducted this pre-saturation up to four times, but the same results were obtained after a single pre-saturation.

2.5.2. Cell Lines and Media

Murine metastatic B16F10 melanoma cell line were cultured in Dulbecco's modified Eagle's medium (DMEM; Invitrogen, Carlsbad, CA, USA) supplemented with 10% or2% heat-inactivated fetal calf serum (FCS) and 100 U/ml of penicillin (Sigma), 100 μg/ml of Streptomycin (Sigma). SK-Mel-28 cells were grown in *Roswell Park Memorial Institute medium* (RPMI) supplemented with 10% FCS, 2mM L-Glutamine, 100 U/ml of penicillin (Sigma), 100 μg/mL streptomycin (Sigma), and 1mM sodium pyruvate. All cell lines were grown in 5% CO_2 at 37°C. MCF-7 cells were grown in MEM media with 10% FCS, 2mM L-Glutamine, 100 U/ml of penicillin (Sigma), 100 μg/mL streptomycin (Sigma), and 1mM sodium pyruvate. SHSY5Y were grown in DMEM with supplemented with 10% heat-inactivated FCS and 100 U/ml of penicillin, 100 μg/ml of Streptomycin.

2.5.3. Cytotoxicity studies

B16F10 or SKMEL-28 cells (10'000 cells) were seeded in 96 well plates and grown for 24 hours prior to their incubation with variable concentrations of Zn-DIGP or DIGP for appropriate time (usually 24 hours). The cellular media were replaced with fresh media containing 86 µM resazurin (Sigma). Fluorescence was measured after 2-4 hours using M5 spectrophotometer with excitation at 560 nm, emission at 590 nm, and a 570 nm cutoff filter. All samples were compared to untreated cells to calculate the % decrease in respiration - from which EC_{50} were calculated.

2.5.4. Quantum Yields of Emission

Quantum yields for photoluminescence were calculated according to:

$$\Phi = \Phi_R \times {I}/{I_R} \times {OD_R}/{OD} \times {n^2}/{n_R^2}$$

Where Φ = quantum yield; R = reference; I = area of emission; OD = optical density; n = refractive index of solvent. As a reference compound, Cy5 (Φ = 0.27) in PBS was used.[1] DIGP derivatives were diluted into DMSO to an optical density of 0.014 - 0.02 at a common wavelength of excitation (620 nm). Background-corrected emission spectra were integrated between 630 – 800 nm using a Spectramax M5 spectrophotometer.

2.5.5. Microscopy

B16F10 cells (~15'000) were seeded in Labtek 8 chambered plate (Nunc) in media containing 10% FCS. After overnight growth, media was replaced with fresh media containing 3µM Zn-DIGP and incubated for 24 hours. Images of the unfixed cells were taken in Leica LX wide field microscope before irradiation and 3 hours following irradiation. For fixation, 3% PFA was added for 15 minutes and washed thrice with PBS. Cells were then added with appropriate concentration of compound and imaged in either fluorescent or confocal microscope.

2.5.6. Microarray Analyses

B16F10 cells (~2×10^5 cells) were seeded in T25 flasks and grown under standard conditions (see Cell Lines and Media section) for 24 hours. Zn-DIGP was added to a final concentration of 5 µM (0.1 % DMSO) in fresh media and the cells grown under standard conditions for 24 hours. The negative control contained only media and DMSO carrier. As a

positive control, 100 µM of cisplatin was used.[22] mRNA was extracted from the isolated cells using a High Pure mRNA Isolation Kit (Roche) according to the manufacturer's protocol. The quality of the isolated RNA was determined with a NanoDrop ND 1000 (NanoDrop Technologies) and a Bioanalyzer 2100 (Agilent). Only samples having a 260 nm / 280 nm ratio between 1.8 – 2.1, and a 28S/18S ratio of 1.5 – 2 were further processed. Total RNA samples (100 ng) were reverse-transcribed into ds cDNA. To assess sample quality, appropriate spike-in controls were included (Agilent). The cDNA were transcribed back into RNA in presence of Cy3 and Cy5-labeled primers using a Low Input Quick Amp labeling, two-color kit (Agilent). The labeled cRNA was purified using an RNeasy mini kit (Qiagen) and its quality and quantity was determined using NanoDrop ND 1000 and Bioanalyzer 2100. Only cRNA samples with a total cRNA yield higher than 1650 ng and a dye incorporation rate above 6 pmol/ µg were considered for hybridization. Cy3- / Cy5-labeled cRNA samples (825 ng each) were mixed with a Blocking Solution (Agilent) and fragmented to ~100-200 bp at 65°C with Fragmentation Buffer and resuspended in Hybridization Buffer using a Gene Expression Hybridization Kit (Agilent). cRNA Samples (50 µl) were hybridized to Agilent Mouse Whole Genome 4 x 44k arrays for 17h at 65°C. Arrays were then washed using Agilent GE Wash Buffers 1 and 2 (Agilent) according to the manufacturer's instructions (Two-Color Microarray-Based Gene Expression Analysis Manual, www.agilent.com). An Agilent Microarray Scanner was used to measure the arrays. Raw data were processed using the Agilent Scan Control and the Agilent Feature Extraction Software Version 10. Quality control measures were considered before performing the statistical analysis. These included inspection of the array hybridization pattern (absence of scratches, bubbles, areas of non hybridization), proper grid alignment, performance of the spike-in controls (linear dynamic range over 5 orders of magnitude) and number of non-uniformity outliers (below 100 for all samples).

2.5.7. qRT-PCR

B16F10 cells (~ 2.5×10^5) were seeded in T25 flasks and grown for 24 hours under standard conditions (see Cell Lines and Media section). Zn-DIGP to a final concentration of 5 µM (0.1 % DMSO) in fresh media was then added and the cells grown under standard conditions for 8 – 24 hours. Appropriate carrier controls (DMSO only) were also included. mRNA was extracted from the isolated cells using a High Pure mRNA Isolation Kit (Roche) according to the manufacturer's protocol. Fluorescence spectroscopy was used to confirm the absence of

Zn-DIGP in the isolated mRNA. mRNA was quantified using a NanoDrop 1000 (Implen). 0.6 µg of mRNA was used for cDNA synthesis in reactions containing 2.5 µl of 10 x buffer (Applied Biosystems), 5.5 µl of $MgCl_2$, 1.25 µl of random hexamer primers, 5 µl of dNTP's, 0.5µl of RNase inhibitor, 0.625 µl of reverse transcriptase (Applied Biosystems) and the total volume adjusted to 25 µl with deionized water. The reactions were then heated at 42 °C for 1 hour and deactivated at 95°C for 10 minutes. 0.75 µl of cDNA was used in real time PCR with 7.5 µl of PCR master mix (Applied biosystems), 0.75 µl of each primer (CXCL10 and β-actin or SDHA) and 6 µl of RNase free water. Experiments were conducted in triplicate and C_t values were determined using software from the 7900HT Fast RT-PCR (Applied Biosystems). C_t values were then converted to relative RNA abundance using the $2^{-\Delta\Delta t}$ method.[23]

2.5.8. DNase/RNase digestion

15`000 SKMEL-28 cells were seeded in Labtec 8 chambered well plate in media containing 10% FCS. After washing once with PBS, cells were fixed with pure methanol for 1 minute at room temperature. Methanol is gently removed and 100µl of Triton X is added and incubated exactly for 2 minutes. After 2 minutes, Triton X was removed and the cells are washed twice with PBS. 1:1000 dilution of Hoeschst 333342 and 30 nM of Zn-APc are added in 2 separate wells for 3 hours. Cells are then washed with PBS. 100 µl of DNAse solution (Sigma D4263) and RNase solution (Roche 1119915) and PBS control are added to the cells and allowed to incubate for 2 hours. Cells were washed several times and imaged using Leica wide field fluorescence microscope.

2.5. References

[1] Braun A., Tscherniac J., **1907**, *40*, 2907.
[2] J. Alzeer, P. J. Roth, N. W. Luedtke, *Chem Commun (Camb)* **2009**, 1970.
[3] J. Alzeer, N. W. Luedtke, *Biochemistry*, *49*, 4339.
[4] T. J. Baker, N. W. Luedtke, Y. Tor, M. Goodman, *J Org Chem* **2000**, *65*, 9054.
[5] N. W. Luedtke, P. Carmichael, Y. Tor, *J Am Chem Soc* **2003**, *125*, 12374.
[6] J. Alzeer, B. R. Vummidi, P. J. Roth, N. W. Luedtke, *Angewandte Chemie-International Edition* **2009**.
[7] H. Ali, J. E. van Lier, *Chem Rev* **1999**, *99*, 2379.
[8] C. G. Claessens, U. Hahn, T. Torres, *Chem Rec* **2008**, *8*, 75.
[9] J. Alzeer, N. W. Luedtke, *Biochemistry* **2010**, *49*, 4339.
[10] G. N. Parkinson, M. P. Lee, S. Neidle, *Nature* **2002**, *417*, 876.
[11] D. Yang, L. H. Hurley, *Nucleosides Nucleotides Nucleic Acids* **2006**, *25*, 951.

[12] A. Siddiqui-Jain, C. L. Grand, D. J. Bearss, L. H. Hurley, *Proc Natl Acad Sci U S A* **2002**, *99*, 11593.
[13] J. Ren, J. B. Chaires, *Biochemistry* **1999**, *38*, 16067.
[14] H. S. Pandha, L. Heinemann, G. R. Simpson, A. Melcher, R. Prestwich, F. Errington, M. Coffey, K. J. Harrington, R. Morgan, *Clin Cancer Res* **2009**, *15*, 6158.
[15] A. Verma, V. K. Yadav, R. Basundra, A. Kumar, S. Chowdhury, *Nucleic Acids Res* **2009**, *37*, 4194.
[16] L. Ren, A. Zhang, J. Huang, P. Wang, X. Weng, L. Zhang, F. Liang, Z. Tan, X. Zhou, *Chembiochem* **2007**, *8*, 775.
[17] Duan W., Wang Z., J. Cook M, *Journal of Porphyrins and Phthalocyanines* **2009**, *13*, 1255.
[18] L. A. Hanakahi, H. Sun, N. Maizels, *J Biol Chem* **1999**, *274*, 15908.
[19] J. L. Huppert, S. Balasubramanian, *Nucleic Acids Res* **2007**, *35*, 406.
[20] A. Verma, K. Halder, R. Halder, V. K. Yadav, P. Rawal, R. K. Thakur, F. Mohd, A. Sharma, S. Chowdhury, *J Med Chem* **2008**, *51*, 5641.
[21] J. Eddy, N. Maizels, *Nucleic Acids Res* **2008**, *36*, 1321.
[22] T. D. Schmittgen, B. A. Zakrajsek, A. G. Mills, V. Gorn, M. J. Singer, M. W. Reed, *Anal Biochem* **2000**, *285*, 194.
[23] L. Goldberg-Bittman, O. Sagi-Assif, T. Meshel, I. Nevo, O. Levy-Nissenbaum, I. Yron, I. P. Witz, A. Ben-Baruch, *Cytokine* **2005**, *29*, 105.

CHAPTER 3. Guanidino phthalocyanines as photosensitizers

3.1. Introduction: Cancer and its treatment

Cancer is a disease characterized by uncontrolled division of abnormal cells. The proliferation of abnormal cells can cause a cluster of neoplastic cells (benign tumor). The tumor is considered to be malignant only if it gains the ability to invade the surrounding tissue and reach the blood stream by metastasis. This process might take several years before its symptoms are apparent. There are currently number of therapies available for cancer treatment such as surgery, chemotherapy, radiotherapy, immunotherapy and their combination. The choice of therapy is based on the type and stage of cancer.[1]

3.1.1. Surgery

Surgery is the frequently used approach to remove solid tumors. Removal of entire tumor mass prior to metastasis can completely eradicate the cancer. However, even a single remaining cancer cell can lead to tumor recurrence. If the tumor is metastasized, complete removal through surgery is not possible. Side effects such as anesthesia complications, infections and immune suppression are associated with surgery. In some cases, the removal of primary tumor was reported to promote metastasis itself.[2]

3.1.2. Radiotherapy

Damaging the genetic material of cells by ionizing radiation inhibits cellular replication in an oxygen-dependent manner. Though normal and cancer cells are both killed by radiation therapy, the treatment is given in low doses so that the normal cells can recover and grow normally. As the radiation focused on a particular region, the treatment is localized. Disadvantages of radiation therapy include skin burns, nausea and vomiting.[3]

3.1.3. Chemotherapy

Chemotherapy is the application of toxic substances to destroy cancer cells. Unlike surgery and radiation therapy, chemotherapy is systemic. Depending on the type of drug, its mode of action can include cell cycle inhibition, kinase inhibition or binding to DNA. Side effects

such as pain, diarrhea, nausea, hair loss and vomiting are typical. Another drawback associated with chemotherapy is prolonged treatment causes drug resistance in cancer cells.[4]

3.2. Photodynamic therapy

3.2.2. Mechanism

Photodynamic therapy (PDT) utilizes the interaction of light with photosensitizers. Upon illumination, the sensitizer absorbs a photon which causes a promotion of one electron from ground state to an excited state. By internal conversion, the electron falls to the lowest vibration level of the excited singlet state. By intersystem crossing, the excited singlet state can be converted to a triplet state. At this stage, the electron can relax to the ground state by radiative phosphorescence. In PDT, the long life time of the excited triplet state allows sufficient time for the photosensitizer to mediate chemical reactions. Two types of toxicity are observed. Type I process involve a photosensitizer that reacts with biomolecules to generate addition products. In a Type II process, molecular triplet oxygen is converted to singlet oxygen and/or other reactive oxygen species (ROS) such as $^{\cdot}OH$ and H_2O_2. These reactive oxygen species can exhibit anti-tumor effects by direct killing of the cell, vascular damage or activation of immune response.[5] Though both type I and type II process can contribute to the generation of reactive oxygen species, it is generally believed that type II is the most important pathway, and that $^1O_2$ is the most important ROS generated.[6] (Figure 3.1 & Figure 3.2)

3.2.3. Singlet Oxygen

Molecular oxygen is one of the most important substances on earth. The electronic configuration of molecular oxygen is $1s^2\ 2s^2\ 2p^4$ and the electronic properties of molecular oxygen are determined by 6 electrons in p-molecular orbitals. After filling the first four electrons in the bonding orbital of p shell, the remaining two electrons can be filled into the anti-bonding orbitals by three possible ways. In triplet state, electrons occupy two different anti-bonding orbitals and in singlet state, both the electrons occupy a single anti-bonding orbital with opposite spins. In its ground state, molecular oxygen exists in a triplet state. (Figure 3.3)

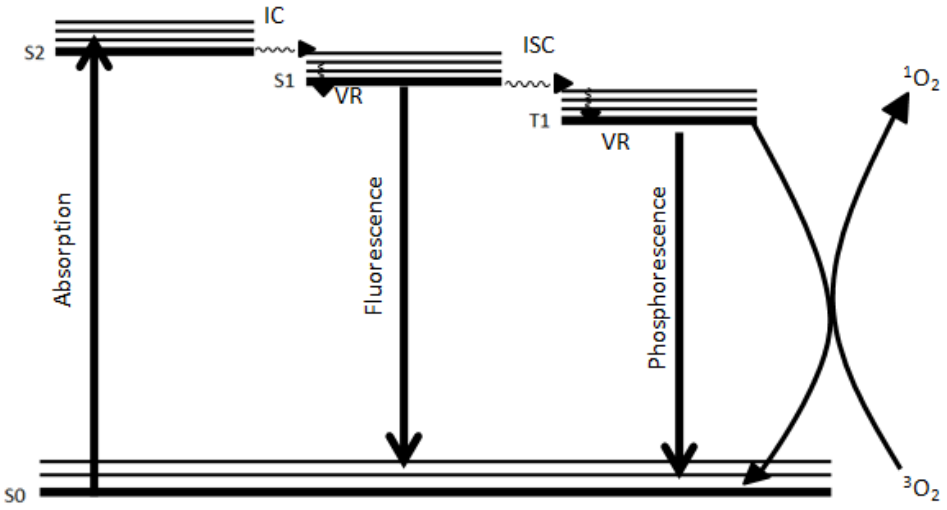

Figure 3.1. Jabaloniski diagram representing possible events of an excitation. S0 : Electronic ground state; S1 and S2 : Electronic excited singlet state; T1 : Triplet state; VR : Vibrational relaxation; IC : internal conversion; ISC : Intersystem crossing.

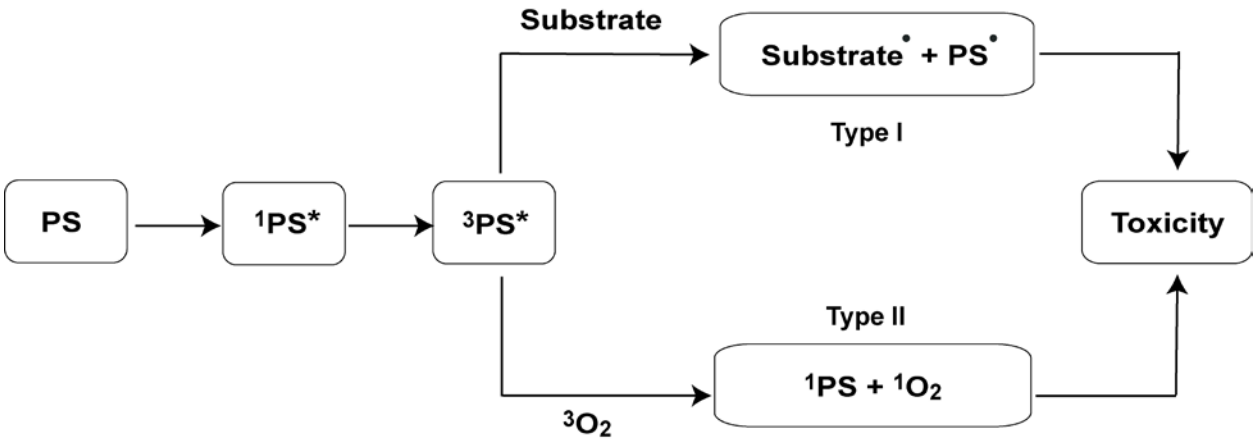

Figure 3.2. Possible mechanisms of photosensitizers in photodynamic therapy.

Unlike triplet oxygen, singlet oxygen can undergo reactions such as ene-, 1,2- and 1,4-cycloaddition reactions. In cells, singlet oxygen is reported to target biological membranes. Components of the cell membrane such as phospholipids, proteins and cholesterol can be readily oxidized by $^1O_2$.[7-9] The products can then break down into free radicals and initiate chain oxidation of other lipids. In proteins, the amino acids tyrosine, tryptophan, histidine, methionine, and cysteine are susceptible to oxidation by singlet oxygen. In DNA, guanine residues can be oxidized by singlet oxygen to generate 8-oxo guanine which triggers strand cleavage.[10]

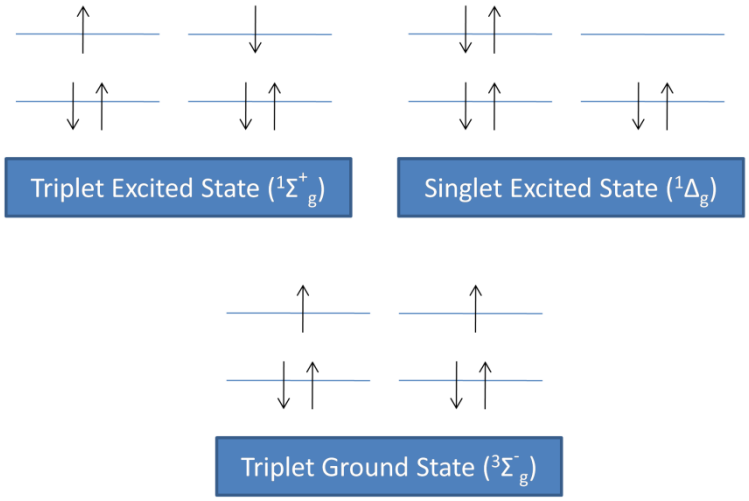

Figure 3.3. Possibilities of electron occupation in p orbital of oxygen.

The efficiency by which photosensitizers generate singlet oxygen is determined by the quantum yield of singlet oxygen formation which is defined as

$$\Phi = \frac{\text{The number of singlet oxygen generated}}{\text{The number of photons absorbed}}$$

3.2.4. Photosensitizers:

By utilizing light energy, photosensitizers can convert triplet oxygen into singlet oxygen and to mediate type II toxicity. An ideal photosensitizer should meet the following requirements to be effective in PDT.[11]

- Water solublity
- Selective uptake in cancerous cells
- Minimum dark toxicity and maximum toxicity in the presence of light
- Non-mutagenic and non-carcinogenic
- Excitation wavelengths in the far red or IR to minimize tissue absorption of light
- High quantum yield and long-lived triplet state
- Rapid excretion from the body

The first attempt to utilize photodynamic effects for the treatment of human tumors was performed by Tappenier and Jesionek in 1903.[5] Inspite of the reported positive effects, further research in PDT was not reported again until 1972 when Diamond and co-workers demonstrated that the haemotoporphyrin, upon activated by white light, caused regression of an experimental glioma in rats.[12] Doherty and coworkers reported that fluorescein activated

by a 488 nm laser and hematoporphyrin activated by red light, resulted in tumor reduction in mice.[13] In 1974, Tomson reported that acridine orange, when activated by an argon laser, caused destruction of a mouse epithelial tumor.[14] In the following year, Kelly and coworkers demonstrated that specific destruction of heterotransplant of human bladder carcinoma in mice could be obtained by local exposure to white light following hematoporphyrin injection.[15] In 1978, Doherty and his coworkers clearly demonstrated that hematoporphyrin derivatives activated by red light resulted in complete or partial response in mouse malignant lesions.[16] Since then, a large number of studies have been reported on photodynamic therapy. Recent research on PDT has been focused on 3 families of photosensitizers. [11]

(i) Porphyrin family
   a. Hematoporphyrin derivative (HpD)
   b. Benzoporphyrin derivative (BPD)
   c. 5-aminolevilinic acid (ALA)
   d. Texaphyrins

(ii) Chlorophyll family
   a. Cholins
   b. Purpurins
   c. Bacteriocholins

(iii) Dyes
   a. Phthalocyanine
   b. Naphthalacyanine

An iron-free derivative of heme, haematoporphyrin derivative (HpD) was one of the first commercially available and clinically-utilized photosensitizers. In 1978, Dougherty and coworkers reported successful results on HpD mediated PDT treatment for many tumor types in humans. In 1995, Food and Drug administration approved Photofrin in USA after which other countries like Canada, Netherlands, France and Italy approved. However, HpD and its derivatives have two important disadvantages. First, they cause severe side effects in skin after PDT treatment. Secondly, they are prepared as a complex mixture instead of a single active component. Overcoming this disadvantage, several 'second generation photosensitizers' have been synthesized. ***5-aminolaevelic acid*** is a prodrug which is converted enzymatically to protoporphyrin IX (Figure 3.4). Protoporphyrin IX has a longer excitation wavelength than photofrin, and it gives better tissue depth penetration of

photoexcitation. ***ALA (Levulan)*** was approved in 1999 for the treatment of cancerous lesions. In 2001, the methyl ester of ***ALA (Metvix)*** was approved for the treatment of basal cell carcinoma and actinic keratosis. However, it must be emphasized that ALA treatments can be painful since high light energy and/or longer treatment times are typically required. ***Foscan*** is another commercially available photosensitizer belonging to the Chlorin group. Though it requires much lower doses than photofrin, the healing time for the side effects remain high. ***Purlytin*** is another chlorin derivative that has excellent properties as a photosensitizer but is poorly soluble in water. Another derivative of chlorin in clinical trial is ***e6*** that is characterized to be effective on cutaneous lesions. However, the lack of tissue selectivity makes it clinically less important than compounds that exhibit selective uptake.[11]

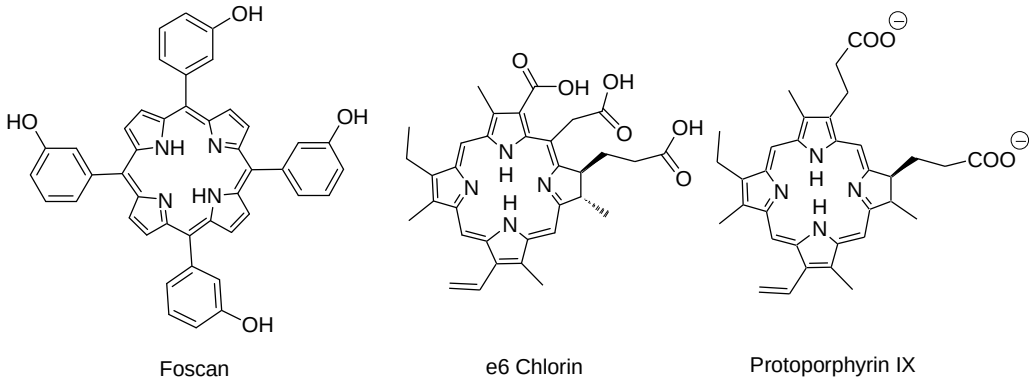

Foscan e6 Chlorin Protoporphyrin IX

Figure 3.4. Structure of Foscan, e6 Chlorin and Protoporphyrin IX

3.2.5. Phthalocyanines

The interest in phthalocyanines for use in PDT started in 1985.[17] The main advantages of phthalocyanines over other photosensitizers are the increased absorption of far-red light, and low cytotoxicity in the dark. The presence of diamagnetic metal-center increases the phototoxicity of phthalocyanines due to long-lived triplet states and the axial substituents on the metal and side groups on the phthalocyanines can have role in solubility. The cellular uptake of phthalocyanines depends on polarity, lipophilicity, central metal ion, axial ligand, serum levels, charge state and delivery vehicles.[18] The accumulation of phthalocyanines appears to be continuous process inside the cell, as the intracellular Pc levels can remain constant after 3 days. Pc accumulates mainly in cytoplasm and lysozomes. Depending on the charge state of Pc, relocation was observed upon exposure to light. Among the many Pc's reported to date, several derivatives such as Zn-Pc and Al-Pc are currently in different phases of clinical trials.[18]

3.3. Aims

According to the fluorescence imaging reported in the previous chapter, Zn-DIGP can cause changes in morphology of cells during live-cell imaging. To explore this further, we decided to evaluate the ability of Zn-DIGP to behave as photosensitizer, and to evaluate its light-dependent toxicity. To evaluate a possible role of G-quadruplex tarrgeting in the phototoxicity of Zn-DIGP and its ability to photocleave plasmid containing G-quadruplex forming sequence was evaluated.

3.4. Results and discussion

Phthalocyanines containing different metal ions including Cadmium, Cobalt, Copper, Iron, Mercury, Nickel, Palladium, Phodium, Tin, Zinc were synthesized by Dr. Jawad Alzeer (Figure 3.5).

3.4.1. Absorbance spectra of M-DIGP

The absorbance spectra of various metal containing DIGP's (M-DIGP) are shown in Figure 3.6. The strongest absorption band is the Q-band which originates from π-π* transitions. M-DIGP exhibits a single Q-band over the range of 650-680 nm whereas DIGP shows split Q-band in same range due to the loss of molecular symmetry (Figure 3.6).[19, 20]

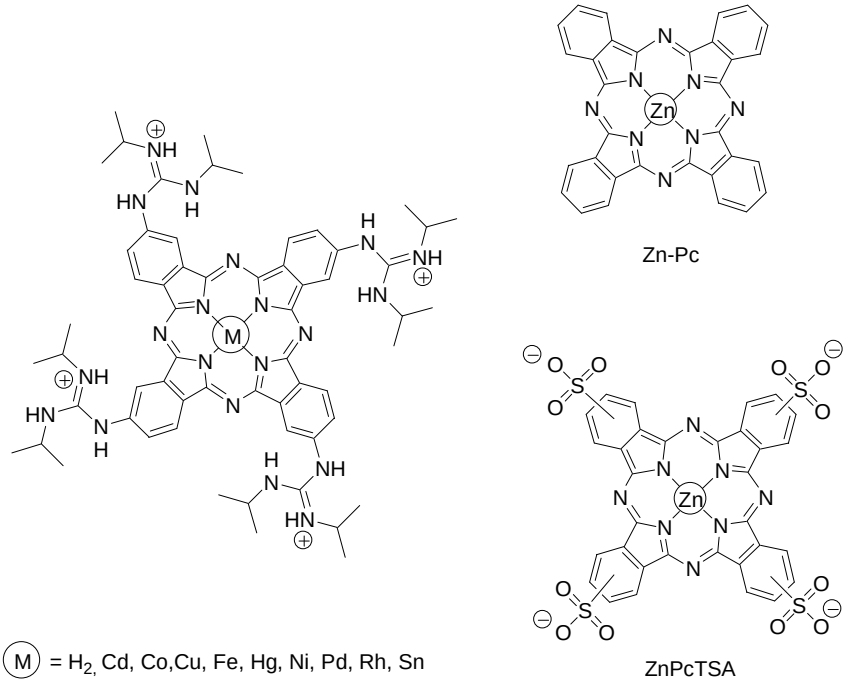

Figure 3.5. Structures of tetrakis-diisopropyl-guanidine-phthalocyanine (DIGP) derivatives containing various metal ions "M", and the reference compounds zinc phthalocyanine (ZnPc) and Zinc tetrasulphonate phthalocyanine (ZnPc.TSA).

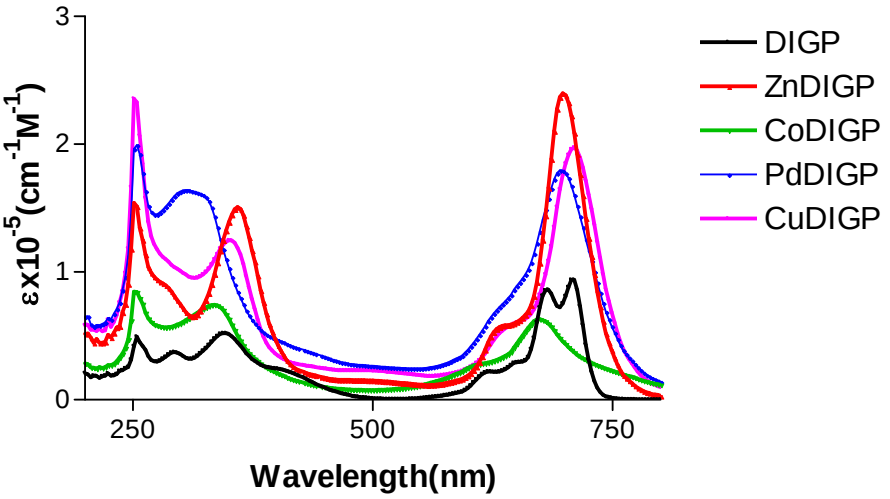

Figure 3.6. Absorption spectra of different metal-containing and metal-free DIGP derivatives in DMSO.

3.4.2. Fluorescence Quantum yield

DIGP derivatives containing Zinc, Cobalt, Palladium and Copper exhibit excellent solubility and obey Beer's law in DMSO over a concentration range of 0.3 – 5 µM. We therefore measured the quantum yields of these compounds for photon emission in DMSO. The known

compounds zinc phthalocyanine “Zn-Pc” and zinc phthalocyanine tetrasulfonic acid “Zn-PcTSA” were included as references (Figure 3.5). The quantum yield of Zn-DIGP for luminescence (Φ = 0.28) was more than 100-fold higher than the other metal-containing DIGPs (Table 3.1). The relatively high quantum yield of Zn-DIGP allows for its direct visualization inside cells using fluorescence microscopy.

Compound	**Φ for emission**
DIGP	0.26
Zn-DIGP	0.28
Cu-DIGP	< 0.001
Co-DIGP	< 0.001
Pd-DIGP	0.002
Zn-Pc	0.34
Zn-PcTSA	0.29

Table 3.1. Luminescence quantum yields of various phthalocyanines.

3.4.3. Microscopy

Upon addition of Zn-DIGP to live B16F10 cells, strong staining of perinuclear organelles and trafficking vesicles by Zn-DIGP was observed. (Figure 3.7).[21] Upon irradiation with 20 joules of far-red light (660 nm), Zn-DIGP-treated cells exhibited large morphological changes and the loss of cellular respiration. Interestingly, a redistribution of Zn-DIGP from the perinuclear organelles of living cells to the nuclei of dead and dying cells was observed following irradiation (Figure 3.7).

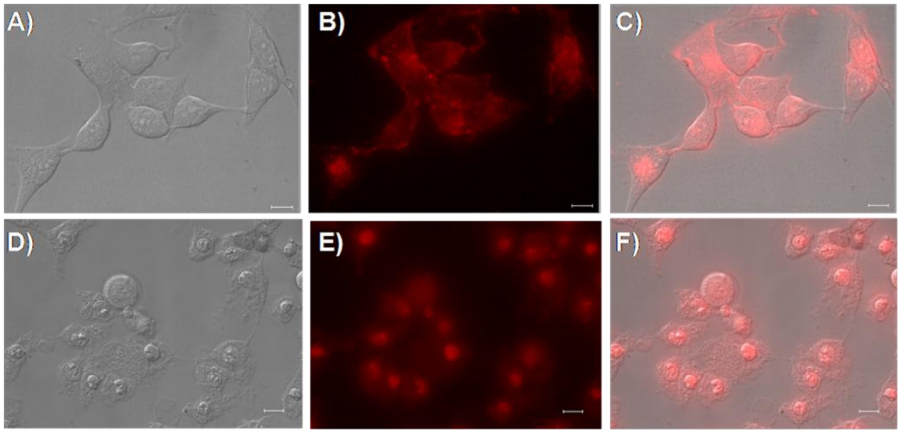

Figure 3.7. Cellular uptake of Zn-DIGP into living B16F10 cells before (A-C) and after (D-F) a 90 second exposure to red laser light at 660 nm. (A) & (D) Brightfield image. (B) & (E) Zn-DIGP fluorescence (Ex = 620 nm, Em = 700 nm). (C) Composite image of (A) – B). (F) Composite image of (D) – (E). Scale bars represent 30 µm.

3.4.4. Phototoxicity

Changes in the morphology of Zn-DIGP-treated cells upon illumination suggested phototoxicity. To quantify the changes in respiration, standard "Alamar Blue" assays were conducted. B16F10 cells were incubated with variable concentrations of DIGP, Co-DIGP, Cu-DIGP, Pd-DIGP, Rh-DIGP, Fe-DIGP, Cd-DIGP, Hg-DIGP, Sn-DIGP or Ni-DIGP and illuminated with red laser light for 90 seconds. After 3 hours, resazurin was added and its conversion into resofurin was quantitated to determine EC_{50} values. As an appropriate control, 0.1% DMSO was serially diluted and added to the cells and subjected to illumination. As shown in Figure 3.8, light did not have any effect on the respiration of DMSO-treated cells.

Cells treated with Pd-DIGP and Zn-DIGP, exhibited light-mediated toxicity at very low concentrations, whereas other M-DIGP derivatives did not exhibit phototoxicity. The EC_{50} values of different M-DIGP derivatives are summarized in Table 4.1. Consistent with microscopy results, Zn-DIGP-treated cells exhibited potent phototoxicity with an EC_{50} of 0.1 µM. This value is roughly 1000-fold lower than samples without light activation. Similarly, Pd-DIGP also exhibited 25-fold lower EC_{50} values upon photoexciation as compared to non-irradiated samples (Figure 3.9).

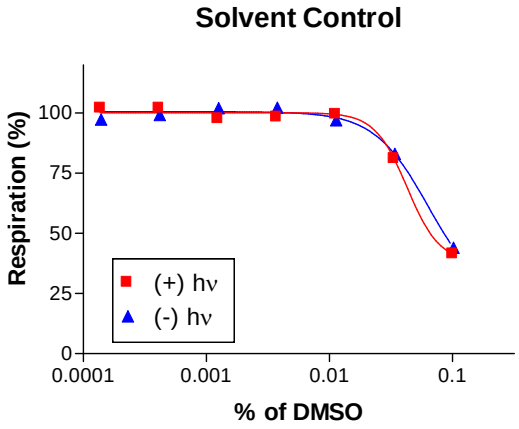

Figure 3.8. Cellular respiration after illumination of DMSO-treated B16F10 cells.

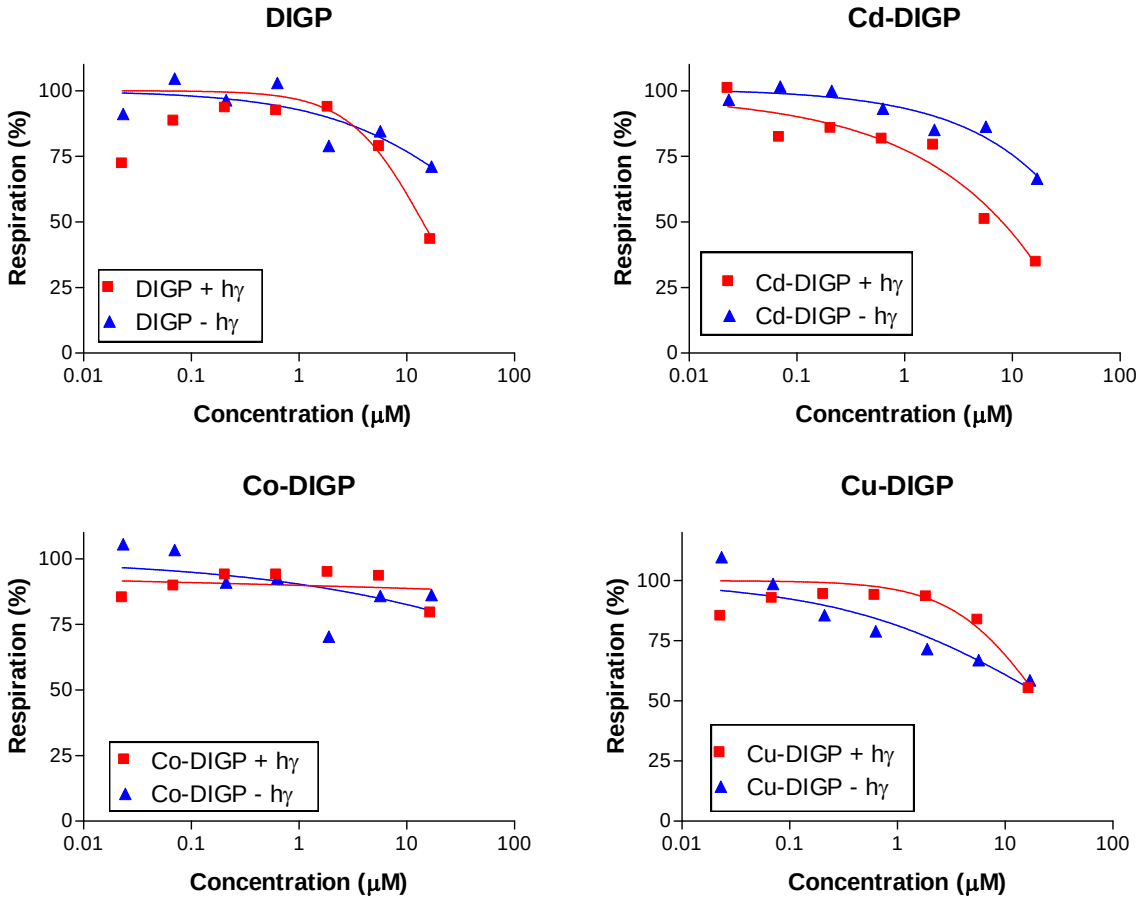

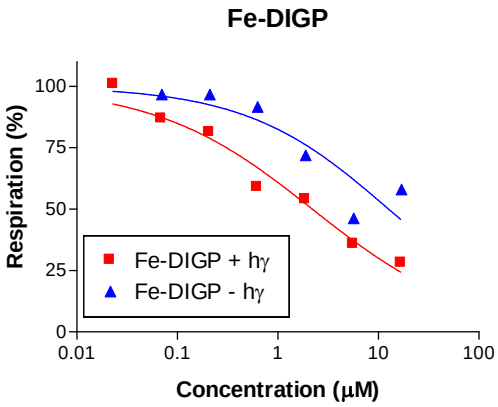
Fe-DIGP
Respiration (%)
100
75
50
25
0
0.01
0.1
1
10
100
Concentration (µM)
Fe-DIGP + hγ
Fe-DIGP - hγ

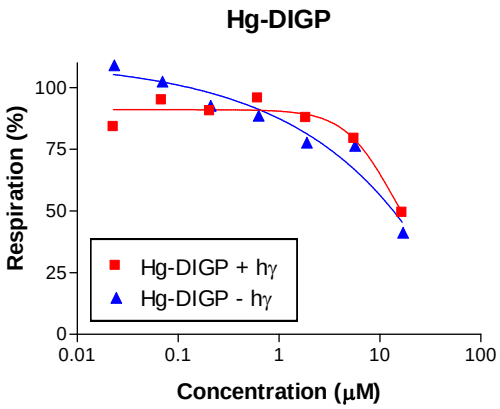
Hg-DIGP
Respiration (%)
100
75
50
25
0
0.01
0.1
1
10
100
Concentration (µM)
Hg-DIGP + hγ
Hg-DIGP - hγ

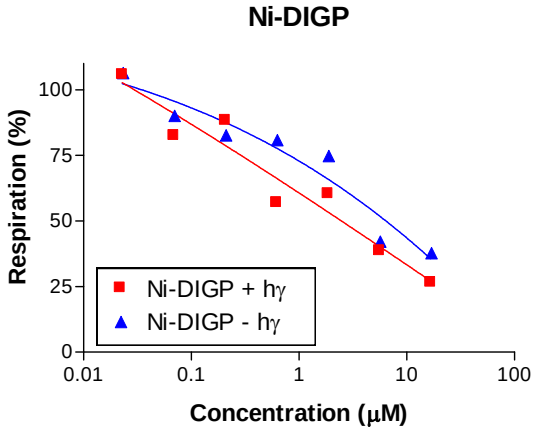
Ni-DIGP
Respiration (%)
100
75
50
25
0
0.01
0.1
1
10
100
Concentration (µM)
Ni-DIGP + hγ
Ni-DIGP - hγ

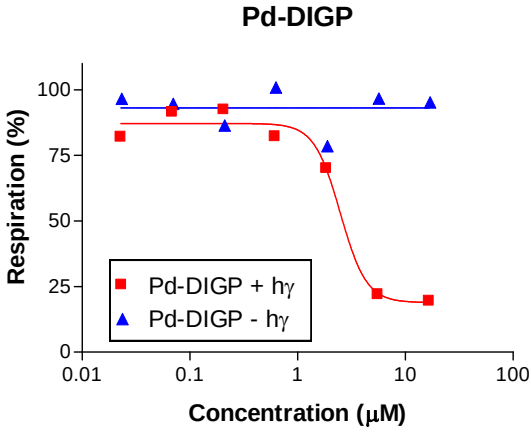
Pd-DIGP
Respiration (%)
100
75
50
25
0
0.01
0.1
1
10
100
Concentration (µM)
Pd-DIGP + hγ
Pd-DIGP - hγ

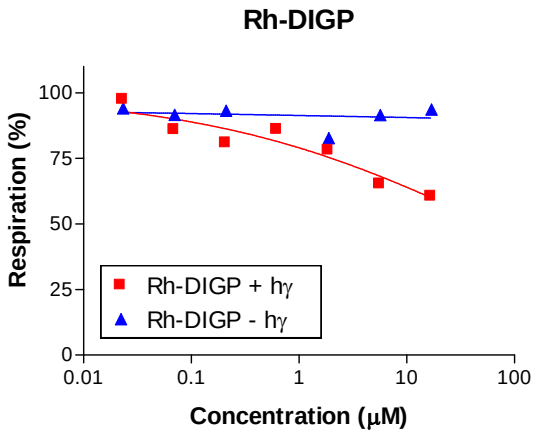
Rh-DIGP
Respiration (%)
100
75
50
25
0
0.01
0.1
1
10
100
Concentration (µM)
Rh-DIGP + hγ
Rh-DIGP - hγ

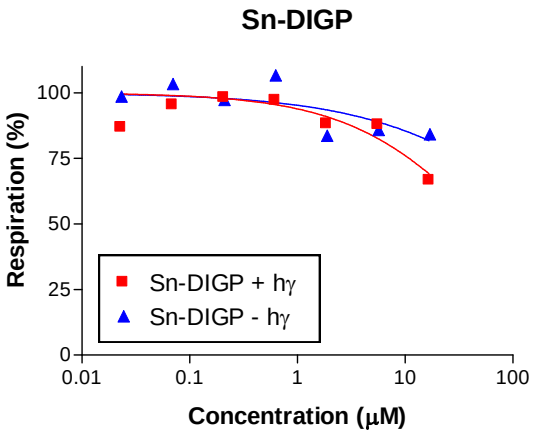
Sn-DIGP
Respiration (%)
100
75
50
25
0
0.01
0.1
1
10
100
Concentration (µM)
Sn-DIGP + hγ
Sn-DIGP - hγ

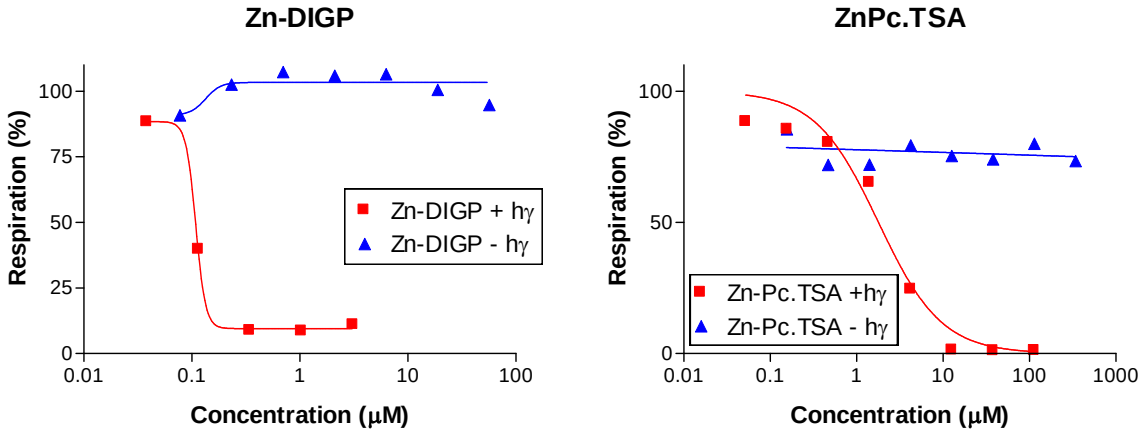

Figure 3.9. Phototoxicity of M-DIGP in B16F10 cells. Blue line indicates the viability (% of total metabolic activity versus untreated cells) of cell cultures incubated with M-DIGP and kept in the dark (-hγ) as compared to M-DIGP-treated cells irradiated with 20 joules of 660 nm light (+hγ) (red).

Compound	EC_{50} (+ hγ) (μM)	EC_{50} (-hγ) (μM)
DIGP	32 ± 6	25 ± 5
Cd-DIGP	7.5	77
Co-DIGP	>80	>80
Cu-DIGP	>80	>80
Fe-DIGP	1.5	9.8
Hg-DIGP	31	15
Ni-DIGP	2.3	4.5
Pd-DIGP	3 ± 0.14	>80
Rh-DIGP	>80	>80
Sn-DIGP	>80	>80
Zn-DIGP	0.15 ± .08	>80
ZnPc.TSA	2.5 ± 0.5	>80

Table 3.2. Summary of effective concentration (EC_{50}) values of M-DIGP derivatives in B16F10 cells. Cells treated with various M-DIGP derivatives were kept in the dark (-hγ) as compared to M-DIGP-treated B16F10 cells that were irradiated with 20 joules of 660 nm light (+hγ).

3.4.5. Singlet oxygen quantum yield

To evaluate why such large differences in phototoxicity were observed for the different metal-containing DIGP derivatives, the quantum yield of singlet oxygen was determined for each compound by monitoring the time-dependent photobleaching of 1,3-diphenyl isobenzofuran (DPBF).[22] Consistent with the relative trends in phototoxicity of each compound, the quantum yields for singlet oxygen formation followed the same trend: Zn > Pd >> Cu / Co /H_2 (Figure 3.10). Differences between the various metals can be explained by the magnetic properties of each metal cation.[23, 24] The paramagnetic ions (copper, cobalt) do not generate singlet oxygen whereas diamagnetic metals (zinc and palladium) generate singlet oxygen and hence exhibit potent phototoxicity. Since all three of the Zn-containing phthalocyanines exhibited similar quantum yields for singlet oxygen formation ($\Phi \approx 0.4 – 0.6$), the large differences in phototoxicity between Zn-DIGP (EC_{50} = 0.16 µM) and Zn-PcTSA (EC_{50} = 2.5 µM) are likely related to the favorable accumulation of Zn-DIGP in living cells.

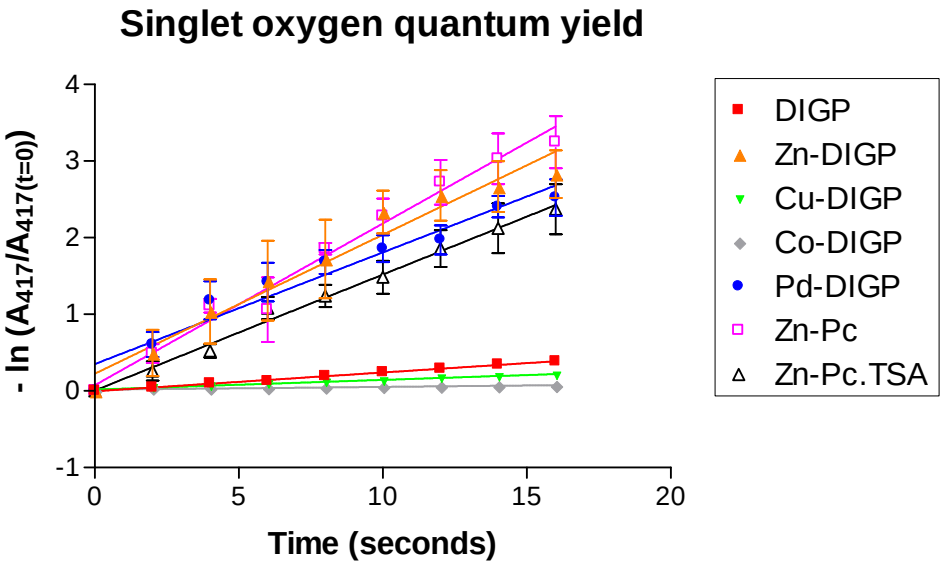

Figure 3.10. Photobleaching of DPBF absorbance in the presence of different metal containing DIGPs (2 µM) and irradiation at 660 nm.

Compound	Φ for $^1O_2$
DIGP	0.06 ± .008
Zn-DIGP	0.51 ± .05
Cu-DIGP	0.03 ± 0.006
Co-DIGP	< 0.01
Pd-DIGP	0.41 ± .02
ZnPc	0.61
ZnPc.TS	0.50 ± .04

Table 3.3. Singlet oxygen quantum yield for various phthalocyanines.

3.4.6. Photocleavage studies

Zn-DIGP generates singlet oxygen upon photoactivation and it binds to G-quadruplex DNA with high affinity and selectivity *in vitro*. (Chapter 2). Since guanosine can be oxidized by singlet oxygen and subsequently cleaved, we speculated that Zn-DIGP could cause G-quadruplex specific photoocleavage. This property could, in theory, allow for site-specific DNA cleavage studies to be conducted in cells. To test this possibility, 1 μM of Zn-DIGP was mixed with pBR322 plasmid and illuminated with 630 nm laser light for variable periods of time. Figure 3.11 demonstrates that irradiation converts the plasmid from supercoiled form to relaxed (nicked) form. This effect was dependent on the duration of illumination. Appropriate control samples lacking Zn-DIGP or without irradiation did not cause any conversion.

To evaluate the possibility of G-quadruplex-specific photocleavage, we decided to incorporate a G-quadruplex sequence from the c-Myc promoter into plasmid DNA and evaluate the concentration at which Zn-DIGP causes photocleavage. For this experiment, we decided to use plasmid DNA that remains unaffected by S1 endonuclease. S1 endonuclease is a restriction enzyme that cleaves single-stranded DNA. In the supercoiled closed form, plasmid DNA has the possibility for the forming single-stranded DNA and assisted secondary structures that can be cleaved by S1 endonuclease.[25] Zn-DIGP could bind to such regions and trigger photocleavage. In order to evaluate G-quadruplex-specific photocleavage, we decided to use a plasmid that does not possess an endogenous S1 nuclease site.

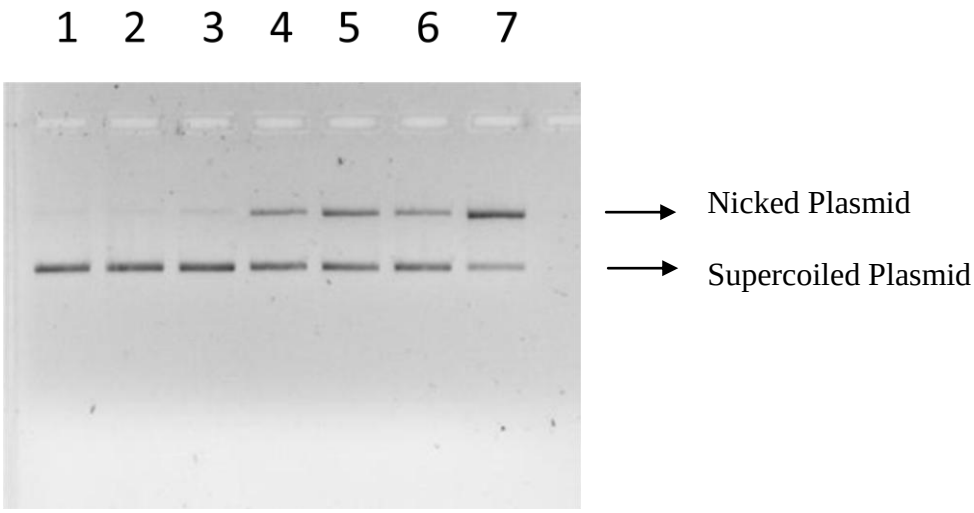

Figure 3.11. Photocleavege of plasmid pBR322 by Zn-DIGP and 660 nm light according to gel electrophoresis based on duration of illumination separated by agarose gel electrophoresis. Lane 1: native Plasmid pBR322; Lane 2: pBR322 + 1 μM of Zn-DIGP; Lane 3: pBR322 + 30 seconds of illumination with 630 nm; Lane 4: pBR322 +1 μM of Zn-DIGP + 30 seconds of illumination with 630 nm; Lane 5: pBR322 + 1 μM of Zn-DIGP + 45 seconds of illumination with 630 nm; Lane 6: pBR322 + 1 μM of Zn-DIGP + 60 seconds of illumination with 630 nm; Lane 7: pBR322 + 1 μM of Zn-DIGP + 90 seconds of illumination with 630 nm.

We screened the available plasmids including pUC18, pHen1 and pET15B for S1 nuclease sensitivity. Figure 3.12 demonstrates that the pHen1 plasmid was not affected by S1 nuclease (Lanes 3 and 4), whereas other plasmids underwent significant changes due to S1 nuclease. To test the ability of Zn-DIGP to photocleave the pHen1 plasmid (no insert), we added 1 μM of Zn-DIGP to pHen1 and tested for the photocleavage. Surprisingly, no conversion to nicked DNA was observed, whereas the plasmid pET15B was converted from supercoiled to nicked form (Figure 3.13). These results indicate that pHen1 could be a useful vector for conducting G-quadruplex-specific photocleavage reactions. Myc-1, a sequence derived from c-Myc oncogene that is well known to form a G-quadruplex even in the context of duplex DNA,[26] was chosen for incorporation in pHen1.

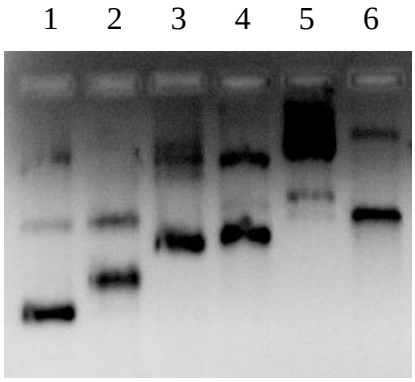

Figure 3.12. Agarose gel electrophoresis of S1 nuclease-treated plasmids. Lane 1: pUC18; Lane 2: pUC18 + S1 nuclease; Lane 3: pHen1; Lane 4: pHen1 + S1 nuclease; Lane 5: pET15B; Lane 6: pET15B + S1 nuclease.

Due to the restriction sites present in the pHen1 plasmid, we decided to amplify Myc-1 with primers containing BamH1 and EcoR1 restriction sites using the polymerase chain reaction (PCR). The PCR product was then digested with BamH1 and EcoR1. Similarly, pHen1 (vector) plasmid was digested using these restriction enzymes. The restricted pHen1 plasmid was separated using agarose gel electrophoresis (Figure 3.14) and the band representing linear DNA was gel extracted. The restricted plasmid and PCR amplified Myc-1 sequence were ligated using DNA ligase. The ligated DNA was transformed into *E.coli* DH5α and selected in ampicillin containing media. The cloning was confirmed by selecting colonies from the plate and subjecting them to colony PCR amplification with the same primers (Table 3.4). Many colonies showed the band of interest (60 bp) in the gel. (circles in Figure 3.15)

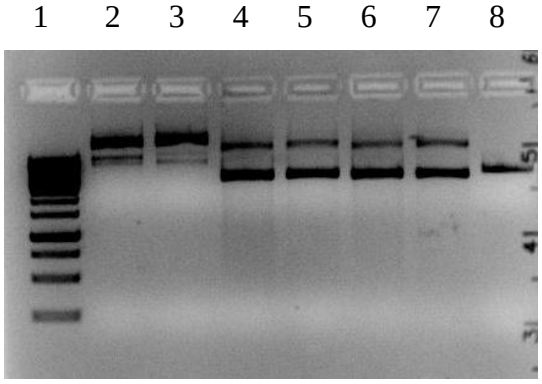

Figure 3.13. Photocleavage of pET15B and pHen1 plasmid by 1 μM of Zn-DIGP. Lane 1: 1kb ladder; Lane 2: pET 15b; Lane 3: pET15b + 1 μM Zn-DIGP + 90 seconds of 660 nm laser. Lane 4: pHen1; Lane 5: pHen1 + 1 μM Zn-DIGP; Lane 6: pHen1 + 90 seconds of 660 nm laser; Lane 7: pHen1 + 1 μM Zn-DIGP + 90 seconds of 660 nm light; Lane 8 : BamH1 restricted pHen1.

Name	Sequence (5`-3`)
Forward Primer	AATTGGATCCGGGAGGGGCG
Reverse Primer	ATATGAATTCCTGAGTTCTCCTCC
Myc-1	GGGAGGGGCGCTTATGGGGAGGG TGGGGAGG GTGGGGAAGGTGGGGAGGAGACTCAG

Table 3.4. Primers used to amplify G-quadruplex forming sequence "Myc-1" from c-Myc template.

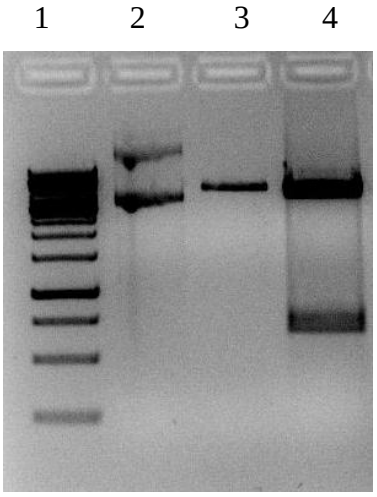

Figure 3.14. Single digestion and double digestion of pHen1 plasmid using BamH1 and BamH1/EcoR1 analyzed by agarose gel electrophoresis. Lane 1: 1kb ladder; Lane 2 : native pHen1; lane 3 : BamH1 digested pHen1; Lane 4 : pHen1 digested with EcoR1 and BamH1.

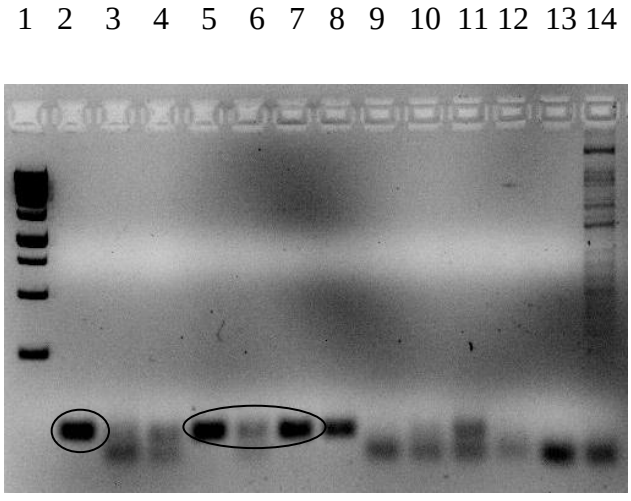

Figure 3.15. Colony PCR of pHen1 transformed *E.coli* cells separated by a 2% agarose gel. Circled bands indicate the clones selected for further studies (Clones A, D, E, F) Lane 1: 1 kb ladder; Lane 2-12: Clones A-K; Lane 13: Negative control; Lane 14: PCR on native pHen1.

Four colonies were selected and the cloning was confirmed by PCR (Figure 3.16). Clones A and E (Lanes 2 and 4 in Figure 3.15) were chosen to study further. As shown in Figure 3.17,

double digestion of clones A and E contained a 60 bp fragment which was not present in native plasmid. Sequencing the samples resulted in the presence of Myc-1 sequence in clone A and E. These results suggest that the c-Myc G-quadruplex forming sequence ”Myc-1” was incorporated into the pHen1 plasmid.

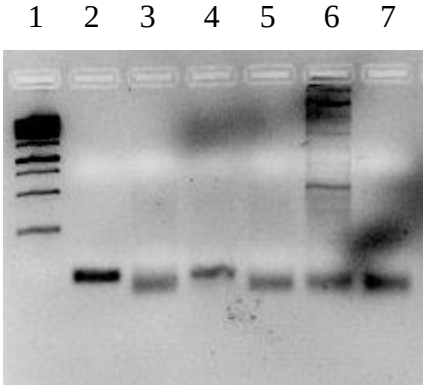

Figure 3.16. PCR of pHen1_clone A-D plasmids. Lane 1: 1kb ladder; Lane 2-5: PCR on clone A, D, E, F; Lane 6: PCR on native phen1; Lane 7: negative control.

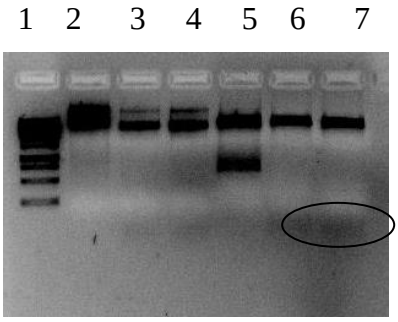

Figure 3.17. Restriction digestion of phen1_cloneA plasmid. Lane 1: 1kb ladder; Lane 2: Native pHen1; Lane 3: pHen1_cloneA; Lane 4: pHen1_cloneE; lane 5: Double digestion – EcoR1 and BamH1 on Native pHen1; Lane 6: Double digestion – EcoR1 and BamH1 on pHen1_A; Lane 7: Double digestion – EcoR1 and BamH1 on pHen1_cloneE.

In order to test for Zn-DIGP-mediated photocleavage, both pHen1 and pHen1_clone A were subjected to varying concentrations of Zn-DIGP and illuminated for 90 seconds of 660 nm light. In both cases (Figure 3.18; Figure 3.19), concentration-dependent conversion of supercoiled form to nicked form was observed. However, we anticipated selective cleavage of the c-Myc containing pHen1 (Phen1_cloneA). Unfortunately, the concentration at which Zn-DIGP caused photocleavage were similar for both pHen1 and pHen1_Clone A. Therefore, no G-quadruplex-specific photocleavage could be confirmed. Strangely, in the lanes of plasmid irradiated with 10 μM of Zn-DIGP, no plasmid was seen. A possible reason for this could be complete destruction of the plasmid due to the presence of high concentration of Zn-DIGP.

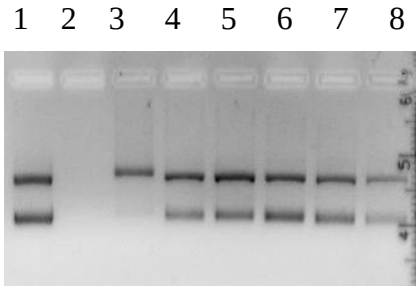

Figure 3.18. Photocleavage of pHen1 plasmid treated various concentration of Zn-DIGP and illuminated with light of 660 nm for 90 seconds. Bands were resolved using agarose gel electrophoresis. Lane 1: Native pHen1; Lane 2: pHen1 + 10 µM Zn-DIGP + irradiation; Lane 3: pHen1 + 5 µM Zn-DIGP + irradiation; Lane 4: pHen1 + 2 µM Zn-DIGP + 90 seconds + irradiation; Lane 5: pHen1 + 1 µM Zn-DIGP + irradiation; Lane 6: pHen1 + 0.5 µM Zn-DIGP + irradiation; Lane 7: pHen1 + 0.25 µM Zn-DIGP + 90 seconds light; Lane 8: pHen1 + 0.125 µM Zn-DIGP + irradiation.

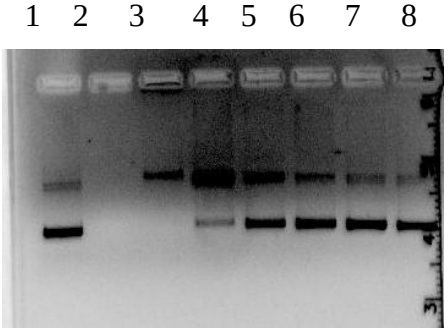

Figure 3.19. Photocleavage of pHen1_cloneA plasmid treated various concentration of Zn-DIGP and illuminated with light of 660 nm for 90 seconds. Bands were resolved using agarose gel electrophoresis. Lane 1: Native pHen1; Lane 2: pHen1 + 10 µM Zn-DIGP + irradiation; Lane 3: pHen1 + 5 µM Zn-DIGP + irradiation; Lane 4: pHen1 + 2 µM Zn-DIGP + 90 seconds + irradiation; Lane 5: pHen1 + 1 µM Zn-DIGP + irradiation; Lane 6: pHen1 + 0.5 µM Zn-DIGP + irradiation; Lane 7: pHen1 + 0.25 µM Zn-DIGP + 90 seconds light; Lane 8 : pHen1 + 0.125 µM Zn-DIGP + irradiation.

3.5. Conclusion

Among the different M-DIGP derivatives tested, Zn-DIGP and Pd-DIGP exhibited high quantum yields for generating singlet oxygen and phototoxicity to treated cells when illuminated with red light. In addition, Zn-DIGP exhibited relocalization from perinuclear organelles to the nucleus upon irradiation. Though this molecule has high affinity for G-quadruplex DNA *in vitro*, no G-quadruplex-specific photocleavage was observed in our c-Myc plasmid construct.

3.6. Experimental Methods

3.6.1. Cytotoxicity and Phototoxicity Studies

B16F10 or SKMel28 cells (10'000 cells) were seeded in 96 well plates and grown for 24 hours prior to their incubation with variable concentrations of M-DIGP derivatives for 24 hours. Individual wells were then photoexcited with a 250 mW diode laser (containing a beam spreader to diameter of 1 cm) at 660 nm for 90 seconds. After 3 hours of incubation in the dark at 37 ºC incubator, the cellular media were replaced with fresh media containing 86 µM resazurin (Sigma). The fluorescence was measured after 2-4 hours using M5 spectrophotometer with excitation at 560 nm, emission at 590 nm, and a 570 nm cutoff filter. All samples were compared to untreated cells to calculate the % decrease in respiration - from which EC_{50} values were calculated.

3.6.2. Microscopy

B16F10 cells (~15'000) were seeded in Labtek 8 chambered plate (Nunc) in media containing 10% FCS. After overnight growth, media was replaced with fresh media containing 3 µM Zn-DIGP and incubated for 24 hours. Individual wells were then photoexcited with a 250 mW diode laser (containing a beam spreader to diameter = 1 cm) at 660 nm for 90 seconds. Images of the unfixed cells were taken in Leica LX wide field microscope before irradiation and 3 hours following irradiation.

3.6.3. Singlet oxygen quantum yield

Quantum yields for singlet oxygen generation were determined from the time-dependent loss of 1,3-diphenylisobenzofuran (DPBF) (Sigma) according to published procedures.[22] Briefly, DPBF (50 µM) and a photosensitizing agent were prepared in DMSO so that the optical density at 660 nm = 0.1. The decrease in DPBF absorbance was monitored at 417 nm as a function of irradiation time at 660 nm using a 250 mW diode laser (containing a beam spreader to diameter = 1 cm). All measurements were carried out in quartz cuvette at room temperature. Singlet oxygen quantum yield was calculated from the following:[27]

$$\phi(S) = \phi(R) \times \frac{m(S)}{m(R)} \times \frac{A(R)}{A(S)}$$

where Φ represents the quantum yield and m represents the slope of DPBF bleaching due to of sample (S) and reference (R) with irradiation time and A represents absorbance of sample (S) and reference (R) at 660 nm.[28] Quantum yields were calculated with respect to ZnPc as a standard (Φ = 0.61).[28, 29] The absorbance of the samples at 660 nm (OD = 0.1) did not change over the course of the experiments.

3.6.4. Photocleavage experiments

Plasmid DNA (350-500 ng) was mixed with 1 μM of Zn-DIGP in TKE buffer and photo illuminated with 90 seconds with a 660nm laser (20 joules). Depending on the type of experiment, the concentration of Zn-DIGP and duration of illumination was varied. After photo illumination, the samples were loaded with DNA dye (Sigma) and separated on a 1.8% agarose gel.

3.6.5. Agarose Gel electrophoresis

1.2 g of agarose was dissolved in 60 ml of Tris-acetate EDTA (TAE) buffer (40mM Tris, 1mM EDTA, pH: 8 adjusted with acetic acid) and heated in a microwave for 2 minutes. After mild cool down, ethidium bromide (final concentration: 0.5 μg/ml) was carefully added and poured on the gel cast and the combs were placed. Upon solidification, gel was transferred to tank filled with TAE buffer and the samples were loaded. An electric field was then applied (50 volt for 30 minutes) and the gel was imaged with a transilluminator.

3.6.6. S1 nuclease treatment

The components in the Table 3.5 were mixed and incubated for 30 minutes at 37 ºC. S1-nuclease treated samples were added with 6X gel loading dye and separated with a 1.8% agarose gel.

S.No	Components	Volume (μl)
1	DNA (500 ng)	4.75
2	S1 nuclease (50U)	0.5
3	5X reaction buffer	4
4	ddH_2O	10.25

Table 3.5. Components of S1 endonuclease digestion

3.6.7. Cloning

Primer	Sequence (5`-3`)
Forward Primer	AATTGGATCCGGGAGGGGCG
Reverse Primer	ATATGAATTCCTGAGTTCTCCTCC

Table 3.6. Primers used for amplification

The sequence of Myc-1 sequence (5'-GGGAGGGGCGCTTATGGGGAGGGTGGGGAGG GTGGGGAAGGTGGGGAGGAGACTCAG-3') was ordered from Sigma. Primers containing the restriction site of BamH1 and EcoR1 were obtained from Microsynth. The mixture containing the components of PCR reaction was prepared as shown in Table 3.7.

Components	Volume (µl)
Forward Primer (10 µM)	1
Reverse primer (10 µM)	1
10X buffer	5
dNTPs (2.5 mM)	4
Taq polymerase	0.5
Template	0.5
ddH_2O	25

Table 3.7. PCR components used for amplification of Myc.

Samples were added and PCR was performed with the following program.

Temperature	95 ºC	95 ºC	55 ºC	72 ºC	72 ºC	4 ºC
Duration	5 mins	15 seconds	15 seconds	15 seconds	5 mins	end

40 cycles

Table 3.8. PCR program used for PCR amplification of Myc

PCR samples were analyzed by gel electrophoresis (1.8% agarose gel). Appropriate negative controls without the template DNA were included.

S.No	Components	Volume (µl)
1	PCR of Myc (22.5 ng/µl)	18.5
2	BamH1	1
3	EcoR1	0.5
4	2X tango buffer	5
5	ddH_2O	-

Table 3.9. Components of restriction digestion of the insert.

S.No	Components	Volume (µl)
1	pHen1 DNA (155 ng/µl)	5
2	BamH1	1
3	EcoR1	0.5
4	2X tango buffer	4
5	ddH_2O	9.5

Table 3.10. Components of restriction digestion of pHen1.

Components were mixed in sterile vial and incubated for 1 hour at 37 ºC. Restricted samples were added with 6X gel loading dye and separated with a 1.8% agarose gel. Insert and vector DNA were extracted from the gel using a gel extraction kit. (Sigma)

S.No	Components	Volume (µl)
1	Insert (20 ng/µl)	3
2	Vector (15 ng/µl)	2
3	10X buffer	2
4	DNA ligase	1
5	ddH_2O	12

Table 3.11. Components of ligation.

Ligation components were added according to Table 3.11. Samples were then left at room temperature for 1 hour. The samples were then added to 100 µl of competent cells and kept on ice for 10 minutes. Meanwhile, a heating block was set to 42 ºC. The vials were kept at 42 ºC exactly for 45 seconds and transferred to ice. Fresh 1 ml of Luria Broth (LB) media was added and incubated at 37 ºC for 1 hour. The transformed cells were plated in LB media containing ampicillin. Plates were incubated at 37 ºC overnight.

Transformed colonies were checked for the presence of plasmid by prescreening colonies by PCR. PCR mixtures according to the table 3.12 were prepared and each colony from the plate

was picked by a sterile tip and added to the vials. After PCR, the samples were analyzed on 2% agarose gel.

Components	Volume (μl)
Forward Primer (10 μM)	1
Reverse primer (10 μM)	1
10X buffer	5
dNTPs (2.5 mM)	4
Taq polymerase	0.5
Template	0.5
ddH_2O	25

Table 3.12. PCR components for performing colony PCR.

3.7. References

[1] M. R. Detty, S. L. Gibson, S. J. Wagner, *J Med Chem* **2004**, *47*, 3897.

[2] Z. Dobronte, T. Wittmann, G. Karacsony, *Endoscopy* **1978**, *10*, 127.

[3] L. H. Gray, A. D. Conger, M. Ebert, S. Hornsey, O. C. Scott, *Br J Radiol* **1953**, *26*, 638.

[4] M. Dean, T. Fojo, S. Bates, *Nat Rev Cancer* **2005**, *5*, 275.

[5] D. E. Dolmans, D. Fukumura, R. K. Jain, *Nat Rev Cancer* **2003**, *3*, 380.

[6] K. R. Weishaupt, C. J. Gomer, T. J. Dougherty, *Cancer Res* **1976**, *36*, 2326.

[7] D. Kessel, *Biochemistry* **1977**, *16*, 3443.

[8] Z. Malik, M. Djaldetti, *Int J Cancer* **1980**, *26*, 495.

[9] D. P. Valenzeno, *Photochem Photobiol* **1987**, *46*, 147.

[10] C. Moucheron, A. Kirsch-De Mesmaeker, J. M. Kelly, *J Photochem Photobiol B* **1997**, *40*, 91.

[11] D. G. H. Allison R. R., Cuenca R., Hu X., Childs C. J. H., Sibata C. H., *Photodiagnosis and Photodynamic therapy* **2004**, *1*, 27.

[12] I. Diamond, S. G. Granelli, A. F. McDonagh, S. Nielsen, C. B. Wilson, R. Jaenicke, *Lancet* **1972**, *2*, 1175.

[13] T. J. Dougherty, *J Natl Cancer Inst* **1974**, *52*, 1333.

[14] S. H. Tomson, E. A. Emmett, S. H. Fox, *Cancer Res* **1974**, *34*, 3124.

[15] J. F. Kelly, M. E. Snell, M. C. Berenbaum, *Br J Cancer* **1975**, *31*, 237.

[16] T. J. Dougherty, J. E. Kaufman, A. Goldfarb, K. R. Weishaupt, D. Boyle, A. Mittleman, *Cancer Res* **1978**, *38*, 2628.

[17] D. A. Bellnier, G. R. Prout, Jr., C. W. Lin, *J Natl Cancer Inst* **1985**, *74*, 617.

[18] Ben-Hur E., Chan W., in *The Porphyrin handbook*, *Vol. 19*, Elsevier, **2003**, pp. 1.

[19] H. Ali, J. E. van Lier, *Chem Rev* **1999**, *99*, 2379.

[20] C. G. Claessens, U. Hahn, T. Torres, *Chem Rec* **2008**, *8*, 75.

[21] J. Alzeer, B. R. Vummidi, P. J. Roth, N. W. Luedtke, *Angew Chem Int Ed Engl* **2009**, *48*, 9362.

[22] S. Hirohara, M. Obata, S. Ogata, K. Kajiwara, C. Ohtsuki, M. Tanihara, S. Yano, *J Photochem Photobiol B* **2006**, *84*, 56.

[23] F. Wilkinson, W. P. Helman, R. A. B., *J. Phys. Chem. Ref. Data* **1993**, *22*.

[24] M. C. De Rosa, R. J. Cruthcley, *Coordination Chemistry Reviews* **2002**, *233*, 354.

[25] J. Sambrook, D. W. Russell, in *Molecular Cloning: A laboratory manual*, **2001**, pp. 7.51.

[26] A. Siddiqui-Jain, C. L. Grand, D. J. Bearss, L. H. Hurley, *Proc Natl Acad Sci U S A* **2002**, *99*, 11593.

[27] Z. Musil, P. Zimcik, M. Miletin, K. Kopecky, M. Link, P. Petrik, J. Schwarz, *Journal of Porphyrins and Phthalocyanines* **2006**, *10*, 122.

[28] M. O. Liu, C. Tai, M. Sain, A. T. Hu, Chou F., *Journal of Photochemistry and Photobiology A: Chemistry* **2004**, *165*, 131.

[29] A. Ogunsipe, D. Maree, T. Nyokung, *Journal of Molecular Structure* **2003**, *650*, 131.

CHAPTER 4. Guanidino phthalocyanines as CXCR3 antagonists

4.1. Introduction

4.1.1. Chemokines

Mammals have two types of fundamental immune functions, the “innate immune system” that consists of monocytes, granulocytes, macrophages, and natural killer cells, and “the adaptive immune system” that consists of T cells and B cells. The communication between these different cell types is largely mediated by chemokines and cytokines.

Chemokines are small (8-10 kDa), extracellular proteins which act as signaling molecules between immune cells. They can be functionally classified into homeostatic chemokines and inflammatory chemokines. Homeostatic chemokines are constitutively expressed for maintaining tissue homeostasis, and perform variety of functions such as directing lymphocytes to lymphoid organs and immuno surveillance. In contrast, inflammatory chemokines are not constitutively expressed, but are induced upon external stimuli and recruit lymphocytes for triggering inflammation or wound healing. There are more than 40 chemokine ligands and 19 receptors identified to date.[1-4]

4.1.1.1. Structure and functions

According to the presence of cysteine (C) residues at the N-terminus, chemokines can be classified into C, C-C, C-X-C, C-X_3-C where X is any amino acid. C-X-C group of chemokines can be further classified according to the presence of a Glu-Leu-Arg (ELR) motif that can be angiogenic (ELR +), or angiostatic (ELR -) when absent. The cysteine residues are known to be important for mediating interactions with receptors.[2, 4]

Chemokine receptors are G-protein coupled receptors that contain 7-transmembrane polypeptide chains. Upon binding to the receptor, the chemokine initiates a conformational change in the receptor and activates it. This leads to an exchange of GDP to GTP in the G

protein which eventually dissociates to G-α and G-βγ subunits. These dissociated G proteins perform variety of downstream signaling events depending on the receptor and ligand type. Broadly, several physiological processes such as cell differentiation, angiogenesis, angiostasis, migration, invasion, immune surveillance and lymphocyte trafficking are all controlled by these chemokine-ligand interactions.[2]

4.1.2. CXCR3-CXCL10

According to the results from microarray analysis and qRT-PCR, Zn-DIGP causes highly selective overexpression of CXCL10 in treated cells. CXCL10 is a chemokine that binds to the receptor CXCR3. Other CXCR3 ligands include CXCL9 and CXCL11. The dissociation constant for murine CXCR3 and the ligands CXCL9, CXCL10 and CXCL11 are 11.65 ± 0.9 nM, 1.35 ± 0.56 nM, and 1.41 ± 0.2 nM respectively.[5]

4.1.2.1 Structure

The CXCL10 gene encodes for a 10 kDa interferon-gamma inducible chemokine with a 21 amino acid signal peptide that gets cleaved during the downstream events. The N-terminus of CXCL10 has one intervening amino acid between two cysteines, so it is classified as a "CXC" chemokine. Moreover, CXCL10 lacks an ELR motif, suggesting that it is angiostatic. An independent NMR study demonstrated that CXCL10 has series of loops and one turn of a 3-10 helix at its N-terminus, followed by three antiparallel β strands packed against C-terminal α helix. Disulfide bridges are formed between cysteines 9-36 and 11-53.[6] Though the NMR study was performed using a mutated CXCL10 that is monomeric, X-ray diffraction studies of wild type CXCL10 suggest that CXCL10 exists as a dimer or tetramer.[7]

CXCR3 is a seven transmembrane G-protein coupled receptor containing 316 amino acids. The structure of the CXCR3 receptor is not fully characterized but CXCR3 is known to be expressed in different forms in different target cells. The classical receptor CXCR3-A is expressed in type 1-helper (Th1) T cells, cytotoxic CD8+ T cells, activated B cells and natural killer cells. CXCR3-A is activated by CXCL9, CXCL10 and CXCL11. A spliced variant CXCR3-B contains a longer N-terminal extracellular domain that mediates its angiostatic effects. CXCL4 is reported to bind specifically to CXCR3-B, but not to CXCR3-

A.[8] Recently, a third CXCL3 variant having a truncated C-terminus that gives only 5 or 6 transmembrane passes was reported to be selectively activated by CXCL11.[9]

4.1.2.2. CXCR3-CXCL10 interaction

The receptor binding and activation of CXCR3 occurs in two steps. In the first step, CXCL10 binds to the N-terminus of the receptor and in the second step, the N-terminus of CXCL10 binds to a second site of the receptor causing activation. Step 1 is mediated by a docking domain located between the first pair of conserved cysteines and the first β strand responsible for recognition. The amino acids responsible for docking include 20s loop (Arg 20, Arg 22), β1 strand (Ile 24) and the 40s loop (Lys 46 and Lys 47). Step 2 is mediated by a triggering domain which is the unstructured N-terminus (Arg 5, Arg 8) of CXCL10. Oligomerization of CXCL10 was found to be necessary for biological functions of CXCL10.[6, 7] Apart from CXCR3, CXCL10 is reported to bind to glycosoaminoglycans like heparin sulphate,[7] another possible target of Zn-DIGP.[10]

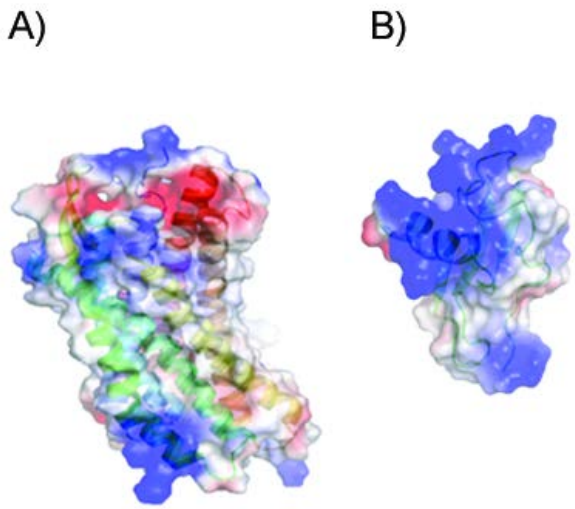

Figure 4.1. Computer-generated model of CXCR3 (A) and NMR structure of CXCL10 (B). Blue and red colors represent cationic and anionic residues.

4.1.2.3. Downstream signaling

Downstream signaling events of CXCR3 activation were studied in pericytes.[11] The binding of ligands to CXCR3 resulted in the activation of the Ras/ERK cascade by triggering components such as Ras, Raf-1 and MEK. The addition of CXCL10 caused increased phosphoinosital 3 kinase (PI3K) activity which further activates Akt kinase and PDK-1. Activation of CXCR3 also caused activation of Src kinases. Moreover, cross-talk between

ERK, Src and PI3K was observed since Src was reported to activate the ERK cascade. Combining the studies, Marra and coworkers proposed that activation of Src results in recruitment of Ras to trigger the ERK cascade. In parallel, activation of PI3K and Akt was also achieved, although the relation between this pathway and activation of Src remains unclear. These pathways mediate critical cellular functions such as cell proliferation, actin polymerization, cell invasion and migration.[11]

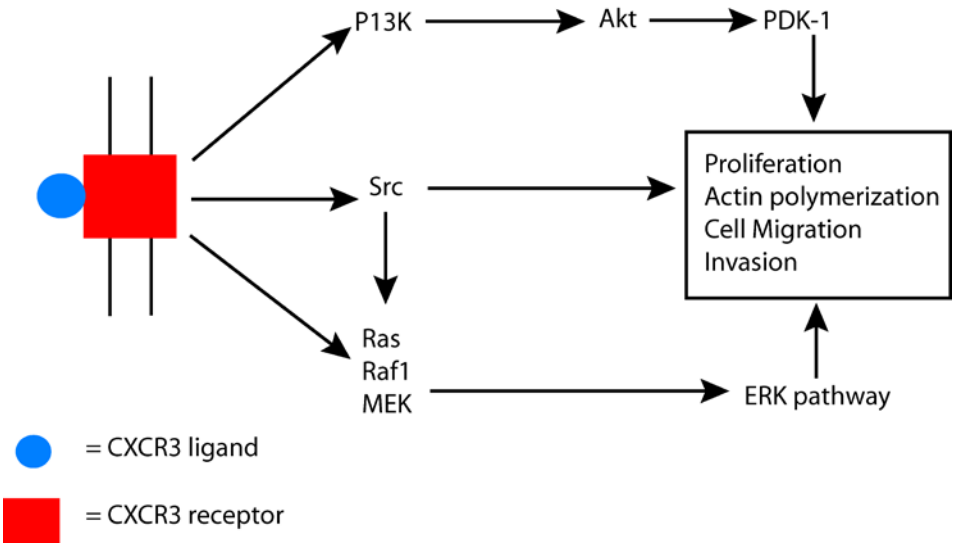

Figure 4.2. CXCR3 activation pathway in pericytes leading to downstream signals such as chemo attraction, invasion, migration and proliferation.

Following receptor activation, CXCR3 is degraded following its internalization. In T-lymphocytes, CXCL11-mediated endocytosis was independent of the clatharin pathway or calveolae pathways. Cell surface replenishment of CXCR3 occurs by de novo synthesis and transport through the endoplasmic reticulum and Golgi.[12] Two distinct domains that contribute to CXCR3 internalization are its carboxy terminus and β-arrestin1 for CXCL9/10 or a third intracellular loop for CXCL11.[13]

4.1.2.4. Expression and Function

CXCR3 is absent in naive T cells, but its expression is induced upon activation by dendritic cells. It remains highly expressed in type-1 helper (Th1)-type CD4+ T cells, effector CD8+ T cells, and innate-type T lymphocytes such as natural killer cells and monocytes. CXCL10 is secreted by activated T-lymphocytes, endothelial sites, monocytes, neutrophils and keritonocytes. The ligands CXCL9, CXCL10 and CXCL11 are thought to have similar functions *in vivo*. Among the differences in regulation, CXCL10 is induced by Interferon

(IFN) α/β/γ, whereas CXCL9 induction is restricted to IFN-γ. CXCL11 is induced by IFN-γ/β.[14]

The CXCL10 promoter contains a functional Interferon Stimulated Response Element (ISRE) and nuclear factor κβ1 binding site. Apart from signal induction by IFN- γ, CXCL10 is also induced by Toll-like receptors and RNA helices including RIG-1 and MID5 through activation of IFN-regulatory factor 3 and the release of IFN-α. Autocrine signaling between IFN-α and STAT1 activates the CXCL10 gene. CXCL10 is also reported to be induced by hypoxia reperfusion injury by NF-κβ activation.[14]

The major functions associated with CXCL10-CXCR3 interactions are chemoattraction of immune cells to target sites, and mediation of angiostatic activities. During inflammation, IFN-γ produced by leukocytes induces the production of CXCR3 ligands in stromal cells, immune cells, and transformed tumor cells. In response, ligands recruit activated T-lymphocytes that express CXCR3 through paracrine signaling and localize it to the target site. The chemokines also bind to CXCR3-B in endothelial cells and activate a p38 pathway that mediates angiostatic activities.[15]

4.1.3. In cancer

Kawada and coworkers demonstrated that CXCR3 promotes colon cancer metastasis to lymph nodes. They constructed cells expressing CXCR3 (‘DLD1CXCR3’) and compared them to non-expressing control cells in nude mice. Both cell lines reached lymph nodes after 2 weeks but, DLD1CXCR3 cells generated colonies that expanded more rapidly than control cells.[16] In another study, CXCR3 was detected in a variety of breast cancer cells such as MDA-MD-231, MCF-7 and T47D.[17] CXCR3 silencing inhibited lung colonization and spontaneous lung metastasis, but had no effect on locally growing tumors. These anti-metastatic activities were compromised in natural killer (NK)-deficient cells, implying an importance of NK cells in inhibiting metastasis.[18] Clinical diagnoses suggested that >85% of cancer patients show moderate CXCR3 staining in breast cancer, and a significant correlation between CXCR3 expression and poor survival rate was observed. In lymphoma, CXCR3 was reported to be expressed in only certain subsets of lymphomas, in contrast to CXCR5 which is expressed by all types of B-cell lymphomas. Hence, Jones and coworkers proposed that CXCR3 could be a marker for B-cell chronic lymphocytic leukemia.[19]

The chemokine CXCL10 is reported to be involved in both tumor progression and inhibition. High levels of endogeneous CXCL10 expression were reported in Hodgkins lymphoma and nasopharyngeal carcinoma,[20] as well as breast cancer cell lines,[17] and renal carcinoma cell lines.[21] Moreover, CXCL10 promotes growth of thyroid cancer cells,[22] and invasion in colorectal cancer cells.[23] In colorectal cancer cells, Raitman and coworkers demonstrated that CXCL10 causes overexpression of matrix metallo proteinase 9 (MMP9) and induces cell migration.[23] Conversely, CXCL10 is also reported to inhibit cell proliferation of neuroblastoma,[24] and prostate cancer cell lines.[25] In hepatocellular carcinoma patients, a correlation between infiltrating lymphocytes and CXCL10 overexpression was observed.[26] In renal cell carcinoma, CXCL10 overexpression facilitated the inhibition of tumor regeneration.[27] Wendel and coworkers demonstrated that exogenous application of CXCL10 to lymphoma increases NK cell accumulation and prolonged survival. Their results further indicated that CXCL10 expression has an important role for NK infiltration into tumors.[28] According to the angiostatic mechanism, Sdgari and coworkers showed that CXCL10 overexpression in human lymphoma causes spontaneous tumor regression in immune-compromised nude mice.[29]

4.1.3.1. Role of CXCL10 and CXCR3 in melanoma

Metastatic melanoma cells such as B16F10, B16F1, BLM and SK-Mel-28 were all reported to express CXCR3.[30, 31] Silencing of the CXCR3 gene in B16F10 cells resulted in reduced migration and invasion upon addition of CXCL9 or CXCL10. CXCR3-deficient B16F10 cells injected into a lymph node metastatic mouse model C57BL/6 demonstrated reduced lymph node metastasis as compared to wildtype B16F10 cells. Similarly, when CXCL9 and CXCL10 were injected with adjuvant into lymph nodes, wild type B16F10 cells caused larger metastatic colonies to form.[30] In another study, using the BLM melanoma cell line, it was shown that CXCL9 activates the small GTPases RhoA and Rac1, inducing the reorganization of actin cytoskeleton to trigger cell chemotaxis.[31] In patients having cutaneous malignant melanoma, a positive correlation between CXCR3 expression with tumor thickness and progression was reported.[32]

The chemokine CXCL10 has an inhibitory role in melanoma metastasis. When CXCL10 was genetically expressed in tumor cells, no significant impact in proliferation was observed but host-mediated anti-tumor effects were observed *in vivo*. The response was reported to be T

cell-dependent, and mediated by lymphocytes, neutrophils and monocytes.[33] When B16F1 cells were transfected with an adenovirus vector expressing CXCL10, reduced melanoma invasion *in vitro* and reduced melanoma metastasis *in vivo* were observed. Furthermore, screening for 30 different chemokines in patients revealed that CXCL10 was overexpressed among patients in remission than progression. These results clearly demonstrated that increase in CXCL10 levels serve to reduce melanoma metastasis.[34]

Results from our microarray analyses and qRT-PCR demonstrate that addition of Zn-DIGP to B16F10 cells causes increase in CXCL10 mRNA (Figure 2.21 and Figure 2.22). Enzyme linked immunosorbent assays (ELISA) were used to quantify the changes in CXCL10 expression at the protein level (Figure 4.3). Depending upon the Zn-DIGP concentration and incubation time, as much as 20-fold upregulation of CXCL10 was observed.

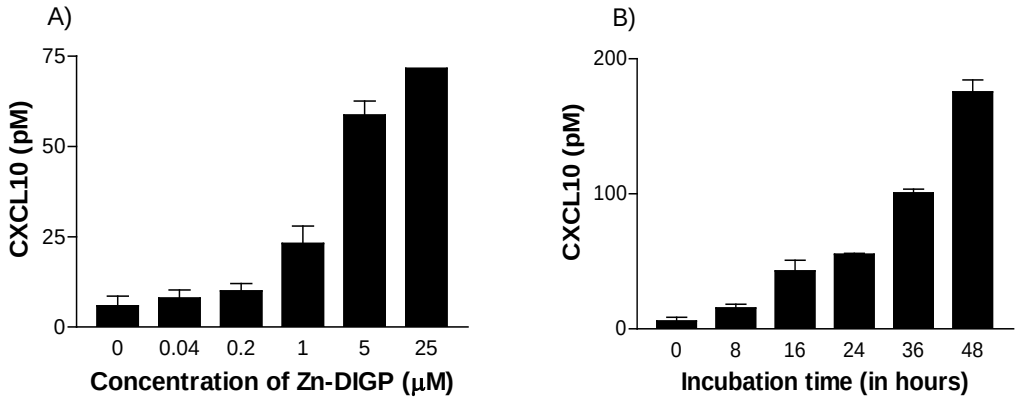

Figure 4.3. Changes in extracellular CXCL10 concentrations according to ELISA. A) Zn-DIGP concentration-dependent changes after 24 hours of treatment. B) Time-dependent changes in CXCL10 concentrations in the presence of 5 μM of Zn-DIGP.

The possible reasons for CXCL10 overexpression upon addition of Zn-DIGP is subjected to further investigation here. According to previous reports,[35] co-expression of TNF-α and IFN-γ cause transcriptional activation of CXCL10. Hence, we evaluated the ability of Zn-DIGP to impact TNF-α and IFN-γ expression. As shown in Figure 4.4, Zn-DIGP did not induce expression of these secreted cytokines. We therefore speculated that CXCL10 overexpression might be related to the ability of Zn-DIGP to inhibit the CXCL10/CXCR3 binding interaction.

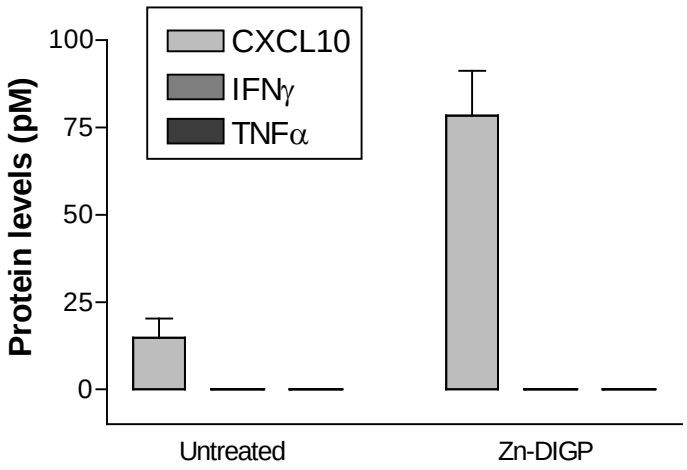

Figure 4.4. Changes in protein concentration (CXCL10, IFN-γ, TNF-α) according to ELISA upon addition of 5 μM of Zn-DIGP to B16F10 cells for 24 hours.

4.1.4. CXCR3 antagonists

CXCR3 activation is well known to promote cancer metastasis, and this has motivated the development of suitable antagonists for CXCR3. One of the most promising antagonists reported to date is AMG-487 (**1**) (Figure 4.5). AMG-487 competitively binds to CXCR3 and displaces CXCL10 and CXCL11 with an IC_{50} of 8 nM and 8.2 nM, respectively. CXCL10- and CXCL9-mediated cell migration was also inhibited by AMG-487. The pharmacokinetic parameters of AMG-487 suggested moderate clearance after intravenous dosing in dogs, and AMG-487 was found to be orally available. A sub-cutaneous dose of 3 mg/kg of AMG-487 showed similar migration inhibition results as using CXCR3-deficient cell lines.[36] Organ-specific inhibition of metastatic colon carcinoma was also observed.[37] AMG-487 inhibits lung metastasis *in vivo*. Studies involving mice deficient in NK cells indicated a reduced anti-metastatic activity, suggesting the possible involvement of natural killer cells in mediating metastasis inhibition.[38] Unfortunately, AMG-487 did not exhibit any efficacy in phase II clinical trials among patients with psoriasis and rheumatoid arthritis and hence the trial was terminated.[39]

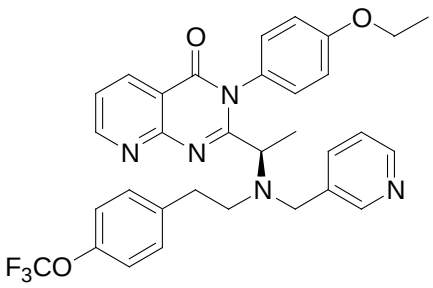

(1)

Figure 4.5. Structure of AMG-487.

Compounds containing a piperdinyl scaffold have also been reported to be CXCR3 inhibitors (Figure 4.6). A series of 1-aryl-3-piperdine-4-yl urea (**2**) were found to be good inhibitors, but they have high log D values, low solubility in water, and therefore poor pharmacokinetics properties.[40] Replacing the urea with thiodiazole,[41] the central piperidine unit to exo-tropanyl[41] or the benzyl urea with 2-amino quinoline[42] resulted in molecules that gave better pharmocodynamics, good potency, good solubility and bioavailability.

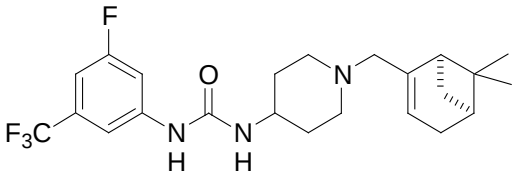

(2)

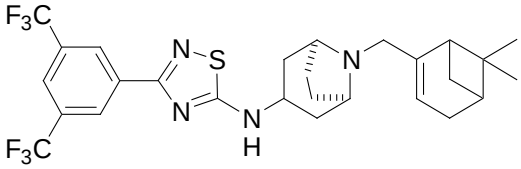

(3)

Figure 4.6. Structure of piperdinyl urea analogs.

High-throughput screening identified a new lead compound containing 4-aryl-[1,4] diazepene ethyl urea as a CXCR3 inhibitor (**4**) (Figure 4.7). One such compound inhibited CXCL10-mediated calcium flux with an IC_{50} as low as 20 nM and CXCL10-mediated migration with an IC_{50} of 100 nM.[43]

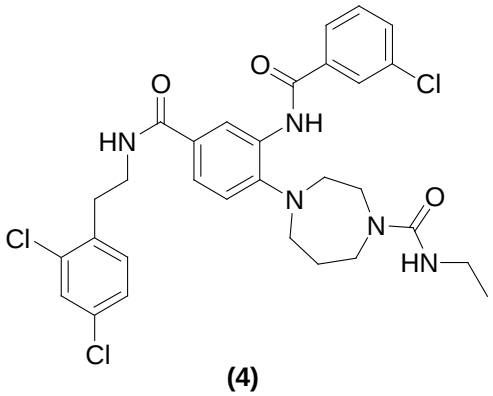

(4)

Figure 4.7. Structure of a 4-aryl-[1,4] diazapene ethyl urea.

High-throughput screening using membrane filtration binding experiments identified a benzimidazole (**5**, Figure 4.8) as a weak inhibitor (IC_{50} = 3 μM) of CXCR3. Modifying the aliphatic substituent at the C4 position improved its potency, and it inhibited CXCR3 with IC_{50} of 80 nM.[44] Further lead optimization resulted in discovery of a new compound (**6**) binding to CXCR3 in the low nM range (20-50 nM).[45] The main disadvantage associated with these molecules was metabolic instablility upon exposure to mouse liver microsomes.[45]

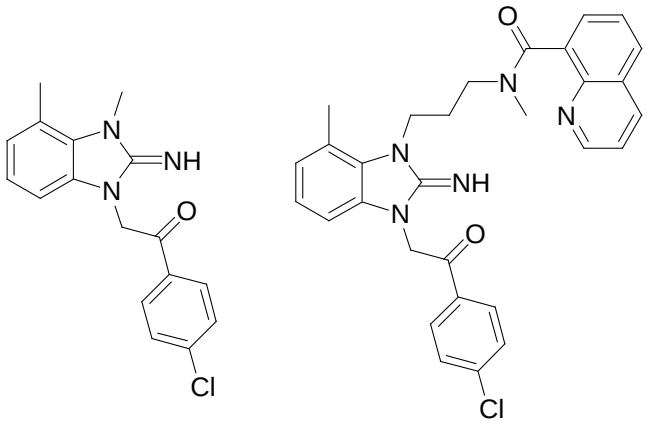

(5) **(6)**

Figure 4.8. Structures of benzimidazole analogs.

A series of 3-disubstituted piperidine-2,6-diones analog of benzamitide (**7**, Figure 4.9) were tested for their ability to inhibit CXCL11-mediated cAMP production in CXCR3-transfected Chinese hamster cells. Apart from binding to CXCR3, this experiment revealed that one enantiomer of the racemic mixture was capable of binding to a muscarinic receptor. Substitutions of 3-piperidine ring with carbonyl functions was found to increase selectivity over the muscarinic receptor.[46]

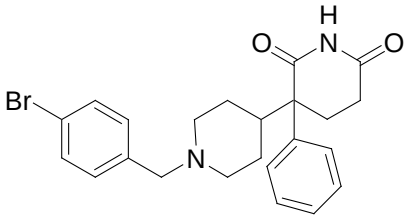

(7)

Figure 4.9. Structure of a 3-disubstituted piperidine-2,6-dione.

Leurs and coworkers reported another scaffold containing a guanidinium group "IPAG" to be a CXCR3 antagonist (**8,** Figure 4.10). IPAG gave moderate CXCR3 affinity with pK_i of 5.4 in the ^{125}I-CXCL10 displacement assays.[47]

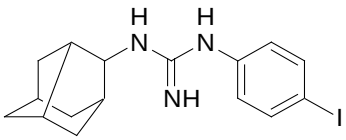

(8)

Figure 4.10. Structure of IPAG.

B16F10 cells are known to express both CXCL10 and CXCR3.[48] The high-affinity interaction between CXCL10 and CXCR3 ($K_d \approx 0.2$ nM) is mediated by arginine, lysine and isoleucine residues of CXCL10 that bind to an acidic patch on CXCR3.[6, 7] Interestingly, all of the CXCR3 antagonists highlighted here contain at least one basic functional group. These compounds can therefore be classified as hydrophobic cations. As hydrophobic cations, the similar physicochemical properties of CXCL10 and Zn-DIGP suggested that Zn-DIGP could mimic CXCL10 to competitively bind CXCR3. Hence, the affinity of Zn-DIGP to CXCR3 was investigated.

4.2. Results and Discussion

4.2.1. CXCR3 binding studies: Radiolabeled ligand displacement assays

Competitive displacement experiments using membrane-immobilized CXCR3 receptors and ^{125}I-labeled CXCL10 were conducted. Human cells Chem 1 overexpressing CXCR3 were membrane purified and immobilized on to filter plate coated with polyethyleneimine. The addition of ^{125}I-labeled CXCL10 to these preparations results in selective binding of the immobilized CXCR3. The addition of variable concentrations of unlabeled CXCL10 or Zn-DIGP causes displacement of ^{125}I-labeled CXCL10 depending from the membrane. This loss of ^{125}I labeled CXCL10 can be monitored using a scintillation counter (Figure 4.11). By plotting the sigmoidal dose response curve, IC_{50} and K_i can be determined. K_i values are summarized in Table 4.1.

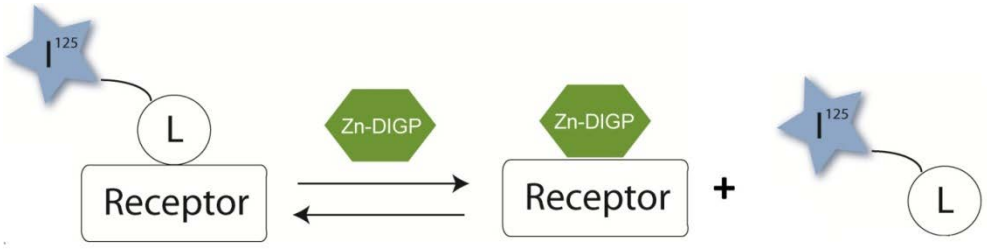

Figure 4.11. Schematic of radiolabeled ligand displacement assays.

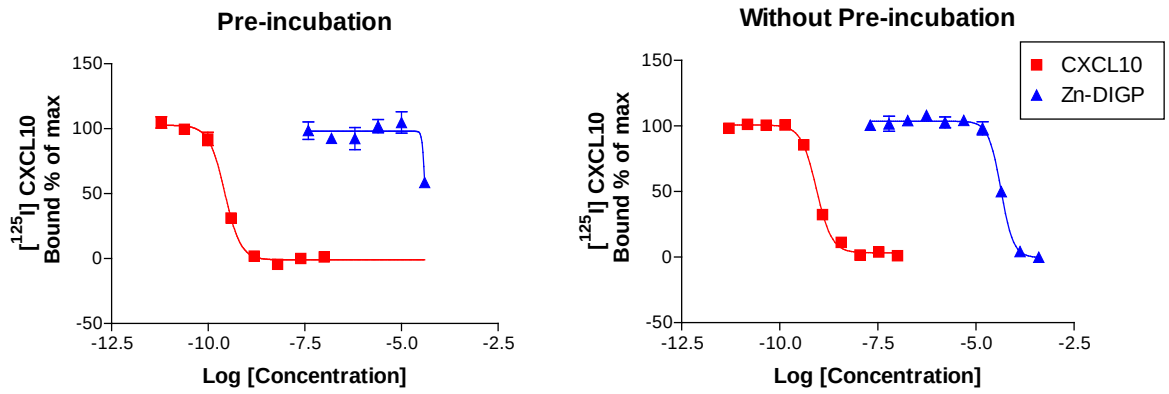

Figure 4.12. Binding studies of Zn-DIGP to CXCR3 with/without prior incubation with Zn-DIGP according to radiolabeled ligand displacement assay.

As a control, unlabeled CXCL10 was titrated and the apparent K_i (0.57 ± 0.02 nM) matched previous reports.[49] Using this assay, Zn-DIGP was found to displace ^{125}I-labelled CXCL10 with an apparent K_i of 29 ± 1 μM (Figure 4.12). To evaluate any possible effect of the order addition, Zn-DIGP was incubated prior to ^{125}I-CXCL10 addition. The pre-incubation step did not affect the K_i values. Hence, Zn-DIGP can reversibly bind to the CXCR3 receptor (Figure 4.12).

Compound	IC_{50}	K_i
CXCL10	0.86 nM	0.57 nM
ZnDIGP	44 μM	29 μM
CXCL10 : 60 minutes pre-incubation	0.26 nM	0.18 nM
ZnDIGP : 60 minutes pre-incubation	37 μM	25 μM

Table 4.1. Results of radiolabeled ligand displacement assays.

4.2.2. Agonist assays

To evaluate the functional impact of Zn-DIGP - CXCR3 binding, agonist assays were performed in Chem 1 cells that over express CXCR3 by monitoring changes in intra-cellular calcium levels. Activation of CXCR3 by CXCL10 causes increases in intra-cellular calcium levels that can be monitored by the fluorescence of a Ca^{2+}-specific dye “fluo-8”. The addition of Zn-DIGP did not increase in calcium levels even at a concentration of 1 mM which is approximately 40 times higher than K_i of Zn-DIGP for displacement of CXCL10 from CXCR3 (Figure 4.13). These results suggest that Zn-DIGP does not activate CXCR3.

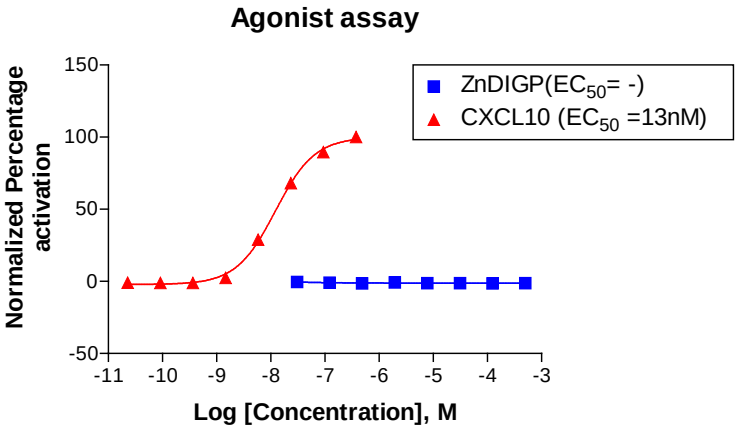

Figure 4.13. Activation of receptor by CXCL10 and Zn-DIGP in CXCR3 expressing Chem 1 cell line according to intra-cellular calcium levels.

4.2.3. Antagonist assays

To test the ability of Zn-DIGP to inhibit CXCL10-mediated activation of CXCR3, Zn-DIGP was incubated with CXCR3 expressing Chem 1 cells for 15 minutes followed by the addition of 13 nM CXCL10 (EC_{50} from agonist assays). Reduced calcium levels were observed in Zn-DIGP treated samples (Figure 4.14). The IC_{50} of Zn-DIGP for CXCL10-CXCR3 inhibition was 3.8 ± 0.6 µM. Notably, the IC_{50} is approximately the same concentration used for most of the experiments (mice studies, microarray, qRT-PCR) reported here. Results from the ligand displacement assays and the agonist assays demonstrate that Zn-DIGP binds to CXCR3 and inhibits receptor activation.

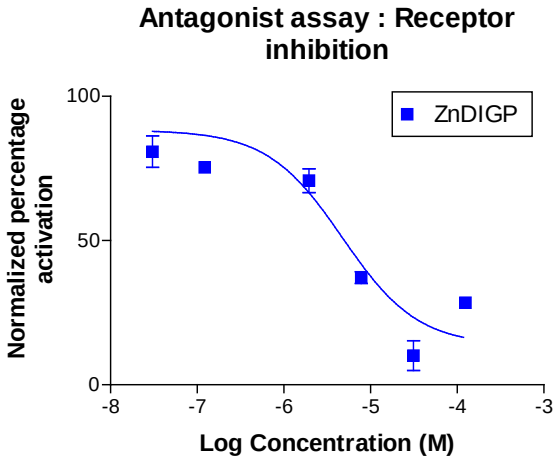

Figure 4.14. Inhibition of the receptor activation in the Zn-DIGP-treated Chem1 cells according to changes in intra-cellular calcium levels.

4.2.4. Receptor Internalization assays

The IC_{50} for CXCR3 inhibition is almost 8-fold lower than the K_i value observed for CXCL10 displacement (29 ± 1 μM). This apparent conundrum can be explained by cell surface dynamics and receptor turnover. It is important to note that ligand displacement assays were performed using CXCR3 embedded on membranes whereas the calcium flux assays were performed using live cells. Since CXCL10 binding is known to initiate internalization of CXCR3 [12, 38, 50], we speculated that Zn-DIGP binding might also cause receptor internalization, albeit without receptor activation. To test this possibility, B16F10 cells were treated with Zn-DIGP or CXCL10, and CXCR3 was visualized by immunofluorescence. In both the cases, a dramatic loss of CXCR3 staining was observed after 1-2 h of incubation (Figure 4.15). The localization of CXCR3 was also distinctly different in treated and untreated cells, where CXCR3 was distributed over the cell surface of control samples, whereas CXCL10 and Zn-DIGP treated cells exhibited perinuclear CXCR3 accumulation consistent with receptor turnover (Figure 4.15). The differences between Zn-DIGP IC_{50} value for CXCR3 inhibition (3.5 μM) and its CXCR3 affinity ligand displacement (K_i = 29 μM) can therefore be attributed to the ability of Zn-DIGP to bind CXCR3 without activation of the receptor, yet causing endocytosis and degradation of CXCR3.

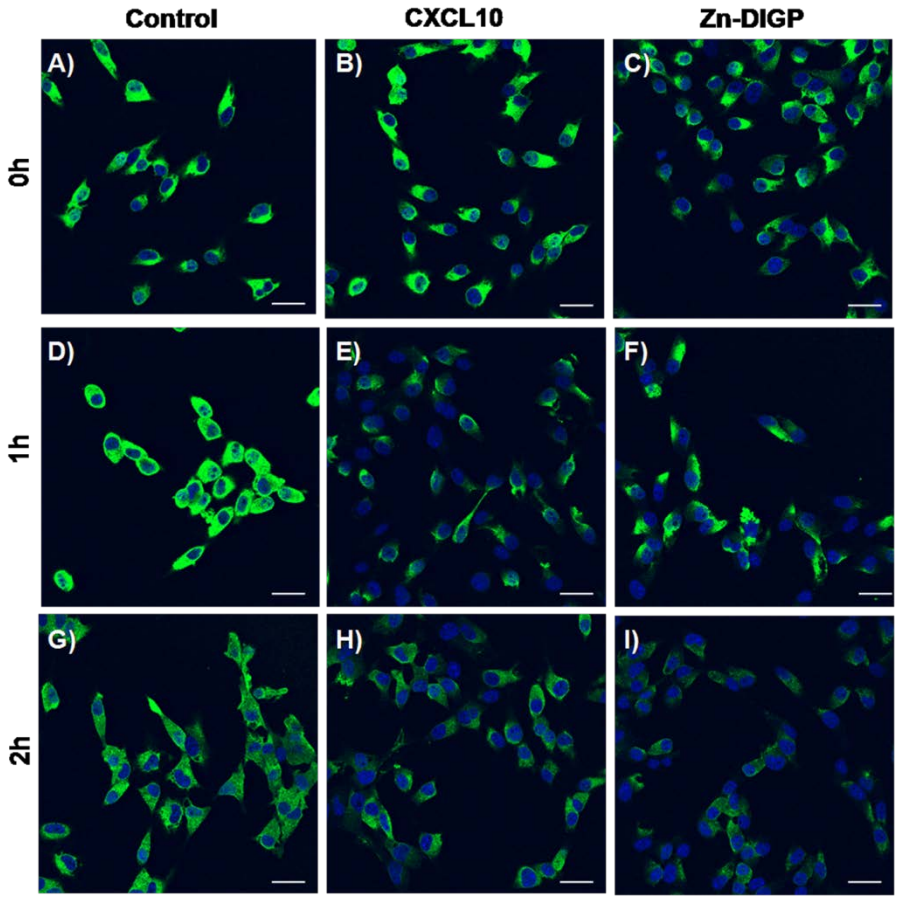

Figure 4.15. Confocal microscopy images of B16F10 cells stained for CXCR3 following the addition of Zn-DIGP (5 μM) or CXCL10 (20 nM). Green staining represents the CXCR3 specific antibody and blue staining represent nucleus specific Hoechst 33258. (A) – (C) are images taken at t = 0 of incubation, (D) – (F) are images taken after 1 hour following the addition of CXCL10 and Zn-DIGP. G-I represents images taken after 2 hours of media, CXCL10 and Zn-DIGP addition. In all cases, cells were fixed prior to imaging. Scale bars represent 30 μm.

4.2.5. Migration assays

Upon CXCL10-mediated activation of CXCR3, the spike in intracellular calcium levels is known to trigger actin polymerization and increased cellular migration.[30, 38] We therefore investigated CXCL10-activated cellular motility using scratch assays (Figure 4.16).[51] As a selectivity control, the chemotactic cytokine CCL21, that binds to receptor CCR7 and Epidermal growth factor (EGF) were also evaluated.[52] The changes in migration indices indicate specific inhibition of CXCL10-mediated cellular migration by Zn-DIGP (Figure 4.17).

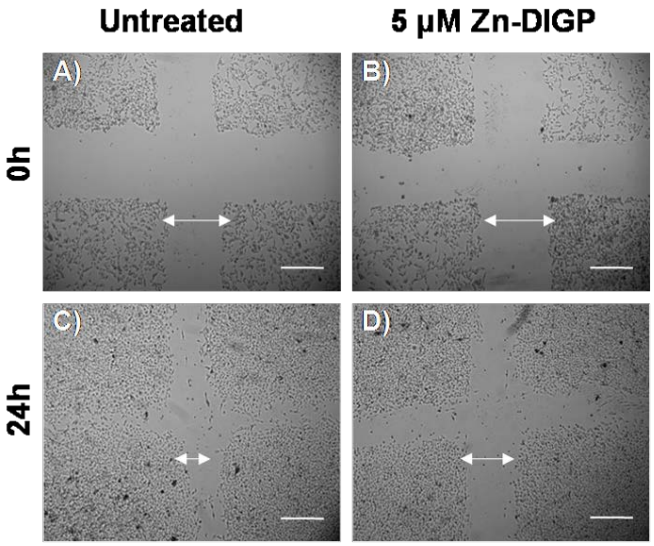

Figure 4.16. Bright field images of scratches made in monolayers of B16F10 cells. (A) – (B) images taken immediately after addition of CXCL10 in untreated and Zn-DIGP treated cells. (C) - (D) are images taken after 24h. Scale bars represent 50 mm.

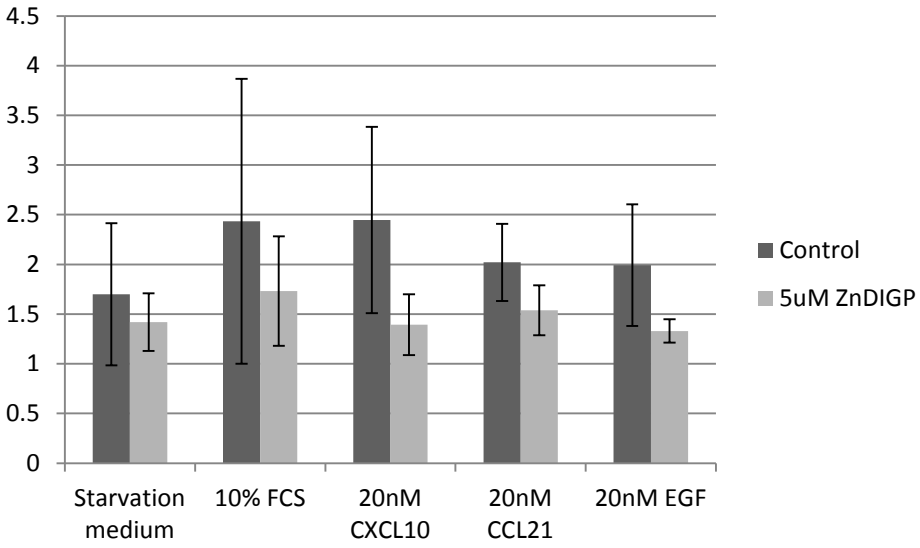

Figure 4.17. Inhibition of CXCL10-induced migration by Zn-DIGP in B16F10 cells according to scratch assays.

Results from these migration results are summarized in Figure 4.17. The use of Zn-DIGP did not cause large changes in migration in samples containing media only. Addition of 20 nM CXCL10 caused a large increase in cell migration that is inhibited by Zn-DIGP. The data can be expressed quantitatively by calculating the “migration effect” which is the ratio of migration indices for Zn-DIGP-treated samples divided by the respective controls. The smaller the migration effect ratio, the greater the influence of Zn-DIGP has on inhibiting

migration. As shown in Table 4.2., the migration effect ratio is smallest for CXCL10. Smaller effects were observed for CCL21, EGF, media containing 10% FCS.

S.No	Condition	Migration Index		Migration effect
		Control	Zn-DIGP	
1	Starvation medium	1.7	1.4	0.83
2	20 nM CXCL10	2.5	1.5	0.56
3	10% FCS	2.4	1.75	0.71
4	20 nM CCL21	2	1.5	0.76
5	20 nM EGF	2	1.4	0.67

Table 4.2. Summary of migration indices according to scratch assays.

To further evaluate these effects, we varied the concentration of CXCL10 (Figure 4.18). As expected, as the concentration of CXCL10 increased, the migration index was also increased. Zn-DIGP-treated cells, however, were not sensitive to increasing concentrations of CXCL10.

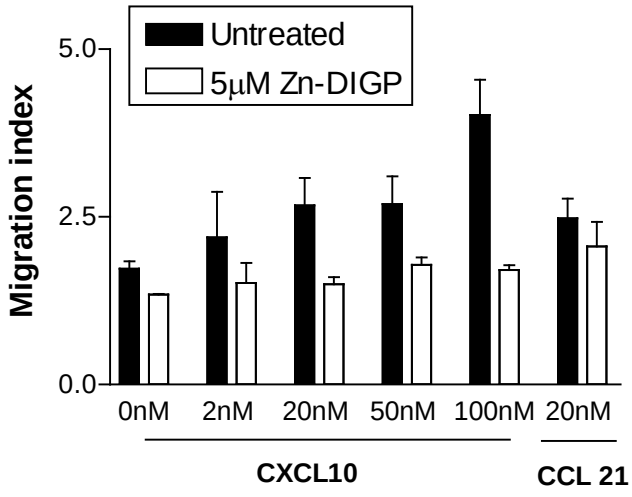

Figure 4.18. Scratch assay results where migration index is defined as the ratio of the area of scratch at 0h to 24h.

Condition	Migration Index		Migration effect
	Control	Zn-DIGP	
Starvation medium	1.5	1.3	0.781
2 nM CXCL10	2	1.45	0.72
20 nM CXCL10	2.1	1.4	0.65
50 nM CXCL10	2.6	1.8	0.67
100 nM CXCL10	3.9	1.7	0.44
20 nM CCL21	2.2	1.85	0.83

Table 4.3. Summary of migration effects with increasing concentration of CXCL10 according to scratch assays.

4.2.6. Invasion assays

CXCL10-CXCR3 activation is reported to activate invasion. According to a matrigel-based invasion assay, cells treated with CXCL10 and Zn-DIGP showed approximately 2-fold decreases in invasion index as compared to cells treated only with CXCL10. In the case of CCL21- activated invasion, little, if any inhibition by Zn-DIGP was observed (Figure 4.19).

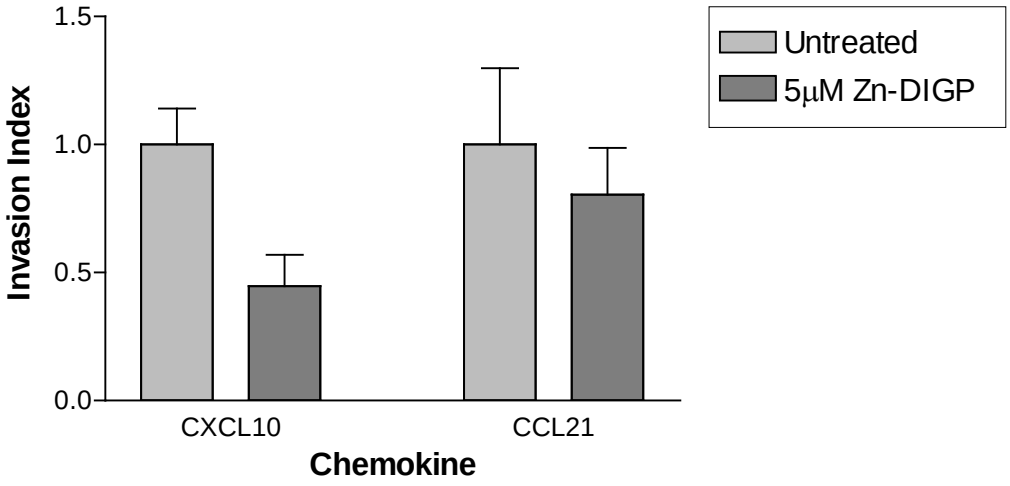

Figure 4.19. Results from Matrigel-based invasion assays using 20 nM of CXCL10 or CCL21 as the chemoattractant.

4.2.7. In vivo studies

As CXCR3 antagonism and CXCL10 overexpression are both known to inhibit melanoma metastases *in vivo*, we decided to evaluate the anti-metastatic activities of Zn-DIGP using a well-known assay that mimics the hematogenous spread of malignant melanoma *in vivo*. In this assay, C57BL/6 mice were intravenously injected into the tail vein with B16F10 cells. After 20 days, the animals were sacrificed and the number of lung metastases determined by visual inspection.[53, 54] Control animals receiving untreated cells or cells treated with the carrier-only (sodium trifluoroacetate in DMSO) contained 38 ± 8 (average ± standard deviation) lung metastases on day 20. When the B16F10 cells were pre-treated 5 μM of Zn-DIGP (Type A) in cell cultures for 16 hours prior to their injection, an almost complete inhibition of lung metastases was observed with only a single animal of six containing four small tumors on day 20. The other five animals were tumor-free (Figure 4.20). In a more stringent experimental design (type B), a solution of Zn-DIGP was injected into the animals directly at 8 mg / kg on day two, following the injection of untreated B16F10 cells into the same animals on day one. All animals treated this way reacted well to the injection, showed no signs of subsequent stress, and survived the duration of the experiment to day 20. In this experiment, the intravenous application of Zn-DIGP caused an approximate 50% reduction in the number and size of lung metastases on day 20. (Figure 4.20)

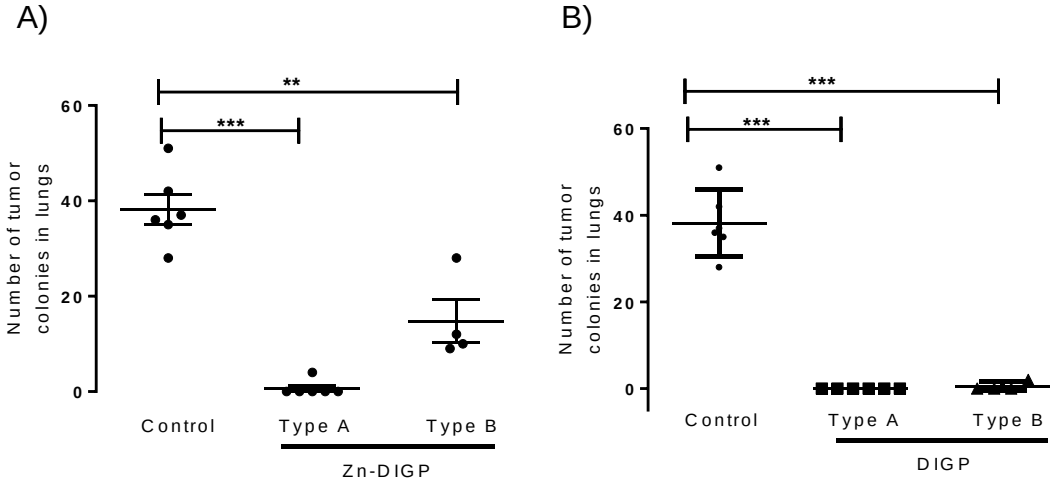

Figure 4.20. *In vivo* effects of Zn-DIGP (A) and DIGP (B) on melanoma tumor growth. Vertical bars represent the mean number and standard error of tumor colonies present in lungs on day 20. *** and ** represent $p < 0.001$ and $p < 0.01$ respectively.

4.3. Conclusion

CXCL10 overexpression caused by Zn-DIGP in B16F10 appears to be independent of both G-quadruplex structures or overexpression of IFN-γ or TNF-α. Zn-DIGP competitively binds to CXCR3 with a K_i of 29 μM, a value approximately 7-fold higher than its IC_{50} value for CXCR3 - CXCL10 inhibition (IC_{50} = 4 μM). The differences between these values can be explained by the ability of Zn-DIGP to bind CXCR3 without activation of the receptor, yet causing endocytosis and degradation of CXCR3. There are few peptide antagonists known to cause internalization of GPCRs.[55, 56] However, to the best of our knowledge, this is the first example of a small molecule GPCR antagonist that has been shown to cause receptor internalization and degradation.[57] Zn-DIGP-mediated overexpression of CXCL10 and antagonism of CXCR3 adds indirect evidence for the presence of an endogenous feedback loop between CXCR3 and CXCL10 expression.

Since CXCR3 antagonism is an attractive anti-cancer target, Zn-DIGP was evaluated for its anti-metastasis activity *in vivo*. Zn-DIGP was found to be well tolerated upon its intravenous injection into mice at 8 mg/kg and was capable of inhibiting the formation of tumor colonies in the lungs of C57BL/6 mice injected with B16F10 cells. This study opened up new avenues for phthalocyanine scaffolds as new antagonists for GPCR's, in particular CXCR3.

We have demonstrated that Zn-DIGP exhibits excellent properties as a PDT agent (Chapter 3) as well as an ability to inhibit formation of tumor colonies in the lungs of C57BL/6 mice injected with B16F10 cells. To the best of our knowledge, Zn-DIGP provides the first example of a preclinical candidate possessing both of these properties.

4.4. Experimental Methods

4.4.1. ELISA

B16F10 cells (~2.5×10^5) were seeded in T25 flasks and grown for 24 hours under standard conditions (see Cell Lines and Media section). Zn-DIGP to a final concentration of 5 μM (0.1 % DMSO) in fresh media was then added and the cells grown under standard conditions for 8 – 48 hours. Appropriate carrier controls (DMSO only) were also included. 5 ml of cell media was concentrated to 750 μl by a biological concentrator (Milipore UFC800324). Murine IFN-γ and TNF-α was quantified by ELISA previously described.[53, 54] Briefly, 0.5 μg/ml of

IFN-γ or TNF-α capture antibody was coated on each well of 96 well Maxisorp plates (Nunc, Cophenagen, Denmark) and incubated overnight at room temperature. After washing with wash buffer (PBS containing 0.05% Tween 20), nonspecific binding was blocked by 1% BSA in PBS for 1 hour. Plates were again washed thrice after which control and Zn-DIGP treated samples were added. Standard samples were prepared by half log dilutions of recombinant IFN-γ and TNF-α (Peprotech). Plates were incubated for 2 hours and washed three times with wash buffer (PBS containing 0.05% Tween-20). 0.25µg/ml of murine IFN-γ and TNF-α specific antibody (polyclonal, developed from rabbit) was then added in diluent (PBS containing 0.1% BSA and 0.05% Tween-20) and incubated for 2 hours at room temperature and washed three times with wash buffer. Avidin-conjugated peroxidase was then added and incubated for 30 minutes. After washing the plated three times with wash buffer, 100µl of 2,2'-azino-bis(3-ethylbenzothiazoline-6-sulphonic acid) (Sigma) was added and the plates incubated for 5 minutes at room temperature for color development. The absorbance of each sample was read at 405 nm using Spectramax M5 spectrophotometer.

4.4.2. [^{125}I] CXCL10 displacement assays

Zn-DIGP was dissolved in DMSO at a concentration of 100 mM and serial dilutions were conducted in DMSO. 60-fold dilutions were then made into an equilibrium binding buffer (water supplemented with 50 mM HEPES, 5 mM $MgCl_2$, 1 mM $CaCl_2$, 0.2% BSA at pH 7.4) to concentrations that were four-fold higher than the final assay concentration. CXCL10 and Zn-DIGP was mixed 1:1 (v/v) with [^{125}I]-CXCL10 to a final concentration of 0.1 nM and added to CXCR3 membranes (Millipore) prepared in assay buffer at 1 unit/well. The assay plate was incubated at room temperature for 120 minutes. Prior to CXCL10 capture, the FC filter plate (Millipore) was pre-coated with 0.3% Polyethyleneimine (PEI) for one hour. Following capture, the FC filter plate was washed three times (50 mM HEPES, pH 7.4, 500 mM NaCl, and 0.1% BSA). The filtration plate was allowed to dry and 50 µL per well of scintillation fluid was added and counted on a Perkin Elmer (Wallac) 1450 Microbeta TriLux liquid scintillation counter. K_i values were calculated based on the Cheng-Prusoff equation; $K_i = IC_{50}/[1 + ([L]/K_d)$, where IC_{50} is the half maximal inhibition concentration, [L] is the CXCL10 ligand concentration (0.1 nM), K_d is the measured equilibrium dissociation constant (0.2 nM) of the CXCL10 / CXCR3 binding interaction.

4.4.3. Ca^{2+} flux assays

CXCR3 expressing Chem1 cells (~ 50,000) were seeded in 96 well plates and incubated at room temperature for 30 minutes before transferring to 37 ºC incubator for overnight incubation. GPCR Profiler Assay Buffer (Hanks Balanced Salt Solution containing 20 mM HEPES and 2.5 mM Probenecid; pH = 7.4) and loading buffer (Assay buffer + 5 mM Fluo-8 dye) were prepared. Fresh cells were then washed once with GPCR profiler assay buffer and incubated with loading buffer for 1.5 hours. Meanwhile, Zn-DIGP was dissolved in DMSO at a concentration of 100 mM and serial dilutions were conducted in DMSO. 1000-fold dilutions were made into Millipore's GPCR Profiler Assay Buffer to concentrations that were three-fold higher than the final assay concentration. Vehicle only and positive controls were prepared in the same way. Wells containing cells were prepared in Millipore's GPCR Profiler Assay Buffer. The CXCR3 agonist assays were conducted using a FLIPR^{TETRA} instrument where Zn-DIGP, vehicle controls, and reference agonist (CXCL10) were added to the assay plates containing Chem1 cells that overexpress CXCR3, and a fluorescence baseline was established in Millipore's GPCR Profiler Assay Buffer. Upon completion of the agonist assay, the assay plate was removed from the FLIPR^{TETRA} instrument and incubated at 25 °C for seven minutes.

4.4.4. Antagonist Assay

The antagonist assay was conducted using the same assay plate that was used for the agonist assay. The antagonist assay was also conducted on a FLIPR^{TETRA} instrument for duration of 180 seconds and was used to assess Zn-DIGP's ability to inhibit CXCR3. Using EC_{50} of CXCL10 determined by the agonist assay, all pre-incubated Zn-DIGP wells were challenged with EC_{50} concentration of CXCL10 after establishment of a fluorescence baseline. All assay plate data were subjected to appropriate baseline corrections. Maximum fluorescence values were then exported and data processed to calculate percentage activation, percentage inhibition (relative to EC_{80} and vehicle control values), and additional statistical values (Z', percentage variation between replicate data values) to assess the quality of each plate. All dose response curves were generated using GraphPad Prism. The curves were fit by utilizing "Sigmoidal Dose Response (Variable Slope)" equation where the bottom parameter was fixed to "0." Where appropriate, the top parameter was fixed to "100" to better predict potency values when a curve was not fully generated by the concentrations assayed.

4.4.5. Receptor Internalization assays

B16F10 cells (~ 70`000) were seeded in 24 well plates containing cover slips in 10% FCS containing media. After 4 hours, 10% FCS containing media was replaced with 0% FCS containing media. After overnight incubation, the used media was replaced with fresh 0% FCS containing media and left for 30 minutes. After 30 minutes, 0% FCS media containing 20 nM of CXCL10 or 5 µM Zn-DIGP were added and incubated for 0 minutes, 1 hour or 2 hours. Cells were then washed twice with 1 ml of PBS, fixed with 3% PFA for 15 minutes and washed twice again with PBS. Cover slips were stained with CXCR3 primary antibody (1:400 dilution in PBS containing 0.1% BSA) (Abcam) and incubated at room temperature for 1 hour and washed twice with PBS. Fluoroscein labeled secondary antibody (Abcam) staining was performed with 1:500 dilution in PBS containing 0.1% BSA and incubated for 1 hour at room temperature. In order to visualize the nucleus, a 1:1000 dilution of 10 mg/ml Hoechst 33258 in PBS was applied for 15 minutes at room temperature. Cells were then washed with PBS 5 times and subjected to imaging by SP2 confocal microscope.

4.4.6. Migration assays

B16F10 cells (~ 75000) were seeded in 24 well plates for approximately 4 hours. The media was then replaced with starvation medium (0% FCS) in the presence or absence of 5µM Zn-DIGP and incubated overnight. Used media were then replaced by PBS and a scratch was made with sterile pipette tip and the detached cells were removed. Starvation media containing variable concentrations of CXCL10 or CXCL10 + 5 µM of Zn-DIGP was added to the cells. Bright field images with 4x objective were taken immediately after the scratch and after 24 hours of incubation. The area of scratch was calculated using Image J software. The migration index is defined as the ratio of the area of scratch made at time 0 h to the area of scratch at 24 hours.

4.4.7. Invasion assays

4 x 10^5 B16F10 cells were seeded in T25 flasks. Once the cells adhered, cells were replaced with 10% FCS media with presence or absence of 5 µM Zn-DIGP. After overnight incubation, 20,000 cells were taken in 0% FCS medium containing 0.1% BSA with or without Zn-DIGP in the upper compartment of invasion chamber. The lower compartment is filled with 20 nM CXCL10 or CCL21 and sometimes 5 µM Zn-DIGP. After 10 hours, cells in the upper compartment were removed using cotton swab. Cells that invaded through the

membrane remain attached on the other side of the membrane. Those cells were washed, fixed, stained with nucleus specific dye Hoechst and counted.

4.4.8. Animal Studies

C57BL/6 mice were bred in the animal facility of the Institute of Medical Virology, University of Zurich, and used at 6-8 weeks of age. All experiments were conducted according to the Guide for the Care and Use of Laboratory Animals. Zn-DIGP (trifluoroacetate salt) was diluted into DMSO at a concentration of 10 mM (15.5 mg/mL). Alternatively, as a control vehicle, 40 mM solutions of sodium trifluoroacetate were prepared in DMSO. Zn-DIGP and control vehicles were diluted 10-fold to make 1 mM and 4 mM solutions, respectively, in DMEM + 10% FCS and sterile filtered immediately prior to their application onto cells or injection into mice. In the first series of experiments (type A), B16F10 cell cultures were incubated with 5 µM of Zn-DIGP or 20 µM sodium trifluoroacetate under standard conditions described above for 16 hours. The cells were then trypsinized and washed twice with PBS and diluted to 2 x 10^5 cells in a total volume of 200 µl. The formation of pulmonary metastases was established by intravenous injection of Zn-DIGP-treated or control cells into the tail vein of C57BL/6 mice. Twenty days later, the animals were sacrificed and numbers of lung metastases were examined by visual inspection of lungs.[58]

In a second series of experiments (type B), 2 x 10^5 cells of B16F10 cells, in 200 µl of PBS were injected into the tail vein of C57BL/6 mice. After one day of growth, the mice were then injected with 100 µL of 1 or 4 mM solutions of Zn-DIGP or sodium trifluoroacetate carrier (prepared in DMEM + 10% FCS as described above). Twenty days later the animals were sacrificed and numbers of metastases were examined by visual inspection of lungs.[8, 9] The results for untreated animals were the same as those receiving the carrier only. The results are shown as numbers of metastases in individual mice. Bars represent relative numbers of metastases +/- standard errors from two independent experiments.

4.5. References

[1] F. Balkwill, *Nat Rev Cancer* **2004**, *4*, 540.
[2] E. J. Fernandez, E. Lolis, *Annu Rev Pharmacol Toxicol* **2002**, *42*, 469.
[3] B. Homey, A. Muller, A. Zlotnik, *Nat Rev Immunol* **2002**, *2*, 175.
[4] J. Vandercappellen, J. Van Damme, S. Struyf, *Cancer Lett* **2008**, *267*, 226.
[5] B. Lu, A. Humbles, D. Bota, C. Gerard, B. Moser, D. Soler, A. D. Luster, N. P. Gerard, *Eur J Immunol* **1999**, *29*, 3804.

[6] V. Booth, D. W. Keizer, M. B. Kamphuis, I. Clark-Lewis, B. D. Sykes, *Biochemistry* **2002**, *41*, 10418.
[7] T. Jabeen, P. Leonard, H. Jamaluddin, K. R. Acharya, *Acta Crystallogr D Biol Crystallogr* **2008**, *64*, 611.
[8] L. Lasagni, M. Francalanci, F. Annunziato, E. Lazzeri, S. Giannini, L. Cosmi, C. Sagrinati, B. Mazzinghi, C. Orlando, E. Maggi, F. Marra, S. Romagnani, M. Serio, P. Romagnani, *J Exp Med* **2003**, *197*, 1537.
[9] J. E. Ehlert, C. A. Addison, M. D. Burdick, S. L. Kunkel, R. M. Strieter, *J Immunol* **2004**, *173*, 6234.
[10] A. V. Dix, L. Fischer, S. Sarrazin, C. P. Redgate, J. D. Esko, Y. Tor, *Chembiochem* **2010**, *11*, 2302.
[11] A. Bonacchi, P. Romagnani, R. G. Romanelli, E. Efsen, F. Annunziato, L. Lasagni, M. Francalanci, M. Serio, G. Laffi, M. Pinzani, P. Gentilini, F. Marra, *J Biol Chem* **2001**, *276*, 9945.
[12] A. Meiser, A. Mueller, E. L. Wise, E. M. McDonagh, S. J. Petit, N. Saran, P. C. Clark, T. J. Williams, J. E. Pease, *J Immunol* **2008**, *180*, 6713.
[13] R. A. Colvin, G. S. Campanella, J. Sun, A. D. Luster, *J Biol Chem* **2004**, *279*, 30219.
[14] J. R. Groom, A. D. Luster, *Immunol Cell Biol*, *89*, 207.
[15] Y. Yu, G. Merlino, *Am J Pathol* **2010**, *176*, 2088.
[16] K. Kawada, H. Hosogi, M. Sonoshita, H. Sakashita, T. Manabe, Y. Shimahara, Y. Sakai, A. Takabayashi, M. Oshima, M. M. Taketo, *Oncogene* **2007**, *26*, 4679.
[17] L. Goldberg-Bittman, E. Neumark, O. Sagi-Assif, E. Azenshtein, T. Meshel, I. P. Witz, A. Ben-Baruch, *Immunol Lett* **2004**, *92*, 171.
[18] X. Ma, K. Norsworthy, N. Kundu, W. H. Rodgers, P. A. Gimotty, O. Goloubeva, M. Lipsky, Y. Li, D. Holt, A. Fulton, *Mol Cancer Ther* **2009**, *8*, 490.
[19] D. Jones, R. J. Benjamin, A. Shahsafaei, D. M. Dorfman, *Blood* **2000**, *95*, 627.
[20] M. Teichmann, B. Meyer, A. Beck, G. Niedobitek, *J Pathol* **2005**, *206*, 68.
[21] T. Suyama, M. Furuya, M. Nishiyama, Y. Kasuya, S. Kimura, T. Ichikawa, T. Ueda, T. Nikaido, H. Ito, H. Ishikura, *Cancer* **2005**, *103*, 258.
[22] D. Datta, J. A. Flaxenburg, S. Laxmanan, C. Geehan, M. Grimm, A. M. Waaga-Gasser, D. M. Briscoe, S. Pal, *Cancer Res* **2006**, *66*, 9509.
[23] A. Zipin-Roitman, T. Meshel, O. Sagi-Assif, B. Shalmon, C. Avivi, R. M. Pfeffer, I. P. Witz, A. Ben-Baruch, *Cancer Res* **2007**, *67*, 3396.
[24] L. Goldberg-Bittman, O. Sagi-Assif, T. Meshel, I. Nevo, O. Levy-Nissenbaum, I. Yron, I. P. Witz, A. Ben-Baruch, *Cytokine* **2005**, *29*, 105.
[25] M. L. Nagpal, J. Davis, T. Lin, *Biochim Biophys Acta* **2006**, *1762*, 811.
[26] S. Hirano, Y. Iwashita, A. Sasaki, S. Kai, M. Ohta, S. Kitano, *J Gastroenterol Hepatol* **2007**, *22*, 690.
[27] T. Kondo, F. Ito, H. Nakazawa, S. Horita, Y. Osaka, H. Toma, *J Urol* **2004**, *171*, 2171.
[28] M. Wendel, I. E. Galani, E. Suri-Payer, A. Cerwenka, *Cancer Res* **2008**, *68*, 8437.
[29] C. Sgadari, A. L. Angiolillo, B. W. Cherney, S. E. Pike, J. M. Farber, L. G. Koniaris, P. Vanguri, P. R. Burd, N. Sheikh, G. Gupta, J. Teruya-Feldstein, G. Tosato, *Proc Natl Acad Sci U S A* **1996**, *93*, 13791.
[30] K. Kawada, M. Sonoshita, H. Sakashita, A. Takabayashi, Y. Yamaoka, T. Manabe, K. Inaba, N. Minato, M. Oshima, M. M. Taketo, *Cancer Res* **2004**, *64*, 4010.
[31] M. M. Robledo, R. A. Bartolome, N. Longo, J. M. Rodriguez-Frade, M. Mellado, I. Longo, G. N. van Muijen, P. Sanchez-Mateos, J. Teixido, *J Biol Chem* **2001**, *276*, 45098.

[32] C. Monteagudo, J. M. Martin, E. Jorda, A. Llombart-Bosch, *J Clin Pathol* **2007**, *60*, 596.
[33] A. D. Luster, P. Leder, *J Exp Med* **1993**, *178*, 1057.
[34] F. Antonicelli, J. Lorin, S. Kurdykowski, S. C. Gangloff, R. Le Naour, J. M. Sallenave, W. Hornebeck, F. Grange, P. Bernard, *Br J Dermatol* **2011**, *164*, 720.
[35] D. L. Clarke, R. L. Clifford, S. Jindarat, D. Proud, L. Pang, M. Belvisi, A. J. Knox, *J Biol Chem* **2010**, *285*, 29101.
[36] M. Johnson, A. R. Li, J. Liu, Z. Fu, L. Zhu, S. Miao, X. Wang, Q. Xu, A. Huang, A. Marcus, F. Xu, K. Ebsworth, E. Sablan, J. Danao, J. Kumer, D. Dairaghi, C. Lawrence, T. Sullivan, G. Tonn, T. Schall, T. Collins, J. Medina, *Bioorg Med Chem Lett* **2007**, *17*, 3339.
[37] B. Cambien, B. F. Karimdjee, P. Richard-Fiardo, H. Bziouech, R. Barthel, M. A. Millet, V. Martini, D. Birnbaum, J. Y. Scoazec, J. Abello, T. Al Saati, M. G. Johnson, T. J. Sullivan, J. C. Medina, T. L. Collins, A. Schmid-Alliana, H. Schmid-Antomarchi, *Br J Cancer* **2009**, *100*, 1755.
[38] T. C. Walser, S. Rifat, X. Ma, N. Kundu, C. Ward, O. Goloubeva, M. G. Johnson, J. C. Medina, T. L. Collins, A. M. Fulton, *Cancer Res* **2006**, *66*, 7701.
[39] J. E. Pease, R. Horuk, *Expert Opin Ther Pat* **2009**, *19*, 199.
[40] D. R. Allen, A. Bolt, G. A. Chapman, R. L. Knight, J. W. Meissner, D. A. Owen, R. J. Watson, *Bioorg Med Chem Lett* **2007**, *17*, 697.
[41] R. J. Watson, D. R. Allen, H. L. Birch, G. A. Chapman, D. R. Hannah, R. L. Knight, J. W. Meissner, D. A. Owen, E. J. Thomas, *Bioorg Med Chem Lett* **2007**, *17*, 6806.
[42] R. L. Knight, D. R. Allen, H. L. Birch, G. A. Chapman, F. C. Galvin, L. A. Jopling, C. J. Lock, J. W. Meissner, D. A. Owen, G. Raphy, R. J. Watson, S. C. Williams, *Bioorg Med Chem Lett* **2008**, *18*, 629.
[43] A. G. Cole, I. L. Stroke, M. R. Brescia, S. Simhadri, J. J. Zhang, Z. Hussain, M. Snider, C. Haskell, S. Ribeiro, K. C. Appell, I. Henderson, M. L. Webb, *Bioorg Med Chem Lett* **2006**, *16*, 200.
[44] M. E. Hayes, G. A. Wallace, P. Grongsaard, A. Bischoff, D. M. George, W. Miao, M. J. McPherson, R. H. Stoffel, D. W. Green, G. P. Roth, *Bioorg Med Chem Lett* **2008**, *18*, 1573.
[45] M. E. Hayes, E. C. Breinlinger, G. A. Wallace, P. Grongsaard, W. Miao, M. J. McPherson, R. H. Stoffel, D. W. Green, G. P. Roth, *Bioorg Med Chem Lett* **2008**, *18*, 2414.
[46] J. P. Bongartz, M. Buntinx, E. Coesemans, B. Hermans, G. V. Lommen, J. V. Wauwe, *Bioorg Med Chem Lett* **2008**, *18*, 5819.
[47] M. Wijtmans, D. Verzijl, S. Bergmans, M. Lai, L. Bosch, M. J. Smit, I. J. de Esch, R. Leurs, *Bioorg Med Chem* **2011**, *19*, 3384.
[48] J. H. Lee, H. N. Kim, K. O. Kim, W. J. Jin, S. Lee, H. H. Kim, H. Ha, Z. H. Lee, *Cancer Res* **2012**, *72*, 3175.
[49] C. E. Heise, A. Pahuja, S. C. Hudson, M. S. Mistry, A. L. Putnam, M. M. Gross, P. A. Gottlieb, W. S. Wade, M. Kiankarimi, D. Schwarz, P. Crowe, A. Zlotnik, D. G. Alleva, *J Pharmacol Exp Ther* **2005**, *313*, 1263.
[50] A. Sauty, R. A. Colvin, L. Wagner, S. Rochat, F. Spertini, A. D. Luster, *J Immunol* **2001**, *167*, 7084.
[51] V. L. Martins, J. J. Vyas, M. Chen, K. Purdie, C. A. Mein, A. P. South, A. Storey, J. A. McGrath, E. A. O'Toole, *J Cell Sci* **2009**, *122*, 1788.
[52] R. Yoshida, M. Nagira, M. Kitaura, N. Imagawa, T. Imai, O. Yoshie, *J Biol Chem* **1998**, *273*, 7118.

[53] J. Schultz, J. Pavlovic, B. Strack, M. Nawrath, K. Moelling, *Hum Gene Ther* **1999**, *10*, 407.
[54] F. Noreen, J. Heinrich, K. Moelling, *Oligonucleotides* **2009**, *19*, 169.
[55] R. Pfeiffer, J. Kirsch, F. Fahrenholz, *Exp Cell Res* **1998**, *244*, 327.
[56] L. H. Pheng, Y. Dumont, A. Fournier, J. G. Chabot, A. Beaudet, R. Quirion, *Br J Pharmacol* **2003**, *139*, 695.
[57] I. Bohme, A. G. Beck-Sickinger, *Cell Commun Signal* **2009**, *7*, 16.
[58] Q. Li, Y. T. Chang, *Nat Protoc* **2006**, *1*, 2922.

Acknowledgment

First of all, I sincerely thank Prof. Dr. Nathan Luedtke for giving me the opportunity to work on this exciting project. In addition to his consistent encouragement and constant involvement, his flexibility towards the project added greater impact in development of this thesis.

I thank Prof. Andreas Plückthun, Prof. Reto Schwendener and Prof. Oliver Zerbe for serving on my thesis committee members, and for their valuable involvement on my thesis.

I would like to thank Prof. Reto Schwendener of Institute of Molecular Cancer Research and his group for allowing access to tissue culture, Alok Behera and Prof. Verrey at the Institute of Physiology for assistance with qRT-PCR. My thanks also go to all the staff, in particular Dr. Caroline Aemisiegger and Dr. Jose Maria Mateos at the Institute of Microscopy for their assistance with fluorescence microscope.

Next, my heartfelt thanks to all former and current member of the Luedtke group : Martin Seyfried, Anaelle Dumas, Sarah Hentschel, Anne Neef, Guillaume Mata, Ulrike Reider, Alessandro Cechi, Therese Triemer, Philippe Roth, Raul Pereira, Sabrina Huber, Olivia Schmidt, Marco Brandstetter and David Oesch for providing a wonderful working atmosphere and friendship. Special thanks to Dr. Jawad Alzeer for frequent discussion about the project.

I thank Swiss National Foundation for their financial support. I am also grateful to Sussanna Bachmann and the Molecular life sciences graduate school for providing opportunity to take different courses and for financial support to attend conferences.

I also thank Balamurugan Periasamy, Harsha Kocherla, Jayamurugan Govindasamy, Chaithanya Maduranthakam, Kiran and Sabyschachi Mishra for their great friendship, and making my time in Zurich memorable.

I am very thankful to my parents Balanarsimhulu and Hamsa Vummidi for their constant support in realizing my career ambitions from the very beginning. Special thanks to my sister

Vasanth Ayswarya for her incredible support and love throughout my PhD studies. I would also like to thank Dr. M.L. Stephen Raj for his guidance and motivation to pursue a scientific career.

Curriculum Vitae

Personal Information

Surname	:	Vummidi
Firstname	:	Bala Yeshwanth Ram
Date of Birth	:	19th August 1985
Nationality	:	Indian

Education

2008-2013	:	University of Zurich, Zurich, Switzerland. PhD in the group of Prof. Nathan Luedtke.
2006-2007	:	Newcastle University, Newcastle, United Kingdom. Masters by Research (Medical and Molecular life sciences).
2002-2006	:	Anna University, Chennai, India. Bachelors of Technology (Industrial Biotechnology).
2002	:	SBOA Higher secondary school, Chennai, India. Higher secondary studies.

Publications

- B. R. Vummidi, J. Alzeer, F. Noreen, K. Moelling, N. W. Luedtke. Photodynamic agents with anti-metastatic activities. *ACS Chemical biology*, 2013, 8 (8), 1737.
- B. R. Vummidi, J. Alzeer, N. W. Luedtke. Fluorescent probes for G-quadruplex. *Chembiochem,* 2013. 14 (5), 540. (Review)
- J. Alzeer, B. R. Vummidi, P. J. C. Roth, N. W. Luedtke. Guanidino phthalocyanines as high affinity G-quadruplex fluorescent probes and transcriptional regulators. *Angew. Chem. Intl. Ed.*, 2009, 48 (29), 9362.
- N. W. Luedtke, J. Alzeer, B. R. Vummidi. Preparation and uses of guanidinium-modified porphyrins and phthalocyanines 2008, PCT/EP application 006417. (Patent)